proton polarization and relaxation in dilute paramagnetic crystals by rotational cooling

h.b. brom

STELLINGEN

1. Het zogenaamde spinflip-proces tussen een proton- en electronspin in het menggebied, zoals door McColl en Jeffries beschreven, is een geval van kruisrelaxatie, waarbij eerste orde tijdsafhankelijke storingstheorie niet van toepassing is. Het kruisrelaxatieproces zal bij een grotere afstand tussen de protonen dan in de ethylsulfaten overgaan in „level anticrossing".
   McColl, J.R. en Jeffries, C.D., Phys. Rev. B 1 (1970) 2917.
   Veeman, W.S., proefschrift Leiden 1972.
   Zweers, A.E., doctoraalscriptie 1972.

2. Metingen van protonspin-roosterrelaxatietijden kunnen waardevolle gegevens over electronspin-roosterrelaxatie verschaffen, die op andere wijze niet of nauwelijks zijn te verkrijgen. Hetzelfde geldt voor metingen van de polarisatiegraad, verkregen met draaikoeling, met betrekking tot de minimum g-waarde van electronspins (voor $g_{min} \leq 0.1$).
   Brom, H.B., Soeteman, J. en van Duyneveldt, A.J., 17de congres Ampere, Turku 1972.
   Dit proefschrift, bijv. hoofdstuk 3.

3. De suggestie van de Wit en Bloom van het bestaan van een korte protonspin-roosterrelaxatietijd in CH_4 bij het absolute nulpunt is aanvechtbaar.
   de Wit, G.A. en Bloom, M., Can. J. Phys. 47 (1969) 1195.
   Glättli, H., Sentz, A. en Eisenkremer, M. Phys.Rev.Lett. 28 (1972) 871.

4. De argumentatie, die Smith en Friedberg geven voor het domineren van wisselwerking tussen naaste buren in $Cs_2MnCl_4 \cdot 2H_2O$ is onjuist.
   Smith, T. en Friedberg, S.A., Phys. Rev. 177 (1969) 1012.

5. De T^2-afhankelijkheid van de soortelijke warmte, die door Pierce en Friedberg wordt verondersteld voor mangaan-formiaat by 2 K, volgt niet uit de spingolftheorie, zoals wordt gesuggereerd.
   Pierce, R.D. en Friedberg, S.A., Phys. Rev. 165 (1968) 680.

6. Bij het gebruik van het begrip Debyetemperatuur dient de definitie duidelijk te zijn aangegeven.
   Anderson, O.L., J. Phys. Chem. Sol. 12 (1959) 41.
   McColl, J.R., proefschrift Un. of California, Berkeley, 1967 (niet gepubliceerd).

7. Bij de beschrijving van warmtegeleidingsmetingen aan kristallen bij lage temperaturen dienen de posities van het stooklichaam en de thermometers, evenals de afmetingen van het preparaat en de richting van de kristalassen t.o.v. de warmtestroomrichting te zijn vermeld.
   Berman, R., Simon, F.E., en Ziman, J.M., Proc.Roy.Soc. A 220 (1953) 171.
   Berman, R.,Foster, E.L. en Ziman, J.M., Proc.Roy.Soc. A 231 (1955) 130.
   Haasbroek, J.H., Int.Conf. on Phonon Scattering in Solids, Parijs 1972, p. 85.

8. Ten onrechte wordt slechts weinig aandacht geschonken aan de polarisatieverschijnselen van de bij optische metingen gebruikte lichtbronnen.
   Winsemius, P. en Lengkeek, H.P., wordt gepubliceerd.
   Pitz, E., Applied Optics 11 (1969) 255.

9. De conclusie van Furtado dat in het door hem gemeten supergeleidend $Ta_{0.92}Nb_{0.08}$ een irreversibele oppervlaktebarriere afwezig is, volgt niet uit zijn argumenten en is onjuist. Aan de waarde van de door hem gevonden „generalized law of a.c. losses" moet dan ook sterk worden getwijfeld.
   Furtado, C.S., Proc. 4th Intern. Cryog. Eng. Conf.„Eindhoven (1972) 140.
   de Klerk, D. en van der Klein, C.A.M., J. Low Temp. Phys. 6 (1972) 1.

10. Campbell en Evetts concluderen ten onrechte dat in een type II supergeleider alleen dan het fluxpatroon in een preparaat bij H_{c2} lineair verloopt, indien de helling van de magnetisatiekromme bij H_{c2} veel kleiner is dan één.
    Campbell, A.M. en Evetts, J.E., Adv. in Physics 21 (1972) 199 (p.283).

11. Ontzilting van zeewater voor het bereiden van drinkwater kan gewenst zijn op grond van milieubeheersing.
    Pieper, G.A., 4thInt. Technical Exhibition on Treatment, Storage, Transport and Usage of Water:„Aquatech 1972" 20 sept. 1972, A'dam.

12. Bij het plaatsen van electriciteitscentrales en/of vuilverbrandingen moet de combinatie met een ontziltingsinstallatie in de beschouwing worden betrokken.
    Wijnstra, O., „Aquatech 1972", 20 sept. 1972, Amsterdam.
    Biemond, C., Water 51 (1967) 396.

13. Het plaatsen van snuffelpalen is niet alleen wenselijk in industriegebieden, maar eveneens in vergaderzalen, cantines en aanverwante gelegenheden.

H.B. Brom

14 februari 1973

PROTON POLARIZATION AND RELAXATION IN DILUTE PARAMAGNETIC CRYSTALS BY ROTATIONAL COOLING

PROTON POLARIZATION AND RELAXATION IN DILUTE PARAMAGNETIC CRYSTALS BY ROTATIONAL COOLING

PROEFSCHRIFT

ter verkrijging van de graad van Doctor in de Wiskunde en Natuurwetenschappen aan de Rijksuniversiteit te Leiden, op gezag van de Rector Magnificus Dr. A.E. Cohen, Hoogleraar in de Faculteit der Letteren, volgens besluit van het college van Dekanen te verdedigen op woensdag 14 februari 1973 te klokke 14.15 uur.

door

HANS BERNARD BROM

geboren te Amsterdam in 1944

Krips Repro - Meppel

PROMOTOR: PROF. DR. W.J. HUISKAMP

This investigation is part of the research program of the "Stichting voor Fundamenteel Onderzoek der Materie (F.O.M.)", which is financially supported by the "Nederlandse Organisatie voor Zuiver-Wetenschappelijk Onderzoek (Z.W.O.)".

Aan mijn ouders

Aan Christa

CONTENTS

Survey.

This thesis deals with experiments on proton-spin polarization and relaxation in diamagnetic crystals doped with small, clearly defined amounts of paramagnetic impurities. Proton polarization was achieved by a special method, called rotational cooling. This method starts from a readily attainable electron-spin polarization, which is subsequently transferred to the nuclear spins by rotation of a magnetic field. The rotational cooling method was investigated under various experimental conditions in order to reach maximum nuclear polarization, e.g. the temperature was varied between $0.05 \leq T \leq 1$ K and the paramagnetic impurity concentration between $0.05 \leq c \leq 2$ %.

Because of the dependence of the degree of polarization on the coupling between proton spins, electronic spins, and lattice vibrations, we have studied the heat transfer between these systems, particularly the nuclear spin-lattice relaxation time, T_{1n}. A second motivation for the T_{1n} study, which comprises a relatively large part of this thesis, derived from the favourable experimental conditions for such an investigation. The very low nuclear-spin temperatures which can be reached by polarization facilitate the nuclear relaxation measurements appreciably. Furthermore, the impurity concentration region below 1% is very suited for examination of e.g. the role of spin-spin interaction in T_{1n}.

In chapter 1 we have mentioned some experiments on polarized nuclei and discussed a few polarization methods, in particular dynamic polarization and nuclear refrigeration, as the rotational cooling method is also called. Further, the relaxation mechanisms, as far as relevant to our experiments, are briefly reviewed. The main topic treated is the manner in which nuclear relaxation proceeds via the Zeeman system and via the dipole reservoir of the electronic spins, including the role of spin diffusion.

The experimental equipment and the measuring procedures are discussed in chapter 2, which is mainly concerned with proton polarization and relaxation experiments in YES (yttrium ethyl sulfate), doped with Yb and Dy ions respectively. With the aid of published data on the electron spin-lattice relaxation time, T_{1e}, a theoretical description of the T_{1n} results is presented in terms of Bloembergen, dipolar, and

cross-relaxation.

Chapter 3 deals with rotational cooling and relaxation experiments in $YCl_3.6H_2O$, doped with Yb ions. The T_{1n} data obtained in these crystals are interpreted in the same terms as in chapter 2, assuming a nearly hexagonal crystal-field symmetry. An estimate of T_{1e} from the T_{1n} results appears to be consistent with the directly measured electron spin-lattice relaxation time in a powdered chloride hexahydrate sample. Finally, from a comparison of the field and angular dependence of the polarization data, the minimum g value of the Yb spins is obtained.

In chapter 4, the optimal conditions for the nuclear-spin refrigerator method are investigated in the crystal samples of the preceding chapters. A theoretical analysis of the data shows that the electron spin-spin interaction plays a prominent role in the degree of polarization attainable by the rotational cooling method.

A few subjects broached in chapter 1 are analyzed in more detail in the appendices, at the end of this thesis. Most of the problems treated are connected with the derivation of the proportionality coefficient between T_{1e} and T_{1n}. Further, a description of adiabatic demagnetization experiments is given, which takes the Kronig-Bouwkamp relaxation mechanism into account. Finally, also a short comment is given concerning the NMR method and concentration analysis.

Chapter 2 of this thesis has been published in Physica 60 (1972); chapters 3 and 4 will be published in the same journal.

CHAPTER 1

INTRODUCTION

1. General remarks. In 1924 Pauli [1] introduced the concept that atomic nuclei possess mechanical angular momentum, which has become familiar as the nuclear spin. The discovery of the nuclear spin, almost simultaneously with that of the electron spin, has posed challenging problems regarding the internal structure of these particles. This refers in particular also to the simplest nuclear constituents, the proton and the neutron, which, unlike the electron, are strongly interacting particles and therefore amenable to a great variety of elastic and inelastic scattering experiments. Particularly in the last decade the internal structure of the proton has been the subject of many experimental studies in the high energy physics. We shall forego a discussion why the use of polarized protons greatly facilitates the task of unravelling the scattering cross-section results. It may be noted [2], however, that many experiments nowadays utilize polarized proton targets and that the results are usually analyzed in terms of a spin-dependent and a spin-independent scattering amplitude (or equivalently in spin-flip and non spin-flip amplitude).

The possibility of polarizing the spins of atomic nuclei was suggested in 1935 by Gorter [3] and by Kurti and Simon [4]. This suggestion was based on the property that atomic nuclei have magnetic moments associated with the nuclear spin I and further on the experimental demonstration, in the same year, that ultralow temperatures could be reached by adiabatic demagnetization. The study of nuclear magnetism was greatly stimulated by the invention of nuclear magnetic resonance (NMR), which has since been applied to many branches of physics, notably also to solid state physics.

From a theoretical point of view, the study of statistical-thermodynamical aspects of interacting spin systems has strongly benefitted

from NMR experiments in solids, where the predominant internuclear magnetic interactions are often entirely of dipolar origin and therefore well defined. This refers, for instance, to many relaxation phenomena in coherently precessing spin systems and to the concept of spin temperature , see section 3.2. Further new theoretical insights may be obtained from the study of nuclear-magnetic phase transitions, as has recently been observed for the first time by Abragam and coworkers [5]. A considerable fraction of the spin entropy had to be removed from the nuclear spin system in order to demonstrate the occurrence of a phase transition point. For comparison, we consider the magnetic ordering of electronic magnetic moments by dipolar interactions. For instance, in $DyCl_3.6H_2O$, about one half of the electron spin entropy needs to be removed to reach the ordered state [6]. This would correspond to 80% polarization of electron spins in a large external field.

Such high degrees of nuclear polarization cannot, at present, be obtained simply by cooling nuclear spin systems in an external field (the brute force method). As will be shown in section 2.1 very low temperatures and high fields would be required. However, in addition, under those circumstances, thermal equilibrium usually is not attained in any reasonable length of time due to exceedingly long nuclear spin-lattice relaxation times. Therefore, other methods for nuclear polarization have been developed, in which electron spin polarization is transferred to nuclear spin systems by the application of electron spin resonance (ESR) techniques or by relaxation processes. In these methods diamagnetic ionic crystals are employed, in which a small percentage paramagnetic ions are substituted.

In this thesis we shall be particularly concerned with the rotational cooling method, which does not require ESR techniques. As will be discussed in section 2.2 both ESR and rotational cooling methods have in common that small amounts of paramagnetic impurities are required in the diamagnetic samples utilized for nuclear polarization. In the rotational cooling method the attainable nuclear polarization depends on the feasibility of cross-relaxation between electronic and nuclear spins as well as on the nuclear relaxation outside the cross-relaxation region. To get nuclear polarization under control it is

expedient to gather information about these relaxation phenomena.

It was suggested in 1949 by Bloembergen that in most diamagnetic solids the nuclei are relaxed to the lattice by intermediary of paramagnetic impurities, see section 3.2.2. He further made the assumption that in view of the low paramagnetic ion concentration usually present ($c \leq 10^{-2}$%), the spin-spin interaction between neighbouring impurity ions are to be neglected. Normally in the ionic crystals, utilized in nuclear polarization, the concentration of the substituted paramagnetic ions is of the order of 0.1% or higher. As argued by several authors after 1965 at these concentrations spin-spin interaction provides an additional relaxation path, which differs in various respects from the "Bloembergen" relaxation. In our experiments we are able to observe both kinds of nuclear relaxation processes. Especially the Bloembergen relaxation rate has been determined carefully, because of the disputable role of the nuclear-spin diffusion. From the dependence of the nuclear relaxation rate on the paramagnetic ion concentration, it is possible to determine the influence of spin-spin interaction. The very low paramagnetic ion concentrations require a special accurate concentration analysis of the crystals, discussed in appendix G.

It may be noted that the availability of polarized protons facilitates the measurements of proton relaxation times for two reasons. Firstly the benefit of polarized spins is based on the circumstance that weak rf fields suffice to measure the nuclear-spin temperature accurately. This is essential because at the very long relaxation times involved low rf fields are required to prevent warming up of the spins during the measurement. Long relaxation times also necessitate a high stability of the NMR equipment, see appendix F. In conventional continuous wave (cw) methods the protons are depolarized by a strong rf pulse. Consequently relatively large rf fields are necessary to determine the return of the nuclear polarization to its equilibrium value. Secondly, large nuclear polarization values have the advantage that initial relaxation effects will give only a small decrease of the NMR signal, while in the usual cw method these effects are relatively strong.

2. Polarization methods. We shall briefly discuss some rather well

known proton-spin polarization methods with particular emphasis on their relation to the rotational cooling method. Following Daniels [7] we roughly divide the polarization methods into two groups.

2.1. *Equilibrium methods.* Let us consider a nuclear spin $I = \frac{1}{2}$ in a magnetic field H. When the probability densities of the nuclear spin in the state $I_z = -\frac{1}{2}$ and $I_z = +\frac{1}{2}$ are denoted by n_1 resp. n_2, the temperature T_I of the spin can be defined according to the Boltzmann distribution $n_1/n_2 = \exp(-g_n\mu_B H/kT)$. Here $\frac{1}{2}g_n\mu_B$ is the nuclear magnetic moment, in which the nuclear gyromagnetic ratio, g_n, is expressed in Bohrmagnetons. The nuclear polarization $p_n = (n_2 - n_1)/(n_1 + n_2) = \tanh(\Delta_n/2kT_I)$, where $\Delta_n = g_n\mu_B H$, see fig. 1. At very low temperatures and very high magnetic

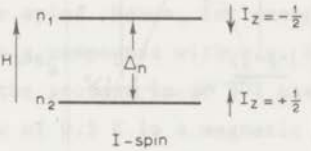

Fig. 1. Zeeman energy levels of a nuclear spin (I), in a magnetic field, with hamiltonian $H = -g_n\mu_B\vec{H}.\vec{I}$. The magnetic field direction coincides with the z axis. The average population of the $I_z = -\frac{1}{2}$ and $I_z = +\frac{1}{2}$ levels, separated by $\Delta_n = g_n\mu_B H$, are denoted by n_1 resp. n_2. The nuclear polarization is defined as $p_n = (n_2 - n_1)/(n_2 + n_1)$.

fields one has $T_I << \Delta_n/k$ and hence the polarization of the nuclear spin would be almost complete ($p_n \approx 1$). For example, for protons $g_n = 0.00304$. Then, in order to satisfy $T_I = \Delta_n/k$, a magnetic field of 10 kOe at $T_I = 2$ mK is required.

2.2. *Non-equilibrium methods.* In this category the dynamic polarization methods, which are based on the Abragam-Jeffries or solid-state effect, are widely used. For a discussion of these methods, we refer in particular to Schmugge and Jeffries [8]. Their treatment is generally

applicable to solids, in which electron spins S and nuclear spins I interact through weak dipolar coupling. In these methods a strong external magnetic field H in conjunction with microwave fields are utilized. The essential points can best be illustrated by considering just one electronic spin and one neighbouring proton spin. In fig. 2a the energy

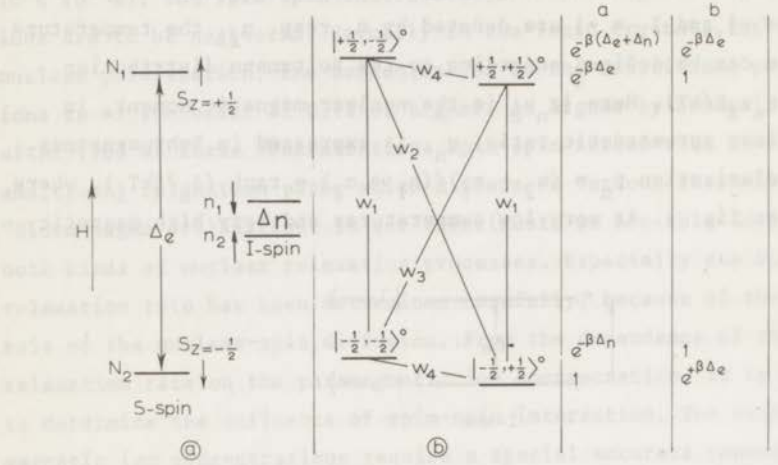

Fig. 2. Energy levels of a nuclear spin (I) and an electronic spin (S). The Zeeman levels of each of the spins are separately illustrated in fig. 2a. The average populations of the S spin are denoted by N_1 and N_2, those of the I spin by n_1 and n_2. The energy levels of the combined S-I system, coupled by dipolar interaction, are given in fig. 2b. The relaxation transitions are denoted by w_1 etc., while the energy levels are labeled by the zeroth-order wave functions $|S_z,I_z\rangle^0$, i.e. omitting the effect of dipolar interaction. Columns a and b show the Boltzmann distributions before resp. after saturation of the w_3 transitions; in the exponents 1/kT is abbreviated as β.

level splittings of the two spins are illustrated. The Zeeman energy splitting, Δ_e, of the electronic spins, is about a factor 10^3 larger than the nuclear Zeeman splitting, Δ_n. The energy levels scheme of the

combined system is given in fig. 2b. The initial Boltzmann distribution, if no microwave field is applied, is given in column a. Allowed transitions with transition probabilities w_1, caused by the interaction with the lattice, can flip the electron spin. The forbidden transitions, in which a paramagnetic ion and a proton spin in weak dipolar coupling are simultaneously flipped, are denoted by w_2 and w_3. Single flips of the nuclear spin have a probability w_4. Suppose $w_1 \gg w_2 \approx w_3 \gg w_4$ (see section 2), which relation holds in most doped diamagnetic crystals. When transitions between the "w_3 levels" are saturated by a strong microwave field, the Boltzmann distributions for the electronic and nuclear spins respectively become approximately equal (column b in fig. 2b). It will be clear that because of the difference by three orders of magnitude in their gyromagnetic ratios, it is much easier to polarize electronic spins than nuclear spins. Hence, for example in the recently intensively studied organic compounds with e.g. free radicals [9,10], dynamic polarization of the protons up to 80% has been attained starting from a sample temperature of 0.5 K in a magnetic field of 25 kOe. It may be mentioned that because of the large hydrogen density and favourable ratio of bound to free protons, these samples are most suited for scattering experiments in elementary particle physics [11].

2.3. *Rotational cooling method.* Also in the nuclear-spin refrigerator method, as the rotational cooling method is frequently called [12-14], one wishes to transfer the electron spin polarization to the nuclear spins. This method is based on reducing the effective Zeeman splitting of the electron spins at constant entropy and nearly constant nuclear Zeeman splitting. The reduction can be realized in various ways, one of which is mentioned below. When the energy splitting of the electron spins matches the nuclear Zeeman energy splitting, the population densities of the energy levels in the two systems tend to equalize through cross-relaxation, induced by dipolar interaction. Abragam [15] and Jeffries [16] have proposed this method e.g. for crystals containing electronic spins with a very anisotropic g value, as for instance ytterbium in yttrium ethyl sulfate, hereafter abbreviated as Yb:YES. At liquid helium temperatures the magnetic behaviour of the electron

spins in Yb:YES can be described by an effective spin $S = \frac{1}{2}$, possessing a very anisotropic g value: $g_{max} = 3.4$ and $g_{min} \approx g_n = 0.003$. A rotation of the magnetic field direction from the g_{max} axis to the g_{min} axis decreases the electron-spin temperature by about a factor thousand (see appendix E) if the Boltzmann distribution remains constant. This requirement is fulfilled if the magnetic field rotation is completed within a time short compared to the electron spin-lattice relaxation time, T_{1e}. In Yb:YES the adiabatic requirement is easily met at low temperatures because of the anisotropy of T_{1e}. In fact, T_{1e} becomes very long when the field is rotated towards the g_{min} direction.

The nuclear-spin refrigerator works most efficiently in diluted systems (see chapter 4). In YbES the ratio of the number of paramagnetic ions to the proton number is 1:33, so for instance in 1% Yb:YES the rotation process must be repeated at least a few thousand times in order to obtain maximum proton polarization. The highest degree of proton polarization, so far attained by the rotational cooling method, is reported to be 35% [13,14].

3. Relaxation mechanisms. 3.1. *Electron spin-lattice relaxation processes.* For a survey of the literature on the theory of the electron spin-lattice relaxation the reader is referred to Manenkov and Orbach [17]. Further review articles are published e.g. of the authors Verstelle and Curtis [18] and recently of Cianchi and Mancini [19]. Of the possible relaxation mechanisms the one-phonon relaxation processes are the most pertinent to our experiments. For a calculation of the direct electron spin-lattice relaxation rate knowledge about the interaction of the electron-spin system with the lattice vibrations is necessary. Because of the problems involved the required parameters of this dynamic orbit-lattice interaction are usually estimated (see also chapter 3). Such estimates provide only an order of magnitude accuracy [20]. However, the qualitative behaviour of T_{1e} predicted by theory, is in good agreement with experimental results [21]. For example, the very anisotropic electron spin-lattice relaxation rate experimentally found in Yb:YES, $T_{1e}^{-1} \propto H^4 T \sin^2\theta\cos^2\theta$, can be derived straightforwardly from theoretical calculations. Here θ denotes the angle between the g_{max} axis and the magnetic

field direction.

3.2. *Nuclear relaxation processes.* We shall discuss nuclear spin-lattice relaxation processes in diamagnetic crystals having a paramagnetic impurity concentration of about 1% or less. The nuclear spins may interact with the lattice in various ways.

3.2.1. *Pure nuclear relaxation.* Waller (1932) [22] has treated spin-lattice and spin-spin interactions in paramagnetic crystals. The proposed relaxation mechanism is also applicable to nuclear spins in a diamagnetic lattice. This mechanism consists of modulation of dipolar interaction by the lattice vibrations (phonons), which effectuates relaxation transitions. In the calculation of Waller lattice vibrations are allowed to change the spin direction of only one spin in a fixed surrounding. Al'tshuler [23] has extended Waller's theory taking into account simultaneous double spin flips, which accelerates the relaxation, because more phonons of higher energy can pariticipate in the relaxation process.

An estimate of the nuclear spin-lattice relaxation time, T_{1n}, in YES crystals, based on the Al'tshuler mechanism, gives typically $T_{1n} \approx 10^{16} H^{-2} T^{-1}$, with the magnetic field H in kOe. Thus at T = 1 K and H = 1 kOe we would expect a relaxation time of the order of 10^{16} s, which is of no practical interest.

3.2.2. *Bloembergen relaxation.* Because the observed nuclear spin-lattice relaxation times are very many orders of magnitude shorter than those predicted by Al'tshuler's theory, obviously other relaxation mechanisms exist. Bloembergen [24] has proposed that T_{1n} would be determined by the influence of paramagnetic ion impurities. These are intimately coupled to the lattice via the interaction between their orbital angular momenta and the crystalline electrical fields. Hence nuclear relaxation can be effectuated by the dipolar interaction of the ionic spins with the nuclei.

Let us consider the influence of the surrounding nuclear and electron spins on a non-equilibrium polarization value, $p_n(\vec{r}_j,t)$, of a nuclear spin at the lattice site $\vec{r}_j$ at time t. Let us further assume a

single paramagnetic impurity ion, located at the origin, to be in thermal equilibrium with the lattice at temperature T_L. Then the relaxation decay of polarization due to the presence of the paramagnetic impurity can be expressed by (see appendix A)

$$\frac{\partial p_n(\vec{r}_j,t)}{\partial t} = Cr_j^{-6}\{p_{no} - p_n(\vec{r}_j,t)\} \tag{3.1}$$

The coefficient C is proportional to $T_{1e}^{-1}H^{-2}$ (in the high temperature approximation), while p_{no} denotes the nuclear polarization assuming equilibrium with the lattice, i.e. $T_I = T_L$ (lattice temperature). On the other hand neighbouring nuclear spins tend to restore the polarization $p_n(r_j,t)$ by cross-relaxation, which process is called spin diffusion. The corresponding relaxation term can be written as

$$\frac{\partial p_n(\vec{r}_j,t)}{\partial t} = \vec{\nabla}\cdot\{D\vec{\nabla}p_n(\vec{r}_j,t)\} \tag{3.2}$$

The right hand side represents the diffusion term, in which D is the diffusion coefficient. As a result the total rate equation for the nuclear polarization of a spin at $\vec{r}_j$ at time t becomes

$$\frac{\partial p_n(\vec{r}_j,t)}{\partial t} = \vec{\nabla}\cdot\{D\vec{\nabla}p_n(\vec{r}_j,t)\} + Cr_j^{-6}\{p_{no} - p_n(\vec{r}_j,t)\} \tag{3.3}$$

Various solutions of this equation have been derived [25-28]. The obtained results strongly depend on the assumptions regarding the nuclear-spin diffusion coefficient D [29]. In the following we shall discuss in particular the supposition that spin diffusion in the immediate vicinity of the paramagnetic ion is blocked by the quasi-static field of the ion.

Let d denote that distance from the origin, where the time averaged field of the impurity spin introduces differences among Zeeman energy level splittings of adjacent nuclei, that exceed the NMR line-width. Now it is usually assumed that at a distance from the origin $r < d$ (diffusion barrier) spin diffusion vanishes ($D \simeq 0$), since the requirement of conservation of Zeeman energy in the cross-relaxation process can no longer be met for $r < d$.

However, against this assumption serious objections can be made.

Grant [30] has shown that cross-relaxation processes are still possible under circumstances, which are rather remote from the situation, where the differences in nuclear Zeeman splittings are smaller than the linewidth. Horvitz [31] has argued on basis of calculations e.g. for CaF_2 with Ce^{3+} paramagnetic impurities, that spin-diffusion coefficients for F nuclei can even be larger within the diffusion barrier than outside. The fluctuating field of the impurity spin has Fourier components at the frequency needed to induce mutual spin flips of adjacent nuclear spins, see appendix B. Further, the contribution of an electronic spin having anisotropic g value to the nuclear Zeeman splitting strongly depends on the position of the nuclei with respect to the paramagnetic ion and the magnetic field direction. The angular dependence of this contribution to the nuclear Zeeman splitting, which is different from that of C in eq. (3.3), is another complicating factor. Measurements e.g. in Yb:YES by King et al.[32] clearly demonstrate the presence of spin diffusion up to those protons which are nearest to the Yb ion. This proves the $D = 0$ assumption for $r < d$ to be incorrect. Our experiments lead to the same conclusion.

Bearing the above arguments in mind, we have to solve eq. (3.3) permitting $D \neq 0$ for $r < d$. In tackling this problem, we shall follow McColl [29], who considered especially the proton relaxation rate in Yb:YES. He started from the reasonable approximation that the protons are uniformly distributed in space, so that $p_n(\vec{r}_j,t) \rightarrow p_n(r,t)$. Let further the crystal be divided into spheres of influence. Each sphere contains one Yb spin at its centre and has a radius R such that the volume of the sphere, $4\pi R^3/3$, equals the crystal volume divided by the number of electronic spins in the crystal. Following a scheme of Khutsishvili [28] McColl has solved eq. (3.3) analytically, which involves complicated combinations of Bessel-functions. If a reasonable value for D is adopted for $r > d$, and a much smaller but finite value for $r < d$ (1% of D for $r > d$) the following result is obtained

$$T_{1n}^{-1} = C/(r_1 R)^3 \qquad (3.4)$$

The radius r_1 designates the distance from the paramagnetic ion to the nearest neighbouring proton (see fig. 3 and fig. 4).

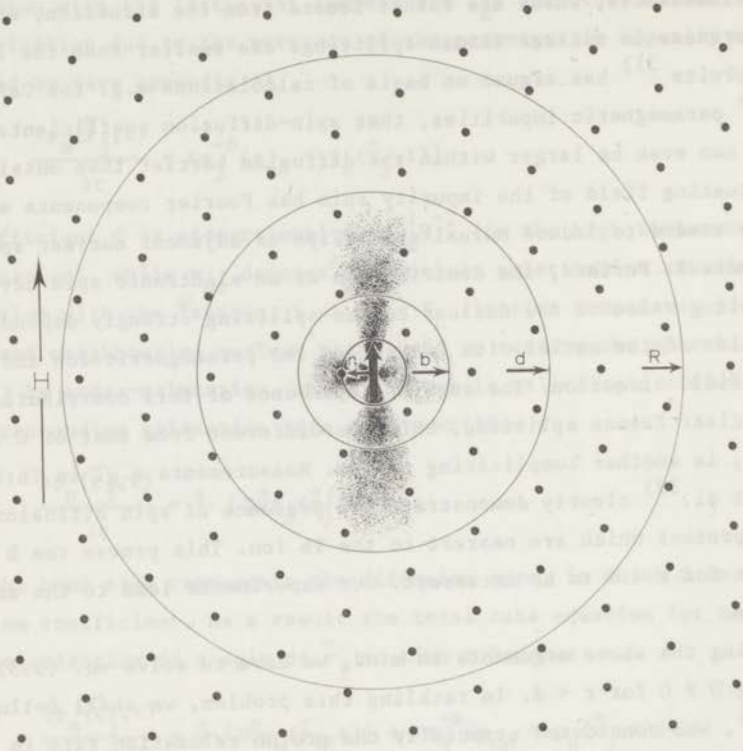

Fig. 3. Cross-section of "sphere of influence" for proton spins surrounding an electronic (impurity) spin S. The minimum distance between proton and impurity ion is denoted by r_1. d designates the diffusion barrier, which normally is taken according to the maximum distance from the origin, at which the quasi-static field of the impurity spin appreciably affects the nuclear energy splitting (see text). The dipolar field pattern of the S spin is shadowed in the figure. The radius b is defined by the relation $b = 0.68(C/D)^{\frac{1}{4}}$. Under the simplifying assumption that d does not play a role in determining the value of D, inside the shell $r_1 \leq r < b$ proton spins relax directly via the impurity spin, while for $r > b$ spin diffusion dominates. The outer radius R equals $R = (3N_e/4\pi)^{-1/3}$, where N_e represents the number of electronic spins per cm^3. In this picture an isotropic electron-spin g tensor is assumed.

It may be noted that for simplicity the positions of only part of the protons in a lattice plane are indicated (i.e. only translation symmetry operators were utilized to generate the proton lattice). Furthermore, the impurity spin position and the field direction do not necessarily coincide with such a plane of drawing.

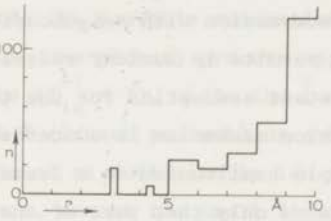

Fig. 4. Radial distribution of protons in the ethyl sulfate crystal. The proton distribution, as calculated in YbES, is illustrated as a function of the distance r from the rare-earth site. n denotes the number of protons per unit distance of 1 Å. The interval 3.0 - 5.0 Å has been subdivided in steps of 0.25 Å in order to draw attention to the proton cluster in the interval $3.0 \leq r \leq 3.2$ Å.

The same result can be derived in a simple way [12,33] without analytical solution of eq. (3.3). In this method also spheres of influence (fig. 3) are used, see also appendix D. In addition to the forementioned spheres with radius R further spheres are introduced having radius $b = 0.68(C/D)^{\frac{1}{4}}$, within which protons relax faster by direct relaxation than by spin diffusion (neglecting static dipolar fields). For protons inside the shell $b < r < R$ the opposite is true. For low Yb concentrations one has $b \ll R$, so the protons in the shell $b < r < R$ are in the vast majority. Consequently, rapid spin diffusion gives a common polarization and an average relaxation rate

$$T_{1n}^{-1} = C/(bR)^3 \qquad (3.5)$$

If $d > b$, and $D = 0$ for $r < d$, the diffusion barrier d must be substituted for b in eq. (3.5). However, assuming not too slow a spin diffusion

inside d and $b \leq r_1$, the final result is identical to eq. (3.4).

3.2.3. *Dipolar relaxation and the spin temperature concept.* In the Bloembergen-relaxation process nuclear relaxation is caused by changes of the z component of the electronic-spin angular momentum due to interaction with the lattice (see appendix A). However, the z component can also be changed by dipolar interaction with neighbouring ions (see appendix C). This process also results in nuclear relaxation, called dipolar relaxation. One important assumption for the theoretical foundation of the dipolar relaxation mechanism is concerned with the subdivision of the electronic-spin hamiltonian in a Zeeman term (H_Z) and a dipolar term (H_D). H_D contains only that part of the dipolar interaction, which commutes with H_Z, see e.g. Goldman [33] or Khutsishvili [34,35]. To each of the two systems a distinct temperature, T_Z resp. T_D, may be assigned. Phillipot [36] has formally shown that the concept of a dipolar system possessing its proper temperature can be justified when the electron-spin polarization is appreciably smaller than unity. As already mentioned in section 2.1, for a spin $\frac{1}{2}$ system a Zeeman temperature can always be defined according to the Boltzmann distribution. The influence of the non-commuting part of the dipolar interaction can be neglected when the energy splitting caused by H_Z strongly exceeds the energy spread, associated with H_D. The electron spin-spin interaction system, corresponding to the dipolar hamiltonian H_D is often called the dipole-dipole reservoir, abbreviated as DDR. It may be recalled that in Bloembergen relaxation the lattice (or more precisely, the resonant phonons, see section 3.2.4) and the electronic Zeeman system are assumed to be already in equilibrium, before energy exchange with the nuclear Zeeman subsystem is becoming effective. However, regarding the dipolar relaxation at sufficiently large impurity concentration, it can be shown that the nuclear spins are tightly bound to the dipolar system and relax jointly to the phonon system. For relatively large ($c \simeq 1\%$) impurity concentrations, dipolar relaxation is the most important. Conversely, for small impurity concentrations, the heat capacity of the DDR may be negligible and then Bloembergen relaxation dominates in the nuclear relaxation.

We like to remark that in the study of nuclear spin-lattice relaxation processes the availability of quite low temperatures is very useful, as may be inferred from the following two arguments.

a). Because both in Bloembergen and dipolar relaxation the nuclear spin-lattice relaxation rate is proportional to the electron spin-lattice relaxation rate, knowledge of T_{1e} is indispensable for the interpretation of T_{1n} data. As regards the possible relaxation processes for the electron spins, the direct (one-phonon) process appears to have the weakest temperature dependence ($T_{1e}^{-1} \propto T$), while the two-phonon processes are either exponential in T (Orbach process) or exhibit a T^7 or T^9 behaviour (Raman relaxation). Hence at sufficiently low temperatures, and, in view of the field dependence, at not too small fields, T_{1e} is entirely determined by the direct process. In our low temperature equipment we are able to choose the temperature region in which indeed the direct process governs T_{1e}, and hence T_{1n} (see chapter 2 and 3).

b). A decrease of temperature appreciably below 1 K provides the opportunity to disentangle the various nuclear spin-lattice relaxation processes, as may be illustrated by an example, borrowing from our results, discussed in chapter 2. Consider an Yb:YES single crystal having an Yb concentration of about 1% at a temperature of 1 K, and let it be placed in a magnetic field such that the electron-spin polarization $p_e \approx 0.2$. Then the nuclear relaxation appears to be determined by relaxation via the DDR of the electronic spins. On the other hand, decreasing the lattice temperature to 0.1 K, enhances the electron-spin polarization to about 0.9. At these high p_e values Bloembergen relaxation becomes the most important relaxation mechanism (see chapter 2), as is also actually observed.

3.2.4. *Phonon bottleneck in nuclear relaxation.* Buishvili et al.[37] have in a recent publication discussed the effects of resonant phonon heating in nuclear spin-lattice relaxation, both for Bloembergen and dipolar relaxation. In the case of Bloembergen relaxation they show that the phonon bottleneck factor in nuclear relaxation, B_n, can be defined as

$$B_n = (C_I/C_R)(T_{PB}/T_{IL}) \qquad (3.6)$$

In eq. (3.6) C_I and C_R are resp. the heat capacities of the nuclear Zeeman system and of the resonant phonons, while T_{PB} and T_{IL} denote the phonon-bath and nuclear spin-phonon relaxation time resp.. As can intuitively be predicted, no bottleneck in nuclear relaxation is present if $B_n << 1$, whereas for $B_n >> 1$ a severe bottleneck exists. In the latter situation the nuclear relaxation time is given by $T_{1n} = T_{PB}C_R^{-1}(C_R + C_S)$ where C_S equals the electronic Zeeman heat capacity. In the same way [38] the bottleneck factor in the electron spin-lattice relaxation is defined as

$$B_e = (C_S/C_R)(T_{PB}/T_{SL}) \tag{3.7}$$

in which T_{SL} denotes the electron spin-phonon relaxation time. A combination of the two equations (3.6 and 3.7) leads to the following relation between B_n and B_e:

$$B_n = (C_I/C_S)(T_{SL}/T_{IL})B_e \tag{3.8}$$

Normally, $C_I \leq C_S$, while $T_{SL} << T_{IL}$. Thus a bottleneck in the electron spin-lattice relaxation does not imply that bottleneck effects would also occur in the nuclear relaxation.

When nuclear relaxation proceeds via the dipole-dipole reservoir of the electronic spins, Buishvili et al. show that the bottleneck factor can be expressed by

$$B_n = 2(C_D/C_S)B_e \tag{3.9}$$

where C_D represents the heat capacity of the DDR. Because usually $C_D << C_S$, B_n will be smaller than unity even if $B_e > 1$.

From eq. (3.8) and eq. (3.9) it may be concluded that in general phonon bottleneck effects in nuclear relaxation can only occur in the presence of a very severe bottleneck in the electron spin-lattice relaxation. In our relaxation experiments we estimate bottleneck effects in T_{1n} to be negligible.

References.

1) Pauli, W., Z. Phys. 20 (1924) 371.
2) Proceedings of the second international conference on polarized targets, ed. Shapiro, G., Berkeley, California, 1971.
3) Gorter, C.J., Phys. Z. 35 (1934) 923.
4) Kurti, N. and Simon, F.E., Proc. Roy. Soc. A 149 (1935) 152.
5) Chapellier, M., Goldman, M., Hoang Chau, V. and Abragam, A., CR Acad. Sci. 268 B (1969) 1530.
6) Lagendijk, E., Blöte, H.W.J. and Huiskamp, W.J., Physica 61 (1972) 220.
7) Daniels, J.M., Oriented Nuclei (Academic Press, New York and London, 1965).
8) Schmugge, T.J. and Jeffries, C.D., Phys. Rev. 138 A (1965) 1785.
9) Borghini, M. and Scheffler, K., Nucl. Instr. Meth. 95 (1971) 93.
10) Odehnal, M. and Bouffard, V., Journal de Phys. 32 (1971) 699.
11) Mango, S., Runolfsson, O. and Borghini, M., Nucl. Instr. Meth. 72 (1969) 45.
12) Langley, K.H. and Jeffries, C.D., Phys. Rev. 152 (1966) 358.
13) McColl, J.R. and Jeffries, C.D., Phys. Rev. B 1 (1970) 2917.
14) Potter, W.H. and Stapleton, H.J., Phys. Rev. B 5 (1972) 1729.
15) Abragam, A., Cryogenics 3 (1963) 42.
16) Jeffries, C.D., Cryogenics 3 (1963) 41.
17) Manenkov, A.A. and Orbach, R., Spin Lattice Relaxation in Ionic Solids (Harper and Row, New York, Evanston and London, 1966).
18) Verstelle, J.C. and Curtis, D.A., Handbuch der Physik Bd 18/1 (1968) 1.
19) Cianchi, L. and Mancini, M., Rev. Nuovo Cimento 2 (1972) 25.
20) Huang, C.Y. and Mostrom, M.A., Phys. Lett. 36 A (1971) 46.
21) Cooke, A.H., Finn, C.B.P., Mangum, B.W. and Orbach, R.L., J. Phys. Soc. Japan 17 suppl. B 1 (1962) 462.
22) Waller, I., Z. Phys. 79 (1932) 370.
23) Al'tshuler, S.A., Izv. Akad. Nauk SSSR 20 (1956) 1207.
24) Bloembergen, N., Physica 15 (1949) 386 (Comm. Kamerlingh Onnes Lab., Leiden, No. 277a).

25) deGennes, P.G., J. Phys. Chem. Solids 3 (1958) 345.

26) Blumberg, W.E., Phys. Rev. 119 (1960) 79.

27) Rorschach, J.R., Physica 30 (1964) 38.

28) Khutsishvili, G.R., Zh. Eksp. Teor. Fiz. 42 (1962) 1311
Sov. Phys. JETP 15 (1962) 909.

29) McColl, J.R., Thesis, University of California at Berkeley, 1967 (unpublished).

30) Grant, W.J.C., Phys. Rev. 134 A (1964) 1554, 1565, 1575;
Phys. Rev. 135 A (1964) 1265.

31) Horvitz, E.P., Phys. Rev. B 3 (1971) 2868.

32) King, A.R., Wolfe, J.P. and Ballard, R.L., Phys. Rev. Lett. 28 (1972) 1099.

33) Goldman, M., Spin Temperature and Nuclear Magnetic Resonance in Solids (Clarendon Press, Oxford, 1970).

34) Khutsishvili, G.R., Uspekhi Fiz. Nauk. 96 (1968) 441.
Sov. Phys. Uspekhi 11 (1969) 802.

35) Khutsishvili, G.R., Progr. in Low Temp. Phys. 6 (1970), ed. C.J. Gorter (North-Holland Publ. Co., Amsterdam).

36) Phillipot, J., Phys. Rev. 133 A (1964) 471.

37) Buishvili, L.L., Giorgadze, N.P. and Khutsishvili, G.R., Zh. Eksp. Teor. Fiz. 60 (1971) 1433.
Sov. Phys. JETP 33 (1971) 776.

38) Scott, P.L. and Jeffries, C.D., Phys. Rev. 127 (1962) 32.

CHAPTER 2

PROTON POLARIZATION AND RELAXATION IN YTTRIUM ETHYL SULFATE DOPED WITH Yb AND Dy IONS

Synopsis

The method of proton polarization by means of rotational cooling is employed in crystals of $Y(C_2H_5SO_4)_3 \cdot 9H_2O$ doped with Yb^{3+} and Dy^{3+} ions. The decay of the proton polarization is observed as a function of magnetic field H (1 kOe $\leq$ H $\leq$ 10 kOe), temperature T (0.05 K $\leq$ T $\leq$ 1 K) and concentration of the rare-earth ions c (0.07% $\leq$ c $\leq$ 3%). For an explanation of the results on proton spin-lattice relaxation times the inclusion of the dipole-dipole reservoir (D.D.R.) of the paramagnetic ions is required. The influence of the concentration of the Yb or Dy ions on the maximum obtainable proton polarization is discussed. The electron spin-lattice relaxation appears to be mainly determined by the direct process.

1. Introduction. Because of the difference by three orders of magnitude in their gyromagnetic ratios, it is much easier to polarize electron spins than nuclear spins and methods have been sought to transfer spin polarization from electrons to nuclei. For instance, Lubbers and Huiskamp [1] have reported 97% polarization of radioactive ^{54}Mn nuclei in a crystal of lanthanum magnesium nitrate (LMN) doped with 0.1% Ce. They obtained cross-relaxation between the polarized Ce spins and the ^{54}Mn nuclear spins through rotation of a magnetic field with respect to the principle axes of the very anisotropic Ce g tensor. As a result the Ce electronic Zeeman splitting was reduced by a factor 50 in such a way as to match the large hyperfine splittings of ^{54}Mn which causes thermal mixing. An analogous method proposed by Abragam [3] and by Jeffries [2] and sometimes called the nuclear spin refrigerator method [4,5], utilizes the even more extreme anisotropy of e.g. Yb^{3+} ions in yttrium ethyl sulfate. By rotation of a magnetic field the electronic Zeeman splittings

could be reduced so much as to equalize the nuclear Zeeman splittings in an external field, hence eliminating the requirement of a large hyperfine field. The polarization method of rotational cooling is experimentally simple, hence relatively inexpensive and an appreciable degree of proton polarization can be obtained. We have extended the experiments of Langley and Jeffries [4] and McColl and Jeffries [5] to lower temperatures and other concentrations of the paramagnetic ions, while also the paramagnetic ions and host crystals are varied.

In this chapter the results of our experiments in yttrium ethyl sulfate, doped with Yb^{3+} and Dy^{3+} ions (hereafter abbreviated as Yb:YES and Dy:YES) are presented and discussed. Special attention is given to the various relaxation mechanisms, acting on the proton spins in the investigated crystals. An explanation of the cooling method is presented in section 2. In section 3 the experimental arrangement is described. Section 4 summarizes the theory of the relaxation phenomena for electron spins in YES and section 5 that for proton spins. The results on relaxation experiments are presented and discussed in sections 6 and 7, while the influence of the concentration of the electron spins on the degree of proton polarization which can be obtained, is the subject of section 8.

2. Nuclear polarization by rotational cooling. Let us consider YES, doped with Dy^{3+} ions. The point symmetry of the Y sites in the YES crystals is C_{3h} [7,8]. At temperatures of liquid helium only the lowest Kramers doublet is populated. The magnetic behaviour of the Dy^{3+} ions can then be described with an effective spin $S = \frac{1}{2}$, associated with a very anisotropic g value. From susceptibility measurements in concentrated DyES crystals one derives [9,10] $g_{\parallel} = 10.8$ and $g_{\perp} \simeq 0$, while EPR in dilute samples [12] gives $g_{\parallel} = 10.94$ and $g_{\perp} \leq 0.05$, in which $g_{\parallel}$ refers to the direction of the hexagonal crystal c axis and $g_{\perp}$ to the plane perpendicular to this symmetry axis. Furthermore, the observed electron-spin-lattice relaxation rate (T_{1e}^{-1}) in concentrated DyES crystals can be fitted by the relation [11,14].

$$T_{1e}^{-1} = AH^4T \sin^2\theta\cos^2\theta. \qquad (2.1)$$

This result is also theoretically predicted (in the high-temperature approximation) in case the relaxation is governed by the direct process [13] between the two Zeeman energy levels originating from a Kramers doublet. H denotes the magnetic field strength, T the temperature and θ the angle between the magnetic-field direction and the $g_{//}$ axis. A is a constant as far as variations of H and T are concerned.

The proton polarization method is based on the establishment of thermal equilibrium between a system of polarized electron spins, S, and nuclear spins, I. This occurs after adiabatic demagnetization of the S spins by rotating the magnetic field from a direction of high g value to that of minimum g. Let us assume that the nuclear spins, I, the electron spins, S, and the lattice, L, can be treated as thermodynamically separated systems, each having its own temperature T_I, T_S and T_L, respectively (at later stages in the discussion a further distinction will be made between Zeeman and dipolar temperatures). Lattice vibrations couple S and L (eq. (2.1)), schematically indicated by switch b in fig.1. The direct exchange of polarization by energy-conserving flip-flop processes, called cross-relaxation [15,16] is represented in switch a. For simplicity the nuclear spin-lattice relaxation is neglected: T_{1n} (the nuclear spin-lattice relaxation time) >> T_{1e}.

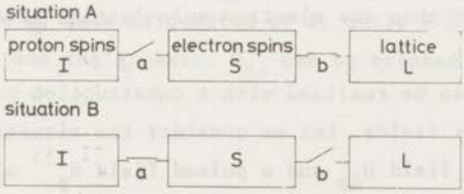

Fig. 1. When the magnetic field H makes an angle $\theta = 45^{\circ}$ with the $g_{//}$ axis (situation A), the equilibrium between electron spins (S) and lattice (L) is established relatively quickly. Hence switch b may be considered to be closed. The proton spins (I) are then nearly isolated: switch a is open. When $\theta \simeq 90^{\circ}$ cross-relaxation equalizes the temperatures of the S and I spin systems but the contact with the lattice is now relatively poor.

When the magnetic field makes an angle $\theta = 45^{\circ}$ with the $g_{//}$ axis, T_{1e} has a minimum, see eq. (2.1). The equilibrium between S and L is established relatively quickly, hence switch b may be considered to be closed as indicated in situation A in fig. 1. The electron-spin polarization p_e becomes

$$p_e = \tanh \frac{g_{eff}\mu_B H}{2kT_L} \approx \tanh \frac{g_{//}\mu_B H\cos\theta}{2kT_L} ,$$

in which

$$g_{eff} = (g_{//}^2\cos^2\theta + g_{\perp}^2\sin^2\theta)^{\frac{1}{2}}, \qquad (2.3)$$

and μ_B is the Bohr magneton. For example, when $H = 2.3$ kOe, $T_L = 0.3$ K and $\theta = 45^{\circ}$, eq. (2.1) gives $T_{1e} \approx 0.6$s and eq. (2.2) predicts $p_e \approx 0.96$. Because of the large difference (factor ≈ 770) of the nuclear and electron-spin Zeeman splittings cross-relaxation does not occur (switch a open).

By rotating the field adiabatically in the Ehrenfest sense [17] from $\theta = 45^{\circ}$ to the $g_{\perp}$ direction ($\theta = 90^{\circ}$), the electron-spin Zeeman splittings can be made equal to the nuclear Zeeman splittings. Under such conditions cross-relaxation equalizes the temperatures in both systems in a time much shorter than the electron spin-lattice relaxation time: situation B in fig. 1.

The same cycle can be realized with a construction comprising two mutually perpendicular fields. Let us consider the situation of a horizontal direct-current field H_{dc} and a pulsed field H_p [5] along the vertical (z) direction (fig. 2). In this situation θ (now defined as the angle between $\vec{H}_{dc}$ and the $g_{//}$ axis) is chosen to be 90°, as will be explained later. The Zeeman splitting of the paramagnetic ions is practically zero, when $H_p = 0$. With H_p directed along the z axis T_{1e}^{-1} becomes in the high-temperature approximation

$$T_{1e}^{-1} = AH_p^2H_{dc}^2T\cos^2\delta, \qquad (2.4)$$

in which δ is defined as the angle between $\vec{H}_p$ and the $g_{//}$ axis. Further,

$$p_e = \tanh(g_{\parallel} \mu_B H_p \cos\delta / 2kT). \qquad (2.5)$$

The case of large H_p (e.g. $H_p \approx H_{dc}$) corresponds to the first scheme A in fig. 1. When $H_p = 0$, the situation corresponds to the second diagram B. In principle the proton-spin polarization can be made equal to that of the electron spins by repeating the above process. McColl and Jeffries [2,5], hereafter referred to as MCJ, mentioned that 35% proton polarization was achieved in their experiment on Yb:YES.

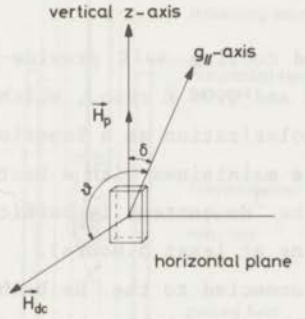

Fig. 2. Orientation of the rectangularly shaped ethyl sulfate crystal with respect to the static field $\vec{H}_{dc}$ and the pulsed field $\vec{H}_p$. The angle between $\vec{H}_p$ and the $g_{\parallel}$ axis is denoted by δ, while θ is defined as the angle between $\vec{H}_{dc}$ and the $g_{\parallel}$ axis. $\vec{H}_{dc}$ can be rotated in the horizontal plane.

3. Experimental arrangement. 3.1. *Low-temperature aspects*. The cryogenic part of the experimental equipment has been described elsewhere [19]. The cryostat consists of glass dewars for liquid nitrogen and liquid helium, surrounding a vacuum space of which the lower part is glass walled. An r.f. coil was wound on a teflon former which can be attached to the glass tube via a press fit (fig. 3). The temperature of the ^{4}He bath can be reduced to about 1 K. With a ^{3}He bath inside the vacuum space temperatures down to 0.28 K can be realized by pumping with an Edwards EM 2 diffusion pump, combined with a Balzer Duo 1

rotary pump. Lower temperatures are reached by adiabatic demagnetization of an iron ammonium alum cooling salt [18], placed inside a superconducting coil ($T_{min} \approx 0.05$ K). This salt is obtained by melting powdered $FeNH_4(SO_4)_2 \cdot 12H_2O$ around a bundle of about 1000 insulated copper wires of 0.07 mm diameter. The superconducting magnet is a coil on a stainless-steel coil form (inner diameter 4 cm, outer diameter 5.7 cm), which is fixed with two clamps onto the brass upper part of the vacuum space. The coil consists of 20 layers of 271 turns NbZr wire (supercon, 0.01 inch diameter, copper plated and insulated). The coil form and each layer are mutually isolated with mylar, to prevent a short-circuit within the coil.

^{4}He bath, ^{3}He bath and cooling salt provide three heat sinks at temperatures of 1 K, 0.4 K and 0.04 K resp., which facilitates a study of the obtainable proton polarization as a function of temperature. A temperature of 0.4 K can be maintained with a heat input in the ^{3}He bath of about 250 erg/s (the ^{3}He content is sufficient to withstand an input of 10^3 erg/s during at least 5 hours).

The cooling salt is connected to the ^{3}He bath by a gas switch [19], the operation of which is based on the heat conductivity of ^{4}He gas. In practice the switch consists of two concentric 12 cm long and 0.04 cm thick epibond cylinders. On the ^{3}He side the outer cylinder is over about 4 cm covered with copper foil, which is thermally connected with the ^{3}He bath. With the aid of Apiezon-N grease the alum cooling pill is stuck in the inner epibond cylinder. The gas space between the two cylinders is filled with 0.1 atm. ^{4}He gas at room temperature. After adiabatic demagnetization of the cooling salt at sufficiently low ^{3}He temperature, the vapour pressure in the gas space becomes so low, that the heat transport between cooling salt and ^{3}He bath becomes negligible. When the temperature of the alum salt becomes higher than $T \approx 0.35$ K the heat conduction through the ^{4}He gas increases very rapidly. The ratio between the heat conduction coefficients at 0.45 K and 0.35 K is about one thousand, as measured by Haasbroek [19].

Each crystal sample, weighing on the average about 0.4 g was mounted between the copper wires leading to the cooling salt. Apiezon-N grease was utilized in order to improve the thermal contact with the

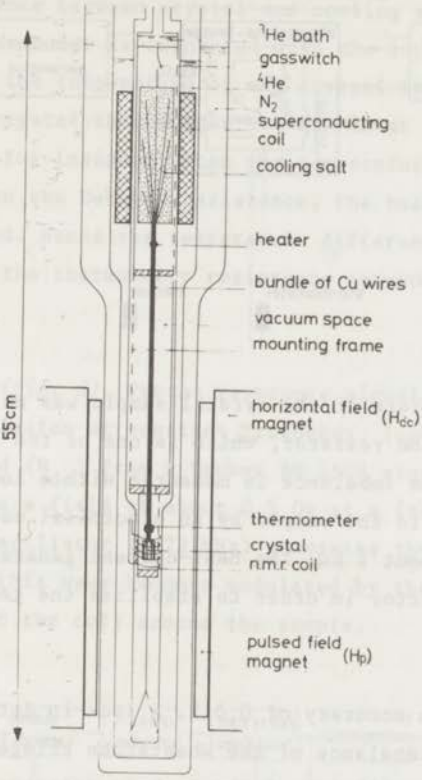

Fig. 3. ^{4}He bath, ^{3}He bath and iron ammonium alum cooling salt provide three heat sinks at temperatures of 1 K, 0.4 K and 0.04 K respectively. ^{3}He bath and cooling salt are linked by a gas switch ("switch" temp. ≈ 0.4 K). The crystal sample is mounted between copper wires leading to the cooling salt in the center of a pulsed-field magnet. The pulsed-field solenoid is clamped between the poles of a direct-current field magnet.

copper bundle. The sample temperature was determined through a calibrated Speer carbon resistor [20], from which the insulating material had been removed. The thermometer was mounted near the sample crystal inside the copper bundle. This resistor is one of the components of a Wheatstone bridge as shown in fig. 4 and can be compensated by a five-decade

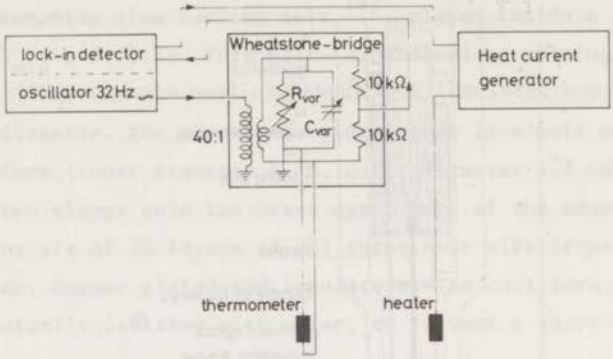

Fig. 4. The temperature of the cyrstal sample was measured with a calibrated Speer carbon resistor, which is one of the components of a Wheatstone bridge. The imbalance is measured with a lock-in detector. Heat can be supplied to the sample by an electrical current through a manganin heater of about 1 kΩ. The heat-current generator is connected with the lock-in detector in order to stabilize the temperature of the crystal sample.

Dekabox resistor with accuracy of 0.01%. A lock-in detection method is used to measure the imbalance of the Wheatstone bridge. The bridge is fed by the internal oscillator of the lock-in detector with a frequency of about 30 Hz and a typical output value of 10 mV, corresponding with about 0.25 mV over the circuit. The resistance R as a function of temperature can be rather well fitted by the semi-empirical relation [21]

$$R = R_o \exp(B/T^{\frac{1}{2}}), \qquad (3.1)$$

with the room-temperature value R_o = 220Ω and B = 1.31 $K^{\frac{1}{2}}$. At R = 70 kΩ (T ≈ 0.05 K) the difference between measured and calculated temperature is 4%.

Heat can be supplied to the crystal sample by an electrical current through a manganin wire of about 1 kΩ twisted around the copper bundle between the cooling salt and the sample. The temperature of the sample crystal could be arbitrarily varied between rather wide limits

by variations of the electrical-current heat supply, which created a temperature difference between crystal and cooling salt or ^{3}He bath. The heat-current generator is connected with the lock-in detector in order to stabilize the temperature of the crystal thermometer. When the resistance of the crystal thermometer becomes lower (the sample temperature may rise, for instance, when the temperature of the cooling salt increases) than the Dekabox resistance, the heat current is correspondingly lowered. Hence the temperature difference with the cooling salt decreases and the thermometer resistance returns to its initial value.

3.2. *NMR apparatus (fig. 5).* Proton resonance signals were obtained by magnetic-field modulation at constant frequency. Superposed on the direct-current field (H_{dc}) from a Bruker BE 25C8 electromagnet, modulation coils produce a field of about 0.5 Oe at a frequency of 30 Hz. A Marconi TF 2002 oscillator (0-72 MHz) generates the r.f. carrier wave. At resonance this wave becomes modulated by the effective change in self-induction of the coil around the sample.

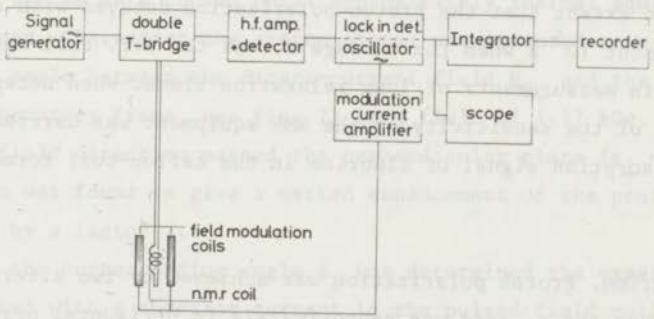

Fig. 5. Scheme of NMR apparatus. The derivative of the NMR absorption signal is obtained by field modulation in a bridge method. After integration the signal is written on a recorder.

The ratio between the modulation depth and the amplitude of the carrier wave is improved by a bridge, constructed after Grivet et al. [23], adjustable at four fixed frequencies (ν) namely 5, 10, 30 and 40 MHz.

The modulated wave from the bridge is applied to an r.f. amplifier and detector. The remaining low-frequency signal is thereafter phase-sensitively detected [22a]. The internal oscillator of this lock-in detector determines also the frequency of the current through the modulation coils. When the direct-current field is swept with constant speed through the resonance value, the output from the lock-in detector is integrated by an R-C network, connected to an operational amplifier. The integrated signal is written on a recorder, while the absorption area under each resonance curve can be easily obtained by a second integration. Short relaxation times were measured by recording the decay of the derivative signal directly at a constant value of H_{dc}. A comparison with the decay time of the twice integrated signals shows practically no difference between the two time constants.

In our type of experiment a very low r.f. voltage over the resonance coil is required. Therefore the bridge method is preferred to the use of marginal oscillator circuits. Relaxation times as long as 10^4 - 10^5 s were measured by observing the absorption signal intermittently during about two minutes with time intervals of 20 to 30 minutes. Continuous irradiation by the r.f. field was found to warm up the proton spin system to such an extent that the proton polarization decayed with a time constant of about 10^5 s when the voltage across the r.f. coil was the same as that in measurements of long relaxation times. When necessary, a calibration of the sensitivity of the NMR equipment was carried out, taking the absorption signal of fluorine in the teflon-coil former as a reference.

3.3. *Polarization.* Proton polarization was achieved by two alternative methods. a) When the $g_{//}$ axis was approximately in horizontal orientation ($\delta \approx 90^{\circ}$), polarization was obtained by rotation of the direct-current field H_{dc}, which may be compared to the method of Langley and Jeffries (LJ). b) When the angle between the $g_{//}$ axis and the vertical axis was less than about 40° the pulsed field was applied in addition to H_{dc}. The pulsed-field coil is a water-cooled solenoid (fig. 3).

A block diagram of the pulse producing circuit is given in fig. 6a. A triangular wave form from an external oscillator and a d.c.

voltage are supplied to the comparator. As a result the desired length of the pulse can now be varied within the vibration period, independently of the oscillator frequency. When the signal has passed a Schmitt trigger, the flanks of the output pulse signal are sufficiently steep to drive a power switch circuit. This circuit serves to switch the current in the pulsed coil, connected to a d.c. power supply of 220 V. The block pulse, driving the power switch, and the final field pattern, as derived from observations by means of a pick-up coil, are sketched in fig. 6b. The pulse duration time τ_1 varies between τ and $10^{-2}\tau$, while the period τ can be changed from 100 s to 1 ms.

The decay time of the field pulse τ_d is determined by the self-inductance of the coil, L = 6 mH. Since R $\approx$ 4Ω, the decay time τ_d is about 1.5 ms. The calibration of the pulsed-field coil gave a field-to-current ratio of 30 Oe/A. The maximum pulsed field used in the experiments was 1.8 kOe.

3.4. *Crystal orientation.* The orientation of the $g_{//}$ axis with respect to the laboratory frame was determined in the following way. After adiabatic demagnetization of the cooling salt the sample and its electron spin system were cooled until approximately thermal equilibrium was obtained. Thereafter the proton signal was measured as a function of ϕ (the angle between the direct-current field H_{dc} and the x axis of the laboratory frame, see fig. 7) in a field of 1.17 kOe. When the magnetic-field direction passed the perpendicular plane ($g_{\perp} = 0$) cross-relaxation was found to give a marked enhancement of the proton signal, typically by a factor 2.

Once the corresponding angle ϕ_1 was determined the experiment was repeated with a constant current in the pulsed field coil. Now cross-relaxation occurred at another angle ϕ_2, different from ϕ_1 by the amount $\Delta\phi$. At ϕ_2, the components of the direct-current field H_{dc} and of the "pulsed" field H_p along the $g_{//}$ axis cancel one another. The orientation of the $g_{//}$ axis with respect to the z axis can now be calculated from the ratio of H_{dc} and H_p, according to

$$\cot\delta = \frac{H_{dc}}{H_p} \sin\Delta\phi \ . \qquad (3.2)$$

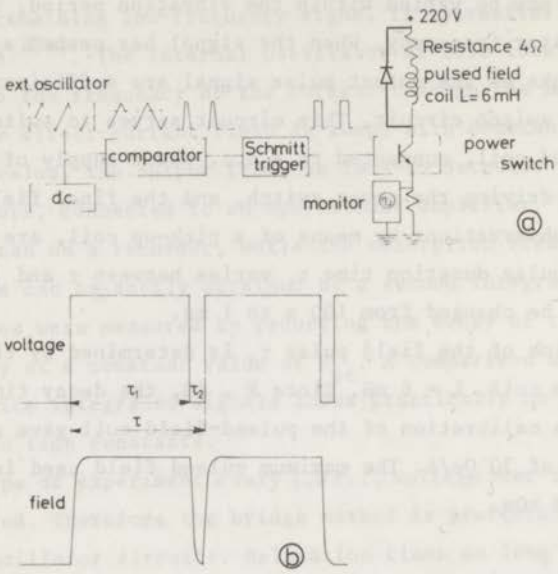

Fig. 6. Apparatus for generating the pulsed field, H_p. In the pulse-producing network a triangular wave of an external oscillator is adapted in such a way as to drive the final power switch with a minimum energy dissipation in the switch itself.

3.5. *The crystals*. Ethyl-sulfate crystals were grown by slowly evaporating an aqueous solution at a temperature of 15 °C. The crystals were prepared from the following oxides: Y_2O_3 with a purity degree of 99.9999%; Yb_2O_3, enriched to 95.8% ^{174}Yb; Dy_2O_3, enriched to 91.04% ^{162}Dy. The isotope concentrations in the crystals were determined by spectral analysis of the induced gamma-ray activity after thermal-neutron activation, using a Ge(Li) spectrometer†.

† We wish to thank Mrs. M.A. Otten-Scholten for preparing the crystals and Dr. E.R. Reddingius of the F.O.M. K IX group at the high-flux reactor of the R.C.N. Petten for the activation analysis.

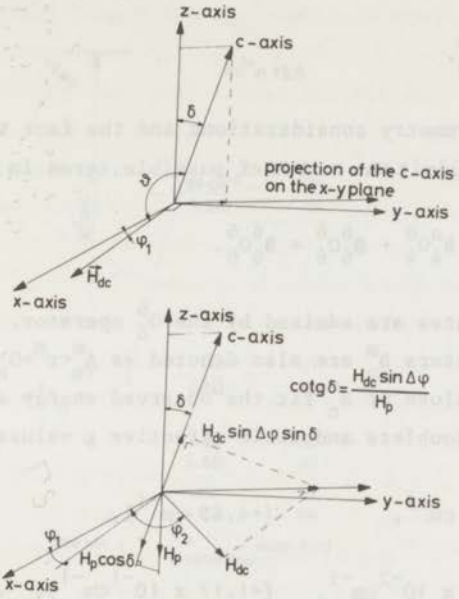

Fig. 7. Diagram showing the determination of the orientation angle, δ, from an auxiliary cross-relaxation experiment. The orientation of the $g_{//}$ axis can be calculated from the cross-relaxation angles ϕ_1 and ϕ_2, respectively, without and with a constant current through the pulsed-field coil.

4. Energy levels and electron spin-lattice relaxation times of Yb^{3+} and Dy^{3+} ions in YES. 4.1. *Yb^{3+}*. First we will pay attention to Yb^{3+} in YES. We refer to MCJ for a description of the crystallographic configuration in the unit cell. Their assumptions on the hydrogen positions are based on the work of Ketelaar [7] and of Fitzwater and Rundle [8], and lead to 12 nearest-neighbour protons for the Y site, at a distance of 3.04 Å, and 6 next nearest-neighbour protons at 3.20 Å.

The energy-level scheme as measured by Wheeler et al. [24] for the $^2F_{7/2}$ ground state of the Yb^{3+} ion in the Yb ethyl-sulfate crystal field, is given in fig. 8. The earlier derived result of LJ is placed within parentheses. The eigenstates of the crystal field can be

calculated from the hamiltonian [25]:

$$H = \sum_{m,n} B_n^m O_n^m. \tag{4.1}$$

Parity and crystal-symmetry considerations and the fact that we deal only with f-electrons limit the number of possible terms in eq. (4.1) to four:

$$H = B_2^0 O_2^0 + B_4^0 O_4^0 + B_6^6 O_6^6 + B_6^6 O_6^6. \tag{4.2}$$

The $|\pm\frac{7}{2}\rangle$ and $|\mp\frac{5}{2}\rangle$ states are admixed by the O_6^6 operator. In the literature [25] the parameters B_n^m are also denoted as $A_n^m\langle r^n\rangle\theta_n$.

The following values of B_n^m fit the observed energy separations between the Kramers doublets and their effective g values:

$$B_2^0 = +4.93\ \text{cm}^{-1}, \qquad (+4.45\ \text{cm}^{-1}),$$

$$B_4^0 = +9.99 \times 10^{-2}\text{cm}^{-1}, \qquad (+1.17 \times 10^{-1}\text{cm}^{-1}),$$

$$B_6^0 = -3.79 \times 10^{-3}\text{cm}^{-1}, \qquad (-4.29 \times 10^{-3}\text{cm}^{-1}),$$

$$B_6^6 = +7.00 \times 10^{-2}\text{cm}^{-1}, \qquad (+6.07 \times 10^{-2}\text{cm}^{-1}).$$

The values between parentheses are estimated values of LJ [4]. The operators O_n^m are tabulated e.g. by Hutchings [25].
With the above-mentioned B_n^m the g values of the lowest doublet become:

$$g_{\parallel} = 2\Lambda\langle a|J_z|a\rangle = 3.43$$

and

$$g_{\perp} = \Lambda\langle a|J_+ + J_-|b\rangle = 0.$$

Λ denotes the Landé factor. The experimental values for the Yb ethyl-sulfate crystals [27,28] are $g_{\parallel} = 3.40$ and $g_{\perp} < 0.05$. Orbach [13] and Scott and Jeffries [26] have shown how the paramagnetic electron spin-lattice relaxation rate T_{1e}^{-1} can be calculated from the B_n^m. One finally obtains the expression

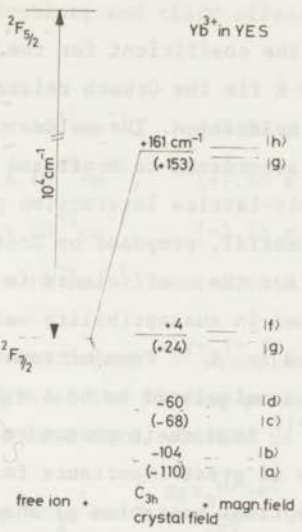

Fig. 8. Energy-level scheme of Yb^{3+} in YES. The $^2F_{7/2}$ ground state of the Yb^{3+} ion in YES, as measured by Wheeler, consists of four Kramers doublets:

$$|a\rangle = |-\tfrac{3}{2}\rangle \quad \text{and}$$

$$|b\rangle = |+\tfrac{3}{2}\rangle \quad ;$$

$$|c\rangle = +0.95|-\tfrac{5}{2}\rangle - 0.31|+\tfrac{7}{2}\rangle \quad \text{and}$$

$$|d\rangle = +0.95|+\tfrac{5}{2}\rangle - 0.31|-\tfrac{7}{2}\rangle \quad ;$$

$$|e\rangle = |-\tfrac{1}{2}\rangle \quad \text{and}$$

$$|f\rangle = |+\tfrac{1}{2}\rangle \quad ;$$

$$|g\rangle = +0.95|+\tfrac{7}{2}\rangle - 0.31|-\tfrac{5}{2}\rangle \quad \text{and}$$

$$|h\rangle = +0.95|-\tfrac{7}{2}\rangle - 0.31|+\tfrac{5}{2}\rangle .$$

The g values of the lowest doublet are $g_{/\!/} = 3.43$ and $g_{\perp} = 0$. The energy-level splitting assumed by LJ is placed within parentheses.

$$T_{1e}^{-1} = AH^5 \sin^2\theta\cos^3\theta\coth\frac{g_{\parallel}\mu_B H\cos\theta}{2kT} + B\, e^{-\Delta E/kT} + CT^9. \qquad (4.3)$$

$A = 1.4 \times 10^{-16}\,Oe^{-5}s^{-1}$ denotes the coefficient for the direct process, $B = 3.3 \times 10^{11}\,s^{-1}$ and $\Delta E/k = 60$ K fix the Orbach relaxation rate and $C = 1.7 \times 10^{-2}\,s^{-1}K^{-9}$ the Raman relaxation. The values of A, B and C in eq. (4.3) are derived by LJ in accordance to Scott and Jeffries and it is assumed that $g_{\perp} = 0$. The orbit-lattice interaction potential, used by Orbach, differs from the potential, proposed by Scott and Jeffries, which gives a different result for the coefficients in eq. (4.3). The parameters B and C, as determined in susceptibility measurements [27] are $B = 7 \times 10^{11}\,s^{-1}$ and $C = 1.6 \times 10^{-2}\,s^{-1}K^{-9}$. From microwave pulse-recovery experiments in 5% Yb:YES [6] A is calculated to be $A = 2.4 \times 10^{-17}\,Oe^{-5}\,s^{-1}$. LJ estimated $A = 3.2 \times 10^{-17}$ from their proton relaxation data.

The precise value of $g_{\perp}$ is of great importance for the operation of the spin refrigerator. For optimal operation $g_{\perp}$ should not exceed the proton g value, g_n, which is defined by $g_n = 2\mu_n/\mu_B$, in which μ_n is the magnetic moment of the proton. The admixing of the wave functions of the various Kramers doublets by the Zeeman interaction in the perpendicular direction can be calculated with perturbation theory. Only the third-order contribution is important, which results in a ground-doublet energy splitting proportional to H^3. In Yb:YES this energy splitting is estimated to be equal to $g_n\mu_B H$ if $H \simeq 30$ kOe. Since the magnetic fields in our experiments are considerably lower, this mechanism may be neglected. The distortion of the static crystal field, due to lattice defects etc. [29,30] may produce $g_{\perp}$ values of the same order of magnitude as g_n. MCJ estimated this contribution to $g_{\perp}$ by assuming that the observed linewidths in all the dilute rare-earth ethyl sulfates are due to random static strains. They define g_0^2 as the second moment of the lorentzian $g_{\perp}$ value distribution and find that $g_0 \simeq 0.003 \simeq g_n$ gives the best fit to the experimental data. Wolfe and Jeffries estimated $g_{\perp} \simeq 0.01$ from their resonance intensity [6].

4.2. *Dy^{3+}*. The energy-level scheme of Dy^{3+} in YES for the ionic ground multiplet $^6H_{15/2}$ with the wave functions according to Hill and Wheeler [31]

is given in fig. 9. The parameters B_n^m (eq. (4.1)) can, as in the Yb^{3+} case, be obtained from an optimal fitting to the energy separations between the Kramers doublets and their effective g values. Hill and Wheeler derived:

$$B_2^0 = -9.14 \times 10^{-1}\,cm^{-1}, \quad (-7.57 \times 10^{-1}\,cm^{-1}),$$
$$B_4^0 = +5.04 \times 10^{-3}\,cm^{-1}, \quad (+1.55 \times 10^{-3}\,cm^{-1}),$$
$$B_6^0 = -3.44 \times 10^{-5}\,cm^{-1}, \quad (-3.23 \times 10^{-5}\,cm^{-1}),$$
$$B_6^6 = +5.54 \times 10^{-4}\,cm^{-1}, \quad (+4.90 \times 10^{-4}\,cm^{-1}).$$

The results of Powell and Orbach [32] are placed in parentheses, in order to illustrate the margin of the fitting procedure. A relaxation formula for T_{1e}^{-1} can be written in a form, similar to eq. (4.3)

$$T_{1e}^{-1} = AH^5 \sin^2\theta\cos^3\theta \coth \frac{g_{\parallel}\mu_B H\cos\theta}{2kT} + B\, e^{-\Delta E/kT} + CT^9 \qquad (4.4)$$

Kump [14] has determined the coefficients A and B from experiments on the Faraday effect: $A = 1.38 \times 10^{-15} s^{-1} Oe^{-5}$ and $B = 0.64 \times 10^7 s^{-1}$. Cooke et al. [33] found from susceptibility measurements $B = 1.1 \times 10^7$ s^{-1} and $\Delta E/k = (23.6 \pm 2)$ K, which is in agreement with $\Delta E/k = 23$ K derived from an investigation of Gramberg [34] of the visible absorption spectrum. $C = 1.3 \times 10^{-5} s^{-1} K^{-9}$ is calculated by Orbach [13] from the crystal-field parameters of Powell and Orbach.

The g values are $g_{\parallel} = 10.9$ and $g_{\perp} \leq 0.05$, as determined by EPR in a sample of 0.5% Dy in YES [12]. Admixture of wave functions of higher states into the ground state by the Zeeman interaction causes an electronic Zeeman splitting along the $g_{\perp}$ direction, which on the basis of Gramberg's data [34] equals the proton Zeeman splitting at H = 3400 Oe. Dweck and Seidel [12] have observed an EPR spectrum of Dy^{3+} in YES which is not expected to occur when $g_{\perp} = 0$. As a possible explanation, they attribute the g-value distribution to the influence of lattice defects and estimated $g_{\perp} \leq 0.05$.

5. Proton spin-lattice relaxation. 5.1. *The electron-spin hamiltonian.* Proton spin-lattice relaxation processes can be illustrated with the model, represented in fig. 10. According to this model the electron spin system is described by the hamiltonian $H = H_Z + H_{D'} + H_{D''}$ in which H_Z is the Zeeman part of the total hamiltonian. $H_{D'}$ denotes that part of the total dipolar interaction (H_D), which commutes with H_Z, and $H_{D''}$ corresponds to the non-commuting part of H_D. The important assumption of the model is, that the electron spin system can be divided into two subsystems, each possessing its own temperature: a Zeeman system (H_Z) at a temperature T_S and a dipolar system ($H_{D'}$) having a temperature T_D. The justification for considering the "dipole-dipole reservoir (D.D.R.)" separately is given by Phillipot [35] in the high-temperature approximation (high-temp. appr.) and is also supported by various experiments [36,37,38]. The non-secular terms ($H_{D''}$) have the effect of mixing the Zeeman and secular spin-spin terms, so as to equalize their temperatures. For external field values several times the local field (i.e. $H_Z > H_D$) this mixing can be neglected [22b].

5.2. *Cross-relaxation.* Direct energy exchange between proton-spin system and electron-spin system through cross-relaxation is possible in the ethyl sulfates when H is directed perpendicular to the $g_{//}$ axis. In that situation, however, the separation of the electron spins in two subsystems is not valid since $H_Z < H_D$. A further discussion is given in section 7.

5.3. *Bloembergen relaxation.* We shall now derive an equation, which gives the magnitude of the nuclear spin-lattice relaxation in accordance with the mechanism, proposed by Bloembergen [39]. He considers magnetically dilute systems in which nuclear spins relax to the lattice via paramagnetic impurities. This relaxation is caused by the modulation of the magnetic-dipole interaction by the electron spin-lattice relaxation. The relaxation mechanism extends to distant protons by intermediary of nuclear-spin diffusion, caused by nuclear magnetic-dipole interaction.

Let us consider the consequences of the Bloembergen relaxation

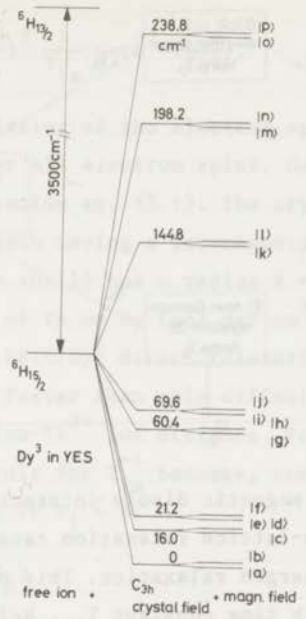

Fig. 9. Energy-level scheme of Dy^{3+} in YES. The wave functions of the 8 Kramers doublets of the $^6H_{15/2}$ ground state of the Dy^{3+} ion in YES are, according to Hill and Wheeler:

$$|a\rangle = \mp 0.05\left|\pm\tfrac{15}{2}\right\rangle \pm 0.28\left|\pm\tfrac{3}{2}\right\rangle \mp 0.96\left|\mp\tfrac{9}{2}\right\rangle;$$
$$|b\rangle$$

$$|c\rangle = \pm 0.51\left|\pm\tfrac{5}{2}\right\rangle \mp 0.86\left|\mp\tfrac{7}{2}\right\rangle;$$
$$|d\rangle$$

$$|e\rangle = \mp 0.08\left|\pm\tfrac{13}{2}\right\rangle \pm 0.2\left|\pm\tfrac{1}{2}\right\rangle \mp 0.98\left|\mp\tfrac{11}{2}\right\rangle;$$
$$|f\rangle$$

$$|g\rangle = 0.99\left|\mp\tfrac{15}{2}\right\rangle - 0.06\left|\mp\tfrac{3}{2}\right\rangle - 0.07\left|\pm\tfrac{9}{2}\right\rangle;$$
$$|h\rangle$$

$$|i\rangle = 0.99\left|\mp\tfrac{13}{2}\right\rangle - 0.13\left|\mp\tfrac{1}{2}\right\rangle - 0.11\left|\pm\tfrac{9}{2}\right\rangle;$$
$$|j\rangle$$

$$|k\rangle = \pm 0.86\left|\mp\tfrac{5}{2}\right\rangle \pm 0.51\left|\pm\tfrac{7}{2}\right\rangle;$$
$$|l\rangle$$

$$|m\rangle = -0.08\left|\mp\tfrac{15}{2}\right\rangle - 0.96\left|\mp\tfrac{3}{2}\right\rangle - 0.27\left|\pm\tfrac{9}{2}\right\rangle;$$
$$|n\rangle$$

$$|o\rangle = 0.14\left|\mp\tfrac{13}{2}\right\rangle + 0.97\left|\mp\tfrac{1}{2}\right\rangle + 0.18\left|\pm\tfrac{11}{2}\right\rangle.$$
$$|p\rangle$$

The g values of the lowest doublet are $g_{/\!/} = 10.8$ and $g_{\perp} = 0$.

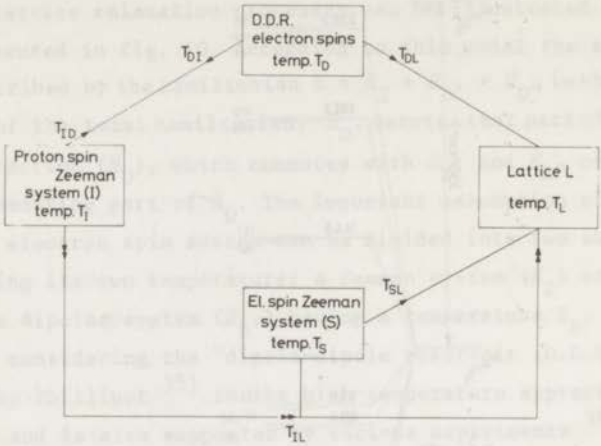

Fig. 10. Modulation of the magnetic dipole interaction between S and I spins by the electron-spin-lattice relaxation causes nuclear relaxation, which is called Bloembergen relaxation. This process is indicated by the double-arrow path with time constant T_{IL}. Relaxation via the D.D.R. of the electron spins is an alternative nuclear-relaxation possibility, which is dominating at high electron-spin concentrations.

(Bl. relax.) on the proton polarization. This may be discussed on the basis of the following equation for the polarization of a proton at $\vec{r}_j$ at the time t.

$$\frac{\partial p_n(\vec{r}_j,t)}{\partial t} = \vec{\nabla}\{D\vec{\nabla}p_n(\vec{r}_j,t)\} + \sum_i \frac{C}{|\vec{r}_j - \vec{r}_i|^6}\{p_{n0} - p_n(\vec{r}_j,t)\}. \qquad (5.1)$$

$p_n(\vec{r}_j,t)$ is an ensemble average (e.g. a large number of identical crystals) of the proton-spin polarization. D is a diffusion coefficient, p_{n0} is the thermal-equilibrium polarization of the proton spin. Only the I_+S_z and I_-S_z operators of the dipolar interaction between S and I spins give an important contribution to C. The angular average of C is

then (assuming $g_\perp \approx 0$):

$$C \approx \frac{3}{10}\left(\frac{g_\parallel \mu_B}{H}\right)^2 \frac{1}{T_{1e}} \operatorname{sech}^2\left(\frac{\hbar\omega_e}{2kT}\right). \qquad (5.2)$$

$\hbar\omega_e$ is the energy splitting of the electron spins. The summation Σ_i in eq. (5.1) is taken over all electron spins. Goldman [40] and LJ have shown a simple way to solve eq. (5.1). The crystal is divided into spheres of influence each having a paramagnetic ion at its centre. The sphere boundary (outer shell) has a radius $R = (3/4\pi N_e)^{1/3}$, in which N_e denotes the number of Yb or Dy ions per cm^3. In a shell of radius $r_1 < r < b$ with $b = 0.68(C/D)^{\frac{1}{3}}$ direct relaxation of the protons via the electron spins is faster than spin diffusion to the nearby protons; r_1 is the minimum proton-Yb^{3+} ion distance. For $b < r < R$ the opposite is true. The final result for T_{1n}^{-1} becomes, for low concentrations of the paramagnetic ions, if $r_1 < b$:

$$1/T_{1n} = C/b^3R^3. \qquad (5.3)$$

The diffusion coefficient D is not constant throughout the crystal as assumed above for simplicity. Roughly speaking, in a shell $r_1 < r < d$ spin diffusion is hindered by the static field of the paramagnetic impurity [41]; d is called the diffusion barrier. If there is no diffusion within a sphere of radius d and if $d > b$, then the relaxation rate is given by

$$1/T_{1n} = C/d^3R^3. \qquad (5.4a)$$

if $d < r_1$ (and $b < r_1$), then T_{1n}^{-1} becomes:

$$1/T_{1n} = C/r_1^3R^3. \qquad (5.4b)$$

In fig. 10 the Bl. relax. rate is represented by the double-arrow path: electron spin-lattice interaction gives nuclear relaxation, because the wave functions of the electron-spin Zeeman system are admixed with those of the proton-spin Zeeman system by the dipolar interaction. The time

constant of this process will be denoted by T_{IL}.

If we consider the Bl. relax. in Yb:YES or Dy:YES and suppose as an example eq. (5.4b) to be valid, then T_{ln}^{-1} will satisfy the proportionality: $T_{ln}^{-1} \propto N_e^{-1} \times H^2 T \sin^2\theta \cos^2\theta$. The field and temperature dependence is only correct in the high-temp. appr. (see eq. 5.2)).

5.4. *Dipole relaxation.* Khutsishvili [41,42] has given a survey concerning the influence of the D.D.R. in the nuclear (proton-)spin relaxation, which was neglected in the above discussion. The hamiltonian of the system is written in the form

$$H = H_I + H_D + H_L + H_{ID} + H_{DL}. \tag{5.5}$$

H_I, H_D, H_L are respectively the hamiltonians of the Zeeman system of the protons, of the secular part of the dipole-dipole interaction (earlier called $H_{D'}$) of the magnetic ions and the hamiltonian of the lattice. It is assumed that the Zeeman degrees of freedom of the magnetic ions are in equilibrium with the lattice. This is certainly valid (except in the cross-relaxation region) because of the relatively very long proton-relaxation times in our experiments. H_{ID} and H_{DL} are the hamiltonians of the interaction between the spins of the nuclei and the magnetic ions resp. those of the magnetic ions and the lattice. The quantum-mechanical equations of motion are solved according to Zubarev's method [43] in the high-temperature approximation, which leads to the following two coupled equations:

$$\dot{\beta}_I = -\frac{\beta_I - \beta_L}{T_I^r} + \frac{\beta_D - \beta_L}{T_{ID}}, \tag{5.6}$$

$$\dot{\beta}_D = +\frac{\beta_I - \beta_L}{T_{ID}} - \frac{\beta_D - \beta_L}{T_D^r}.$$

To avoid confusion in the notation of temperatures and relaxation times sometimes the symbol r is added as a superscript to the T symbol, i.e.

T^r denotes a relaxation time. β_I in eq. (5.6) is defined as $1/T_I$; β_D as $1/T_D$ and β_L as $1/T_L$.

$1/T_I^r$ can be written as

$$1/T_I^r = 1/T_{IL} + 1/T_{ID}$$

and

$$1/T_D^r = 1/T_{DL} + 1/T_{DI}. \qquad (5.7a)$$

The meaning of the time constants in eq. (5.7a) is illustrated in fig. 10. The ratio between T_{DI} and T_{ID} is equal to the ratio between the heat capacity of the D.D.R. (C_D) and the heat capacity of the nuclear Zeeman system (C_I)

$$T_{DI}/T_{ID} = C_D/C_I. \qquad (5.7b)$$

The contact between the D.D.R. and the nuclear Zeeman system depends on the spin-spin relaxation time of the electron spins and the Zeeman splitting of the nuclear spins (Δ_n). In general, when M_2 (the second moment of the EPR resonance line) $<< \Delta_n^2$ the electron spin-spin interaction has negligible influence on the nuclear relaxation ($T_{ID} > T_{IL}$). The nuclear spins relax directly to the lattice via the Zeeman degrees of freedom of the magnetic ions. One particular situation, considered by Khutsishvili is $T_{ID} \leq T_{IL}$, $T_{DI} << T_{DL}$ and $T_{DI} << T_{ID}$, which is expected to occur at low temperatures and at not too low electron-spin concentrations. He shows that under those conditions β_I and β_D relax first rapidly to a common value. Then both the nuclear Zeeman system and the electronic-dipole system approach the lattice temperature at a rate T_{1n}^{-1}, given by:

$$T_{1n}^{-1} = \left(\frac{C_D}{C_I + C_D}\right) T_{DL}^{-1} + \left(\frac{C_I}{C_I + C_D}\right) T_{IL}^{-1}. \qquad (5.8)$$

C_D and C_I are the heat capacities of the D.D.R. and proton Zeeman system respectively. When $C_D/C_I >> T_{DL}/T_{IL}$, T_{1n}^{-1} is proportional to C_D. Further the heat capacity of the paramagnetic ions, C_D, depends quadratically on the concentration of the electron spins, so $T_{1n}^{-1} \propto N_e^2$.

Bendiashvili et al. [44] have discussed the situation, in which the

line broadening is not entirely of dipolar origin, as assumed above, but in which also inhomogeneous line broadening is present. The nuclear relaxation time is calculated in the case of fast spectral diffusion, i.e. when the exchange of energy among the different spins occurs within the spin-lattice relaxation time. If D.D.R. heating is important, then T_{1n}^{-1} is determined by

$$T_{1n}^{-1} \approx \frac{N_e S(S+1)}{N_n I(I+1)} \frac{(\Delta^{*2} + \Delta_{SS}^2)}{\Delta_n^2} \frac{1}{T_{DL}} \qquad (5.9)$$

where $(\Delta_{SS})^2$ is the second moment of the homogeneous line and (Δ^*) the second moment of the inhomogeneous line. N_n denotes the number of nuclear spins per cm^3. If $\Delta_{SS} \ll \Delta^*$, T_{1n}^{-1} becomes proportional to the electron-spin concentration N_e. The proportionality between T_{1n}^{-1} and N_e is also expected for the Bloembergen relaxation, while the angular, field and temperature dependence are similar in both cases too.

When spectral diffusion is slow, the formulae of Khutsishvili remain valid for the separate spin packets [42], in particular eq. (5.8).

6. Experimental results on Dy:YES. In figs. 11, 12, 13 and 14 the measured proton spin-lattice relaxation times T_{1n} in Dy:YES are plotted versus the angle, θ, subtended by the direct current field, $\vec{H}_{dc}$, and the $g_{//}$ axis. The results on various concentrations have been simultaneously shown in one figure. The four diagrams represent data taken at the same temperature, T = 0.45 K, and at different magnetic-field strengths, hence different proton-resonance frequencies (5, 10, 30 and 40 MHz resp.). It is seen that the figures have the following qualitative features in common:

a) the relaxation times become shorter at increasing Dy^{3+} concentrations;

b) the influence of the concentration on T_{1n} increases with decreasing field strength;

c) T_{1n} varies over many orders of magnitude when θ is varied from 0^o to 90^o.

We now present a discussion of these experimental results.

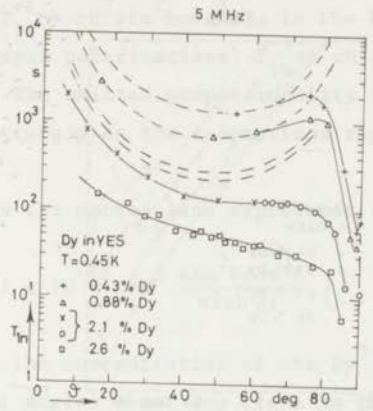

Fig. 11. Proton spin-lattice relaxation time T_{1n} (in s) in Dy:YES, measured at ν = 5 MHz and T = 0.45 K, plotted versus θ. θ is the angle between magnetic field and the $g_{//}$ direction. As in all the following figures, the drawn lines connect the experimental data points. The theoretical predictions are dotted in the figures. Varying the concentration by a factor 6 (at $\theta = 60^{o}$) results in a change in T_{1n} by a factor 35 .

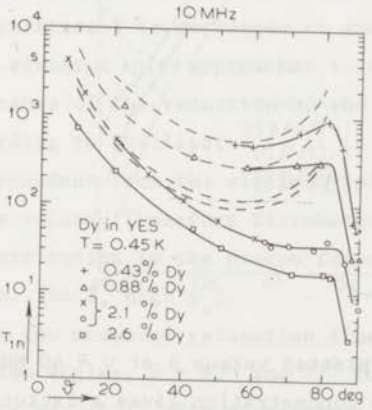

Fig. 12. T_{1n} in Dy:YES is plotted versus θ at ν = 10 MHz and T = 0.45 K. Changing the Dy concentration by a factor 6 gives (at $\theta = 60^{o}$) a variation in T_{1n} of a factor 17.

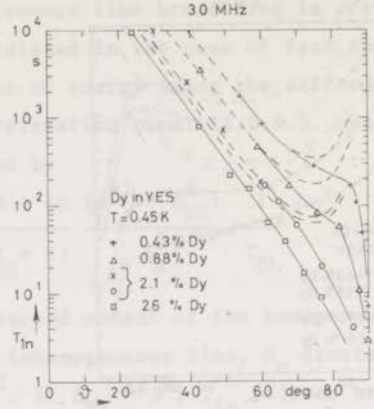

Fig. 13. T_{1n} in Dy:YES is plotted versus θ at ν = 30 MHz and T = 0.45 K. A factor 6 variation in the concentration yields a factor 10 variation in T_{1n}.

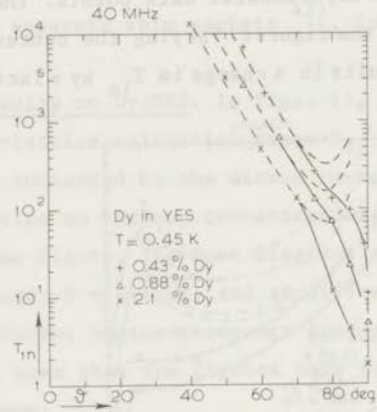

Fig. 14. T_{1n} in Dy:YES is plotted versus θ at ν = 40 MHz and T = 0.45 K. A factor 5 variation in the concentration gives a factor 5 variation in T_{1n} at $\theta = 60^{\circ}$.

6.1. *Bloembergen relaxation.* According to the discussion of the Bl. relax. in section 5, we expect the proton spin-lattice relaxation rate to be proportional to $T_{1n}^{-1} \propto CR^{-3}f(d,b)$. If we suppose the function

f(d,b) to be angular, field and temperature independent, see for example eq. (5.4b), then: $T_{1n}^{-1} \propto cH^2 \sin^2\theta\cos^2\theta T$, in the high-temp. appr.; and for high electron-spin polarizations: $T_{1n}^{-1} \propto cH^3 \sin^2\theta\cos^3\theta/\sinh 2\chi$, with $\chi = g_{//}\mu_B H\cos\theta/2kT$. The omitted proportionality constant in the above equation depends strongly on the assumptions regarding the function f(d,b).

In all figures the dotted line represents the formula

$$\frac{1}{T_{1n}} = 1.1 \times 10^{-11}\, cH^3\, \frac{\sin^2\theta\cos^3\theta}{\sinh 2\chi} \qquad (6.1)$$

in which c denotes the concentration of the Dy^{3+} ions in at.%. Eq. (6.1) fits the results at angles θ not too close to the perpendicular direction and for the lowest concentrations (c < 1%). The angular, field and temperature dependence, combined with the observed linear proportionality between T_{1n}^{-1} and c suggest predominance of the Bl. relax. mechanism. One might argue, however, that such a proportionality can also occur in other situations (section 5). As will be shown, an examination of the T dependence of the relaxation times proves that eq. (6.1) gives the magnitude of Bl. relax..

When the temperature T is decreased to such a degree, that the polarization of the electron spins approaches 1, the inequality $M_2 \ll \Delta_n^2$ becomes valid, because of the reduction of the second moment (section 8). Further, according to Phillipot [35], it is not allowed to treat the D.D.R. as independent from the electron-spin Zeeman system for these high magnetization values. Therefore Bloembergen relaxation gives the most important contribution to the proton relaxation rate under these circumstances (i.e. low T, high p_e).

Fig. 15 shows the measured relaxation times as a function of 1/T at ν = 30 MHz at two angles, $\theta = 63^\circ$ and 71° for c = 2.1% Dy. The dotted line represents eq. (6.1). For an electron polarization $p_e > 0.9$ the experimental curve coincides with the predictions of eq. (6.1). We conclude that the proportionality constant in eq. (6.1) determines the magnitude of the Bl. relax. for the protons in Dy:YES. LJ have made a theoretical calculation (section 5) for T_{1n} caused by the Bl. relax. for the protons in Yb:YES. When the appropriate $g_{//}(Dy)/g_{//}(Yb)$ ratio

is taken into account and when for T_{1n}^{-1} the earlier mentioned result of Kump is substituted:

$$T_{1e}^{-1} = 1.38 \times 10^{-15} H^5 \sin^2\theta\cos^3\theta\coth\chi ,$$

we derive for $1/T_{1n}$:

$$T_{1n}^{-1} = 2.0 \times 10^{-11} cH^3 \sin^2\theta\cos^3\theta/\sinh 2\chi . \qquad (6.2)$$

The agreement between eq. (6.1) and eq. (6.2) is better than could have been expected in view of the approximations made in the calculation. Relation (6.2) is derived from eq. (5.4) by replacement of the diffusion barrier d by r_1. Within the shell $r_1 < r < d$, the proton spin diffusion time will be shorter than the average time, required to induce a proton spin flip by a neighbouring Dy ion. This is probably caused by the non-spherical symmetry of the Dy field at the proton sites or by the so-called "induced" spin diffusion [50].

A high value of the electron-spin polarization, which leads to the reduction of the influence of the dipole relaxation, is also present near the parallel direction ($\theta = 0^\circ$) at T = 0.45 K. This mechanism causes the closer agreement between relation (6.1) and the measured relaxation times in the $\theta = 0^\circ$ angular region.

6.2. *Dipole relaxation.* In small fields over almost the whole angular region and in high magnetic fields in the perpendicular region ($\theta > 80^\circ$) the proton spin-lattice relaxation time is proportional to c^n with $2 \leq n < 3$ (see section 5). A proportionality $T_{1n}^{-1} \propto c^n$, where $n > 2$ may be caused by a concentration dependence of the electron spin-lattice relaxation rate T_{1e}^{-1}. A c dependence of T_{1e}^{-1} was found e.g. by De Vroomen et al. [49] for Cu^{2+} in zinc ammonium Tutton salt, even for field values several times larger than the local field. The relaxation times predicted by eq. (5.8) for the dipole relaxation, assuming $T_{DL} = T_{1e}/2$, a homogeneously broadened resonance line, T = 0.45 K, c = 2.6% Dy, $\theta = 60^\circ$ at ν = 30 MHz and ν = 5 MHz are respectively T_{1n} = 0.5 ms and T_n = 1.5 s. The experimental values are, respectively, 100 s and 40 s. The

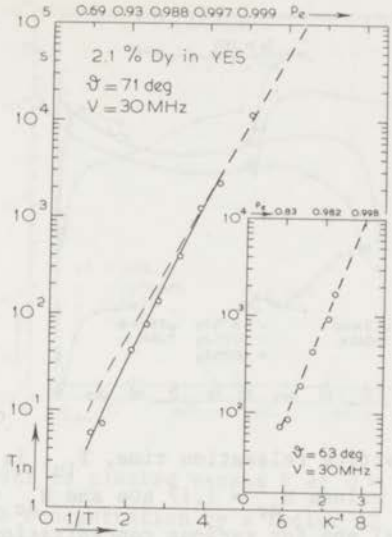

Fig. 15. T_{1n}, measured in YES with 2.1% Dy at ν = 30 MHz and at the angles $\theta = 63^{\circ}$ and $\theta = 71^{\circ}$, is plotted on a linear scale as a function of 1/T. The corresponding scale for the calculated electron-spin polarization, p_e, is indicated at the top. For $p_e > 0.9$ the experimental curve coincides with the predictions of eq. (6.1) (dotted line in the figure).

differences in the measured and theoretical values will be explained, when the Yb results are discussed (section 7).

6.3. *Cross-relaxation.* Fig. 16 illustrates the appreciable shortening of T_{1n} in the cross-relaxation region. The proton spin-lattice relaxation times are plotted versus θ for different concentrations at the fields H = 7 kOe and 1.17 kOe. A discussion of these results will be given in section 7.3.

7. Experimental results on Yb:YES. The figs. 17, 18, 19 and 20 are analogous to figs. 11, 12, 13 and 14 inasmuch as the frequency or field

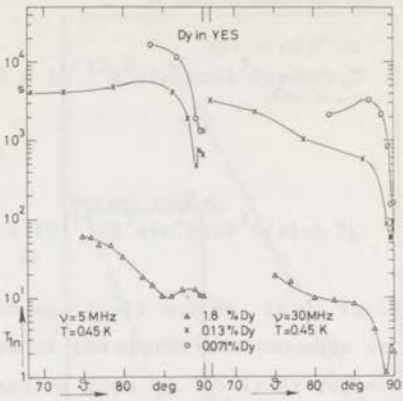

Fig. 16. Proton spin-lattice relaxation time, T_{1n}, is plotted versus θ at two magnetic-field values H_{dc} = 1.17 kOe and H_{dc} = 7 kOe (resp. ν = 5 MHz and ν = 30 MHz) and for various concentrations of Dy. The T_{1n} versus θ plot is confined to the region ($\theta > 80^{o}$) of small electronic Zeeman splittings, where cross-relaxation effects are seen to give appreciable shortening of T_{1n}.

variation is concerned. We have chosen a temperature of 1 K in order to compare our results with those of LJ and because the relaxation times become very long already at 1 K for the lowest concentrations. A discussion of these experimental results now follows.

7.1. *Bloembergen relaxation.* The results for low concentration of the Yb ions ($c \leq 0.2\%$) at high fields ($H \geq 7$ kOe) can be reasonable described by

$$T_{1n}^{-1} = 1.8 \times 10^{-14} c H^3 \sin^2\theta \cos^3\theta / \sinh 2\chi. \qquad (7.1)$$

The T_{1n} values calculated from eq. (7.1) are dotted in the figures.

Again (compare section 6.1) the linear proportionality between T_{1n}^{-1} and c is not sufficient to conclude that the proportionality constant in eq. (7.1) is given by the Bl. relax.. Under conditions of high electron-spin polarization Bl. relax. gives the most important

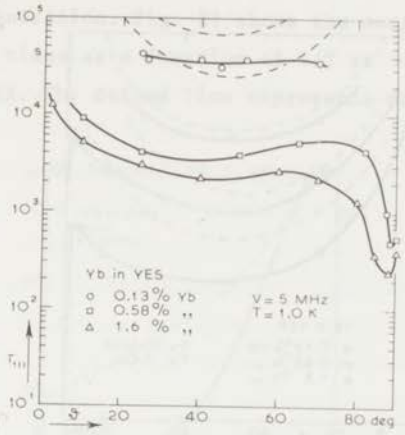

Fig. 17. T_{1n} in Yb:YES is plotted versus θ at ν = 5 MHz and T = 1.0 K. A variation in the Yb concentration by a factor 12 gives (at $\theta = 40^{o}$) a variation in T_{1n} of a factor 15. The influence of impurities cannot be neglected, when c ≈ 0.13%. As in all the following figures the drawn lines connect the experimental data points. The theoretical predictions are dotted in the figures.

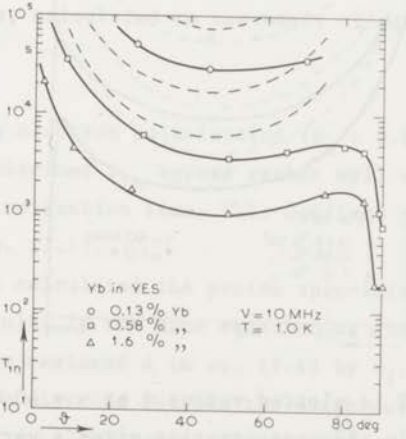

Fig. 18. T_{1n} in Yb:YES is plotted versus θ at ν = 10 MHz and T = 1.0 K. A variation in the concentration by a factor 12 gives (at $\theta = 40^{o}$) a factor 29 variation in T_{1n}.

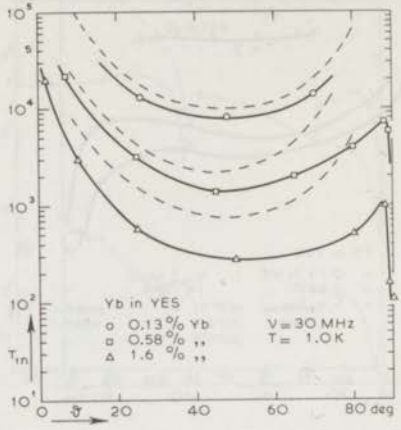

Fig. 19. T_{1n} in Yb:YES is plotted versus θ at ν = 30 MHz and T = 1.0 K. A factor 12 variation in the Yb concentration yields a factor 26 variation in T_{1n} (at $\theta = 40^{o}$).

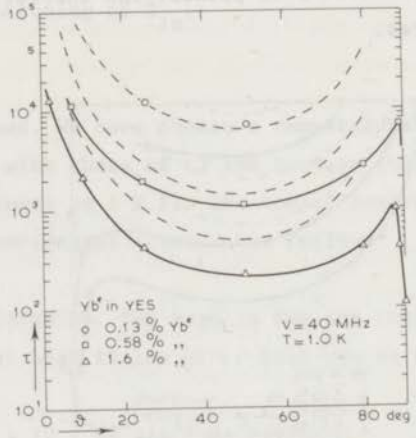

Fig. 20. T_{1n} in Yb:YES is plotted versus θ at ν = 40 MHz and T = 1.0 K. A factor 12 variation in the concentration gives a variation of a factor 28 in T_{1n} (at $\theta = 40^{o}$).

contribution to T_{1n}, even at moderate field and relatively high electron-spin concentration. Fig. 21 shows the measured proton spin-lattice relaxation times as a function of 1/T at ν = 10 MHz and at $\theta = 60^{\circ}$ for c = 1.5%. The dotted line represents formula (7.1). It is

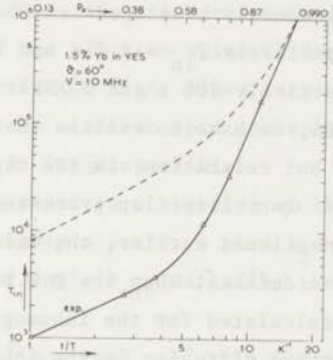

Fig. 21. T_{1n}, measured in YES with 1.5% Yb at ν = 10 MHz and at $\theta = 60^{\circ}$ is plotted on a logarithmic scale as a function of 1/T. The corresponding scale for the calculated electron-spin polarization, p_e, is indicated at the top. In the limit of strong electron-spin polarization ($p_e \approx 0.9$), the extrapolated experimental data nearly coincide with the dotted line, calculated on the basis of eq. (7.1).

seen that for strong electron polarization ($p_e \approx 0.9$) the magnitude of the experimentally obtained T_{1n} agrees rather well with the calculated proton spin-lattice relaxation time. This confirms that the Bl. relax. is represented by eq. (7.1).

MCJ and LJ have calculated the proton spin-lattice relaxation rate. Their derivation results in the same equation as the experimental relation (7.1), when they replaced d in eq. (5.4) by r_1. If $d = (2Sg/g_n)^{\frac{1}{4}}a$, taking a equal to the distance between the neighbouring proton spins and g equal to $g_{//}$, the calculated result for T_{1n}^{-1} would differ by more than 2 orders of magnitude from that of eq. (7.1).

7.2. *Dipole relaxation.* At small magnetic fields and high electron-spin

concentrations there is a difference between the measured T_{1n} values and the predictions of relation (7.1): the Bl. relax. is dominated by another concurring process. Under conditions of small Δ_n and large M_2 it is to be expected that the dipole relaxation is important. However, the relaxation times predicted by eq. (5.8) for T = 1.0 K, c = 1.6% and $\theta = 45^{\circ}$, assuming a homogeneously broadened resonance line are for ν = 30 MHz and ν = 5 MHz respectively T_{1n} = 2.7 s and T_{1n} = 750 s. The experimental values are respectively 200 s and 3 000 s. To understand the 5 MHz results in Yb/Dy:YES, we have to realize that Bl. relax. is independent of the $g_\perp$ value, but relaxation via the dipole-dipole reservoir is directly dependent upon flip-flop processes, in which $g_\perp$ plays an essential role. As mentioned earlier, the main contribution to $g_\perp$ has its origin in lattice defects. When the D.D.R. is taken into account, its effect must be calculated for the inhomogeneously broadened resonance line. Most probably the diffusion in the inhomogeneous line will be slow, due to the small $g_\perp$ values. Because eq. (5.8) was derived assuming $T_{ID} \ll T_{IL}$, C_D in this equation is reduced to the heat capacity of the spin packets with sufficiently high $g_\perp$ values. This reduction will give longer relaxation times. For the same reason there is no rigorous rule for the concentration dependence. The imperfections, responsible for the $g_\perp$ value distribution and the heat capacities of the spin packets, can differ from crystal to crystal.

At ν = 30 MHz eq. (5.8) (even, when corrected for the above-mentioned effect) predicts too short relaxation times. Apparently the increasing nuclear Zeeman splitting reduces the contact between the nuclear-spin Zeeman system and the D.D.R. of the electron spins. So the assumption $T_{ID} \ll T_{IL}$ is no longer valid, resulting in longer nuclear spin-lattice relaxation times.

7.3. *Cross-relaxation.* First we shall fix our attention on the case in which the proton spins are relaxed to the lattice via the dipole-dipole reservoir of the electron spins. When the Zeeman splitting of the electron spins Δ_Z becomes of the same order of magnitude as the linewidth (the width at half intensity), $\Delta_{\frac{1}{2}}$, the distinction between Zeeman and dipolar system loses its meaning. The total heat capacity of this

connected system $H = H_Z + H_D$ becomes about 4 times larger than the heat capacity of the D.D.R. before cross-relaxation. If $g_\perp \approx 0$, this extra contribution in the heat capacity will vanish, when $\vec{H}$ is directed perpendicular to the $g_{//}$ axis ($\theta = 90^o$). Further, the heat capacity in the cross-relaxation region can be enlarged by a distribution in the $g_\perp$ values (section 4). This effect becomes relatively more important when the concentration of the electron spins is decreased. In Dy:YES the "field-induced" $g_\perp$ value is eight times larger than the proton g value at $\nu = 30$ MHz: when the electron-spin concentration is low enough, cross-relaxation is no longer possible.

Summarizing, we expect a shortening of the dipole relaxation time of the protons by roughly a factor 4 when Δ_Z becomes of the order of $\Delta_{\frac{1}{2}}$. The corresponding angle θ_{min} satisfies the equation:

$$\Delta_{min} = H_{dc}\left[(g_{//}\mu_B\cos\theta_{min})^2 + (g_\perp\mu_B\sin\theta_{min})^2\right]^{\frac{1}{2}}, \qquad (7.2)$$

in which Δ_{min} is field independent.

Now we shall consider the situation when the concentration of the paramagnetic ions is so low that the electron spin-spin interaction can be neglected. The proton relaxation time T_{1n} in the cross-relaxation region, divided by T_{1e} will be of the order of the ratio of the number of proton spins (N_n) and electron spins (N_e) per cm^3. For example, in Yb:YES crystals

$$T_{1n,cross} \approx 0.5 \times 10^{23} T_{1e}/N_e. \qquad (7.3)$$

For angles $\theta \approx 90^o$ the Bl. relax. eq. (7.1) for the proton spins can be written as

$$T_{1n,Bl.} \approx 0.23 \times 10^{23} H_{dc}^2 T_{1e}/N_e, \qquad (7.4)$$

with the magnetic field H_{dc} in kOe. Eq. (7.4) predicts even shorter proton relaxation times than eq. (7.3) for field values $H_{dc} \leq 1$ kOe.

To understand this result it should be recalled that eq. (7.3) was derived from eq. (5.2). In eq. (5.2) C is calculated under the assumption

of a very small admixture of the pure Zeeman wave functions of the electron spins by the dipolar interaction with the proton spins. This approximation is certainly not allowed for the low-field calculations: at ν = 5 MHz the nuclear Zeeman splitting is of the same order as the dipole interaction term. In the limit of very strong dipolar admixture, the ratio between the allowed transitions, w_1, and the forbidden transitions (forbidden when no dipolar interaction is present) w_2^i, approaches unity. The symbol w_1 denotes the probability of a transition $\Delta m_s = \pm 1$, $\Delta m_n = 0$ between two levels differing only in m_s, the magnetic quantum number of the electron. w_2^i gives the probability of the transition $\Delta m_s = \pm 1$, $\Delta m_n = \mp 1$ for a proton at $\vec{r}_i$; m_n denotes the nuclear magnetic quantum number. So we have to expect (in the case of Bl. relaxation) that for high fields there is a shortening of the proton relaxation time in the cross-relaxation region proportional to H_{dc}^2. In Yb:YES (eqs. (7.3) and (7.4)) T_{1n} (cross)/T_{1n}(Bl.) = $2H_{dc}^{-2}$. For low-field values the admixture of the wave functions is so strong, that no appreciable shortening is expected to occur when the cross-relaxation transitions with $\Delta m_s = \pm 1$, $\Delta m_p = \pm 1$ become probable.

Now let us compare these considerations with the experimental results. The decrease of T_{1n} in the cross-relaxation region is present in all measured crystals, as is illustrated for Dy:YES in fig. 16 and for Yb:YES in fig. 22. In both figures the concentration of the paramagnetic ion is varied over a wide range. Because of the measured relaxation times outside $\theta \simeq 90^\circ$ region, we think that in every crystal the limit of the Bl. relax. is not yet reached. This assumption is in agreement with the increasing polarization for lower concentrations in Dy:YES. (see section 8). In Yb:YES there are indications of a saturation of the proton-spin polarization for the lowest concentrations, but here the influence of impurities cannot be neglected. From the nuclear spin-lattice relaxation times near $\theta \simeq 90^\circ$ we conclude that the heat capacity of the spin-spin interaction system is of the same order in the perpendicular direction ($\theta = 90^\circ$) as for $\theta = \theta_{min}$, probably because of the $g_\perp$-value distribution. A minimum in T_{1n} for $\theta = \theta_{min}$, as expected in the case of dipole relaxation, is found in yttrium chloride hexahydrate crystals [51] doped with Yb^{3+} ions.

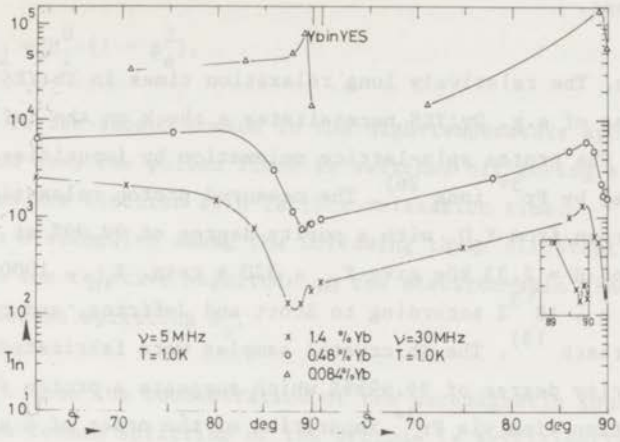

Fig. 22. T_{1n} is plotted versus θ at two field values H_{dc} = 1.17 kOe and H_{dc} = 7 kOe (resp. ν = 5 MHz and ν = 30 MHz) and for various concentrations of Yb. The T_{1n} versus θ plot is confined to the region ($\theta > 80^{o}$) of small electronic Zeeman splittings, where cross-relaxation effects are seen to give appreciable shortening of T_{1n}.

Formula (7.2) appears to be valid both in Dy:YES and in Yb:YES. Application of eq. (7.2) to YES with 1.8% Dy yields $\Delta_{min} = 1.0 \times 10^{-17}$ erg. A calculation of the linewidth, assuming a dipolar broadened gaussian resonance line, gives $\Delta_{\frac{1}{2}} = 1.6 \times 10^{-17}$ erg. In YES with 0.13% Dy the experimentally determined Δ_{min} is $\Delta_{min} = 2.1 \times 10^{-18}$ erg, while the computed $\Delta_{\frac{1}{2}}$ becomes $\Delta_{\frac{1}{2}} = 4.3 \times 10^{-18}$ erg. When a lorentzian line shape is assumed, which is more likely at the lower concentrations (c < 1%), the calculated linewidth becomes smaller. In YES with 1.4% Yb formula (7.2) yields $\Delta_{min} = 1.2 \times 10^{-18}$ erg, while a calculation of $\Delta_{\frac{1}{2}}$ gives $\Delta_{\frac{1}{2}} = 1.3 \times 10^{-18}$ erg.

The reasonable fit of the experimental results with the predictions of eq. (7.2) confirms the important role of the electron spin-spin interaction, also in the cross-relaxation region.

In Dy:YES at ν = 30 MHz cross-relaxation is possible even at the

lowest concentration ($c \simeq 0.07\%$). The third-order Zeeman splitting is not yet important.

7.4. *Impurities.* The relatively long relaxation times in Yb:YES, compared with those of e.g. Dy:YES necessitates a check on the influence of impurities. The proton spin-lattice relaxation by impurities is most likely dominated by Pr^{3+} ions [26]. The measured proton relaxation times in a crystal grown from Y_2O_3 with a purity degree of 99.99% at T = 1.0 K, H = 1.17 kOe and H = 2.33 kOe give $T_{1n} \simeq 320$ s resp. $T_{1n} \simeq 1000$ s, which corresponds to $c \simeq 10^{-3}\%$ according to Scott and Jeffries, and $c \simeq 10^{-2}\%$ according to Orbach [13]. The Yb crystal samples were fabricated from Y_2O_3 with a purity degree of 99.9999% which suggests a proton spin-lattice relaxation time via Pr^{3+} impurities of the order of 3×10^4s at H = 1.17 kOe and T = 1.0 K. Therefore the proton relaxation times for the lowest Yb concentrations at H = 1.17 kOe may be influenced by Pr impurities (fig. 20).

7.5. *Phonon bottleneck.* In order to investigate whether bottleneck effects have influenced the results presented in the figs. 15 and 21, we have estimated the bottlenecked electron spin-lattice relaxation time (T_{1b}), according to Scott and Jeffries [26]. Assuming the phonon mean free path $\bar{l}$ equal to $\bar{l} = 0.2$ cm and calculating the linewidth from the homogeneously broadened resonance line, T_{1b} was computed for both crystals. The bottlenecked relaxation times, as far as relevant for the figure, appear to be of the same order as the electron spin-phonon relaxation times (T_{SP}) or shorter. Because of these estimated magnitudes of $T_{1b}/T_{SP} \leq 1$, no appreciable influence of a phonon bottleneck in the nuclear relaxation is expected [52], see also chapter 1.

8. Proton polarization. We shall consider the degree of polarization which can be obtained in the pulsed-field method and illustrate the importance of the relaxation mechanisms. The first step of the polarization cycle consists of switching on the pulsed field. The electron-spin polarization becomes (eq. (2.5)) $p_e = \tanh(g_{\parallel}\mu_B H_p \cos\delta/2kT_L)$. When the EPR resonance line is homogeneously broadened its central second moment

M_2 will be reduced [45,46] by the increase in polarization:

$$M_2 = M_2^0 (1 - p_e^2), \tag{8.1}$$

in which M_2^0 is the second moment in the high-temperature approximation. In the second step the pulsed field is switched off during a time short compared with the electron spin-lattice relaxation time.

One can distinguish among the following three different situations, depending on the relative magnitude of the electron-spin linewidth to the proton Zeeman splitting Δ_n.

8.1. $M_2^0 << \Delta_n^2$. When the concentration of the paramagnetic ions is very small and the Zeeman splitting of the protons is sufficiently high, then $M_2^0 << \Delta_n^2$, in which $\Delta_n = g_n \mu_B H_{dc}$. This case is extensively treated by MCJ, whose notation we shall follow. Important factors in the polarization process are the following.

8.1.1. *The electron-spin polarization just before cross-relaxation:* $\overline{p_e}$. The pulsed field is switched off in a time τ_0, which in practice amounts to a few times τ_d (section 3). The polarization $p_e(t)$ of the electron spins at a time $t < \tau_0$ will relax to an equilibrium value $p_{e0}(t)$, determined by the instantaneous field value H(t) and by the lattice temperature T_L, expressed by the following equation

$$\frac{\partial p_e}{\partial t} = \frac{1}{T_{1e}(t)}\left[p_{e0}(t) - p_e(t)\right], \tag{8.2}$$

in which $T_{1e}(t)$ is given by eq. (2.4).

We take as an example Dy:YES with H_p = 1.5 kOe, H_{dc} = 7 kOe, $\delta = 0^\circ$, T = 0.40 K. With a decay time, τ_d, of the pulsed field τ_d = 6 ms, the electron-spin polarization just before cross-relaxation (computed from eq. (8.2)) is practically equal to the intial value: $\overline{p}_e \approx 0.9$.

8.1.2. *Multiple spin flips.* The influence of multiple spin flips will be illustrated in the high temp. approx.. We consider here only

the situation in which one electron spin causes multiple proton spin flips. The probability of one proton spin flip in combination with multiple electron spin flips is too low to be of practical significance. When further the proton spin-lattice relaxation can be neglected, the temperature of the proton system, T_n, and that of the electron spin system, T_S, become equal.

In the high temp. approx.

$$T_n \simeq \Delta_n / 2\,k p_n \quad \text{and} \quad T_S \simeq \varepsilon \Delta_n / 2\,k \bar{p}_e, \tag{8.3}$$

when ε is the number of proton spins which simultaneously flip with one electron spin and p_n denotes the proton polarization. Therefore p_n approaches $\bar{p}_e/\varepsilon$. For example, when H_p = 1.5 kOe, H_{dc} = 7 kOe, $\delta = 0^o$, T = 0.40 K, τ_d = 6 ms, $g_\perp = \frac{1}{2} g_n$ and if H_0 (the field value of H_p at which the cross-relaxation takes place) equals 200 Oe, then for Dy^{3+} in YES one has $f_1 = 1$, $f_2 = 1$ and $f_3 = 0.7$. The symbol f_n denotes the probability for a one Yb spin -n proton spin flip. The f values are calculated in accordance with the formulas of MCJ. The derivation of the expressions for f_n is based on time-dependent perturbation theory, which is only valid when the spin-flip part of the dipole-dipole interaction between protons and Yb ions (V_{ij}) will be less than the proton linewidth (δE). Adiabatic passage corrections [4,42] are needed for the protons nearest Yb sites, where perturbation theory breaks down. The probability for 1:1 spin flips remains still large, when we consider protons at lattice sites where $|V_{ij}| < \delta E$, because of the slow decay time of the pulsed field (minimum $\tau_d \simeq 1.5$ ms).

When the high-temp. appr. is no longer allowed the process becomes more complicated. When $\bar{p}_e = 1$, then p_n approaches 1, provided that the influence of the proton spin-lattice relaxation can be neglected.

The final proton polarization p_f in the high-temp. appr. when T_{1n} is taken into account, becomes [5]

$$p_f = (E\langle C\rangle \tau p_{n0} + \langle\langle \varepsilon f_\varepsilon \rangle\rangle \bar{p}_e)/(E\langle C\rangle \tau + \langle\langle \varepsilon^2 f_\varepsilon \rangle\rangle), \tag{8.4}$$

in which $E = 4\pi N_n / 3 r_1^3$ and N_n is the number of protons per cm^3; $\langle C\rangle$

denotes the average of C (eq. (5.2)) over a refrigerator cycle; $p_{n0} = \tanh g_n \mu_B H_{dc}/2kT_L$, $\langle \varepsilon f_\varepsilon \rangle$ represents the net effect of all orders of cross-relaxation while in the double bracketed $\langle\langle \varepsilon f_\varepsilon \rangle\rangle$ the average value over the distribution of g values (section 4.1) is taken. Eq. (8.4) is valid if the pulse duration time τ_1 is several times longer than the electron spin-lattice relaxation time during the pulse. For example, let us consider a crystal of 1% Dy in YES at T = 0.40 K, H_{dc} = 7 kOe, H_p = 1.5 kOe, $\delta = 0^o$, τ_d = 6 ms, a pulse period τ = 1 s and $\tau_1 \simeq \tau$. With $\langle\langle \varepsilon f_\varepsilon \rangle\rangle = 3$ and $\langle\langle \varepsilon^2 f_\varepsilon \rangle\rangle = 11$ (section 8.1.2), $\langle C \rangle \simeq 10^{-45}$ and $E = 6.7 \times 10^{45}$ eq. (8.4) gives $p_f = 0.17\ \bar{p}_e$. In this case the proton relaxation cannot be neglected within the pulse period. At a higher frequency $E\langle C \rangle \tau$ will become much smaller than $\langle\langle \varepsilon^2 f_\varepsilon \rangle\rangle$ and eq. (8.4) can be simplified to

$$p_f \simeq \frac{\langle\langle \varepsilon f_\varepsilon \rangle\rangle}{\langle\langle \varepsilon^2 f_\varepsilon \rangle\rangle} \bar{p}_e, \tag{8.5}$$

which results in $p_f = 0.3\ \bar{p}_e$. When the direct-current field is 6 times lower (H_{dc} = 1.17 kOe), $\langle C \rangle$ will be 6^2 times smaller. This means, that even with τ = 1 s the final polarization is completely determined by the the multiple spin-flip process and eq. (8.5) can be applied.

8.2. $M_2 \gg \Delta_n^2$. This situation occurs, when the concentration of the paramagnetic ions is, e.g., a few percent. The proton spin system will then be in equilibrium with the D.D.R. of the paramagnetic ions (section 5). The proton spin temperature, again neglecting the nuclear spin-lattice relaxation, will approach the final electron spin temperature. The latter, reached after adiabatic demagnetization of the electron spins from H_p, is given by

$$\frac{T_i^2(\text{initial temp.})}{T_f^2(\text{final temp.})} = \frac{\mathrm{Tr}(H_i^2)}{\mathrm{Tr}(H_f^2)} \tag{8.6}$$

The initial hamiltonian H_i is the sum of the Zeeman interaction term $\mu_B \Sigma_j \vec{H} \cdot \vec{g} \cdot \vec{S}_j$ and the dipolar interaction $\Sigma_{j,k} H_{j,k}$. When the direct-current field $\vec{H}_{dc}$ points in the perpendicular direction, the Zeeman term vanishes: the final hamiltonian becomes $H_f = \Sigma_{j,k} H_{j,k}$. With the usual definitions

of the local field $\vec{H}_L$ for $\vec{H} \| z$ axis $H_{Lz}^2 = \mathrm{Tr}\{H_f^2\}/\mathrm{Tr}\{\Sigma_j S_{zj}^2\}$ and local-field energy splitting $\Delta_{Lz}^2 = g_z^2 \mu_B^2 H_{Lz}^2$ eq. (8.6) becomes

$$T_i^2/T_f^2 = (\Delta_Z^2 + \Delta_L^2)/\Delta_L^2, \tag{8.7}$$

in which $\Delta_L^2 = g_{eff}^2 \mu_B H_L^2$ is over a wide angular region equal [48] to Δ_{Lz}^2 and $\Delta_Z = g_{/\!/} \mu_B H_p \cos\delta$.

When $g_{/\!/} >> g_\perp$, one finds [48] that $2\Delta_L^2 \simeq M_2$, so

$$\frac{T_i^2}{T_f^2} = \frac{2\Delta_Z^2 + M_2}{M_2} . \tag{8.8}$$

For example: let us consider YES with 1% Dy ions at T = 0.40 K, H_{dc} = 7 kOe, H_p = 1.5 kOe, τ_d = 6 ms and $\delta = 0^o$. When we suppose M_2 in eq. (8.8) to be equal to $M_2 \simeq 2 \times 10^{-35} \mathrm{erg}^2$, the ratio between initial and final temperature becomes $T_i/T_f \simeq 40$ or $p_f \simeq 0.08\ \bar{p}_e$.

8.3. $M_2^0 > \Delta_n^2$ *and* $\bar{M}_2 < \Delta_n^2$. $\bar{M}_2$ denotes the second moment of the EPR line, just before cross-relaxation. In the beginning of the recurrent cross-relaxation cycles, M_2 after cross-relaxation will stay larger than Δ_n^2, but finally because of the decreasing temperature of the protons, M_2 may become smaller than Δ_n^2.

The proton spin-lattice relaxation time is shorter than expected from the Bl. relax. relation (eq. (5.4b)), when the contact between proton spin system and D.D.R. of the electron spins is important. In that situation eq. (8.8) gives the degree of proton polarization. The influence of the D.D.R. becomes negligible in T_{1n} when the concentration of the paramagnetic ions is sufficiently small. Concomittantly also eq. (8.4) becomes valid. For example, a concentration of about 0.07% Dy in YES is not sufficiently low to reach the limit of eq. (8.4). We conclude from our experiment that the final polarization degree of the protons can still be enlarged by a further decrease of the Dy concentration in the crystals.

For inhomogeneous line broadening the treatment given above remains valid in the slow diffusion limit for the separated spin packets. In order to avoid an enlargement of the heat capacity of the D.D.R. by the

hyperfine splittings even isotopes of Yb and Dy have been selected for the experiments.

9. Conclusion. Proton polarizations can be obtained in ^{162}Dy:YES and ^{174}Yb:YES by the nuclear spin refrigerator method. Under the experimental conditions the electron spin-lattice relaxation appears to be governed by the direct process, while the nuclear spins usually relax to the lattice via the dipolar part of the electron spin system. Under conditions of high electron-spin polarization (reached by cooling the sample crystal to sufficiently low temperatures by means of adiabatic demagnetization), or sufficiently low electron-spin concentration the nuclear spin-lattice relaxation time can be reasonably well described by the Bloembergen relaxation process. An appreciable shortening of T_{1n} occurs when the electron-spin Zeeman splitting becomes of the order of the dipolar linewidth in the crystal.

We have shown that in order to reach high proton polarization via rotational cooling the concentration of the paramagnetic ions must be very low (in Dy:YES $c < 0.07\%$). Only then the electron spin-spin interaction, which normally restricts the degree of proton polarization can be neglected.

References.

1) Lubbers, J. and Huiskamp, W.J., Physica 34 (1967) 193 (Commun. Kamerlingh Onnes Lab., Leiden No. 353b).
2) Jeffries, C.D., Cryogenics 3 (1963) 41.
3) Abragam, A., Cryogenics 3 (1963) 42.
4) Langley, K.H. and Jeffries, C.D., Phys. Rev. 152 (1966) 358.
5) McColl, J.R. and Jeffries, C.D., Phys. Rev. B 1 (1970) 2917.
6) Wolfe, J.P. and Jeffries, C.D., Phys. Rev. B 4 (1971) 731.
7) Ketelaar, J.A.A., Physica 4 (1937) 619.
8) Fitzwater, D.R. and Rundle, R.L., Z. Krist. 112 (1952) 362.
9) De Haas, W.J., Van den Handel, J. and Gorter, C.J., Phys. Rev. 43 (1933) 81.
10) Cooke, A.H., Edmonds, D.T., McKim, F.R. and Wolfe, W.P., Proc. Roy. Soc. A 252 (1959) 246.

11) Cooke, A.H., Finn, C.B.P., Mangum, B.W. and Orbach, R.L., J. Phys. Soc. Japan 17 suppl. B 1 (1962) 462.
12) Dweck, J. and Seidel, G., Phys. Rev. 155 (1967) 267.
13) Orbach, R., Proc. Roy. Soc. A 264 (1961) 458.
14) Kump, U., Phys. Status Solidi 34 (1969) 691.
15) Grant, W.J.C., Phys. Rev. 134A (1964) 1554, 1565, 1575; Phys. Rev. 135A (1964) 1265.
16) Provotorov, B.N., Zh. Eksper. Teor. Fiz. 42 (1962) 882; Soviet Physics-JETP 15 (1962) 611.
17) See, for example:
Abragam, A.: The Principles of Nuclear Magnetization, Clarendon Press (Oxford, 1961), p. 135.
18) Vilches, O.E. and Wheatley, J.C., Phys. Rev. 148 (1966) 509.
19) Haasbroek, J.N., thesis (Leiden, 1971).
20) Nicol, J. and Soller, T., Bull. Amer. Phys. Soc. 2 (1957) 63.
21) Rafolowisz, J. and Sujak, B., Acta Phys. Polon. 25 (1964) 599.
22a) Goldman, M.: Spin Temperature and Nuclear Magnetic Resonance in Solids, Clarendon Press (Oxford, 1970), p. 108.
22b) Id. p. 138.
23) Grivet, P., Soutif, M. and Buyle-Bodin, M., CR Acad. Sci. 229 (1949) 113.
24) Wheeler, R.G., Reames, F.M. and Wachtel, E.J., J. Appl. Phys. 39 (1968) 915.
25) See, for example:
Hutchings, M.T., Solid State Phys. 16 (1964) 227.
26) Scott, P.L. and Jeffries, C.D., Phys. Rev. 127 (1962) 32.
27) Van den Broek, J. and Van der Marel, L.C., Physica 29 (1963) 948 (Commun. Kamerlingh Onnes Lab., Leiden, No. 335c), Physica 30 (1964) 565 (Commun. Kamerlingh Onnes Lab., Leiden, No. 337b).
28) Cooke, A.H., McKim, F.R., Meyer, H. and Wolf, W.P., Phil. Mag. 2 (1957) 928.
29) Stoneham, A.M., Proc. Phys. Soc. (London) 89 (1966) 909; J. Phys. C 1 (1968) 565.
30) McMahon, D.H., Phys. Rev. 134A (1964) 128.
31) Hill, J.C. and Wheeler, R.G., Phys. Rev. 152 (1966) 482.

32) Powell, M.J.D. and Orbach, R., Proc. Phys. Soc. (London) 58 (1961) 753.
33) Cooke, A.H., Finn, C.B.P. and Orbach, R., Arch. Sci. 13 (1960) 111.
34) Gramberg, G., Z. Phys. 159 (1960) 125.
35) Phillipot, J., Phys. Rev. 133A (1964) 471.
36) Jeener, J., Eisendratht, H. and Van Steenwinkel, R., Phys. Rev. 133A (1968) 478.
37) Swanenburg, T.J.B., thesis (Leiden, 1967).
38) Atsarkin, V.A., Mefeod, A.E. and Rodak, M.I., Zh. Eksper. Teor. Fiz. 55 (1968) 1671. Soviet Physics-JETP 28 (1969) 877.
39) Bloembergen, N., Physica 15 (1949) 386 (Commun. Kamerlingh Onnes Lab., Leiden, No. 277a).
40) Goldman, M., Phys. Rev. 138A (1965) 1675.
41) Khutsishvili, G.R., Uspekhi Fiz. Nauk. 96 (1968) 441, Soviet Physics-Uspekhi 11 (1969) 802.
42) Khutsishvili, G.R., Progr. in Low Temp. Phys. 6 (1970), ed. C.J. Gorter (North-Holland Publ. Co., Amsterdam).
43) Zubarev, D.N., Fortschr. Phys. 18 (1970) 125.
44) Bendiashvili, N.S., Buishvili, L.I. and Zviadadze, M.D., Zh. Eksper. Teor. Fiz. 58 (1970) 597, Soviet Physics-JETP 31 (1970) 321.
45) McMillan, M. and Opechowski, W., Canad. J. Phys. 38 (1963) 1168.
46) Svare, I. and Seidel, G., Phys. Rev. 134A (1964) 172.
47) Wannier, G.H., Physics 1 (1965) 251.
48) De Boo, N., private communication.
49) De Vroomen, A.C., Lijphart, E.E. and Poulis, N.J., Physica 47 (1970) 458 (Commun. Kamerlingh Onnes Lab., Leiden, No. 377b).
50) Horvitz, E.P., Phys. Rev. B 3 (1971) 2868.
51) Brom, H.B. and Huiskamp, W.J., to be published.
52a) Murtazin, Sh.V., Fiz. Tverd. Tela 8 (1966) 1847, Soviet Physics-Solid State 8 (1966) 1465.
52b) Buishvili, L.L., Giorgadze, N.P. and Khutsishvili, G.R., Zh. Eksper. Teor. Fiz. 60 (1971) 1433, Soviet Physics-JETP 33 (1971) 776.

CHAPTER 3

PROTON POLARIZATION AND RELAXATION IN YTTRIUM CHLORIDE HEXAHYDRATE DOPED WITH Yb IONS

Synopsis

A rotational-cooling method is employed to obtain proton polarization in crystals of $YCl_3 \cdot 6H_2O$ doped with Yb^{3+} ions. The relaxation behaviour of the protons is investigated as a function of magnetic field H (1 kOe $\leq$ H $\leq$ 10 kOe), temperature T (0.05 K $\leq$ T $\leq$ 1 K) and concentration c of the rare-earth ions (0.05% $\leq$ c $\leq$ 1.4%). For concentrations of the Yb ions in the range 0.3 $\leq$ c $\leq$ 1.4% the relaxation times are strongly influenced by the dipole-dipole reservoir of the electron spins. The electron spin-lattice relaxation rate is calculated on the basis of the proton spin-lattice relaxation rates (T_{1n}^{-1}) at the lower Yb concentrations. Because the T_{1n} measurements are reasonably well described by a hexagonal crystal-field interaction on the Yb ions, a hexagonal crystal-field hamiltonian is proposed. Polarization measurements give $g_{min} = 0.08 \pm 0.01$.

1. Introduction. In the second chapter of this thesis [1], referred to as I, a proton polarization and relaxation study was presented, proton polarization being achieved by the rotational-cooling method in Yb- and Dy-doped yttrium ethyl sulfate crystals. The degree of proton polarization and its time dependence was measured by NMR at various frequencies and at temperatures down to about 0.05 K. In this chapter similar results on yttrium chloride hexahydrate crystals, doped with Yb^{3+} ions enriched to 95% ^{174}Yb, will be discussed. Since rotational cooling is based on the anisotropy of the electron-spin g value and particularly on the occurrence of a small g value in at least one direction of the crystal, the Yb-doped hydrated chlorides are expected to be favourable. The electron-spin g values for the lowest Kramers doublet

of the Yb spins are determined as $g_{max} = 5.6$ and $g_{min} < 0.5$ (see section 2).

The experimental arrangement is the same as described in I. The subject of section 2 is the energy-level splitting of the $^2F_{7/2}$ ground state of the Yb ion. Formulae for the electron spin-lattice and proton spin-lattice relaxation times, resp. abbreviated as T_{1e} and T_{1n}, are derived in sections 3 and 4, while the experimental results on T_{1n} are presented and discussed in section 5. In section 6 an estimate of the minimum g value is obtained from measurements of the influence of the electron-spin Zeeman-energy splitting on the maximum obtainable proton polarization.

2. Energy level splitting of the $^2F_{7/2}$ ground state of the Yb^{3+} ion in $YCl_3 \cdot 6H_2O$. Rare-earth ions in hydrated chloride crystals have been extensively investigated, e.g. with respect to their paramagnetic resonance spectra and relaxation behaviour [2-5]; also the crystal structure is known.

2.1. *Crystal structure and proton positions.* The chloride hexahydrates of the rare-earth ions and yttrium form a series of isostructural compounds [6]. The crystal structure is determined in detail for gadolinium trichloride hexahydrate from X-ray data [7]. The crystal is monoclinic (point group of the rare-earth sites is C_2) with two molecules in the unit cell, which for $GdCl_3 \cdot 6H_2O$ has dimensions a = 9.651, b = 6.525, c = 7.923 Å and $\beta = 93.6^\circ$. In $YCl_3 \cdot 6H_2O$ [2a] β is somewhat smaller, $\beta = 92^\circ$. The hydrogen positions, tabulated by Marezio et al., are based on the assumption that the H atoms are situated between the oxygen and chlorine atoms at a distance of 0.96 Å from the oxygen atom; the minimum H-Gd distance will be 3.0 Å. The two Gd sites are magnetically and electrically equivalent. Optical data on the chloride hexahydrates of Yb [2a], Tm and Ho [8] suggest a pseudo-hexagonal axis perpendicular to the twofold symmetry axis, while EPR data on $YCl_3 \cdot 6H_2O$ doped with various rare-earth ions [4] are reasonably well described by assuming hexagonal symmetry of the electric crystal field.

2.2. *Spin hamiltonian.* Harrop [9] has calculated the crystal-field parameters explicitly for $ErCl_3 \cdot 6H_2O$ on the basis of the monoclinic crystal structure and extrapolated his results to the other rare-earth crystals. We have constructed a hexagonal spin hamiltonian for Yb: $YCl_3 \cdot 6H_2O$ which gives the same energy-level splitting as Harrop's monoclinic spin hamiltonian (fig. 1) and which reproduces also the experimental g values for the lowest Kramers doublet. (A hexagonal spin hamiltonian, derived by Eisenstein [10] for $YbCl_3 \cdot 6H_2O$ gives completely different level splittings). Further also the eigenfunctions belonging to the energy levels were correlated to the results of Harrop. Predictions for the proton relaxation times from both hamiltonians will be compared with the experimental results.

The spin hamiltonian which describes the interaction of an Yb^{3+} ion with the crystal field can be written in the form [11]

$$H = \sum_{m,n} B_n^m O_n^m + iB_n^m(s) O_n^m(s). \qquad (2.1)$$

The O_n^m and $O_n^m(s)$ operators have an immediate correspondence with the tesseral harmonics Z_{nm}^c and Z_{nm}^s [11]. When hexagonal symmetry is present it is possible to choose the coordinate system in such a way that no imaginary operator equivalents are necessary. Harrop has derived the following values for the coefficients B_n^m and $B_n^m(s)$: $B_2^0 = +3.39\ cm^{-1}$; $B_2^2 = +4.62\ cm^{-1}$ and $B_2^2(s) = -7.66\ cm^{-1}$; $B_4^0 = +0.130\ cm^{-1}$; $B_4^2 = +0.285\ cm^{-1}$ and $B_4^2(s) = -0.511\ cm^{-1}$; $B_4^4 = -0.490\ cm^{-1}$ and $B_4^4(s) = -0.233\ cm^{-1}$; $B_6^0 = -0.114 \times 10^{-2} cm^{-1}$; $B_6^2 = -0.811 \times 10^{-2} cm^{-1}$ and $B_6^2(s) = +0.163 \times 10^{-1} cm^{-1}$; $B_6^4 = +0.276 \times 10^{-1} cm^{-1}$ and $B_6^4(s) = -0.138 \times 10^{-1} cm^{-1}$; $B_6^6 = +0.276 \times 10^{-1} cm^{-1}$ and $B_6^6(s) = -0.127 \times 10^{-2} cm^{-1}$.

The energy-level splitting of the $^2F_{7/2}$ multiplet, illustrated in fig. 1, is derived with the coefficients given above. The corresponding wave functions in case a magnetic field of 7 kOe is present (used in the majority of our experiments) parallel to the monoclinic axis, become for the lowest doublets:

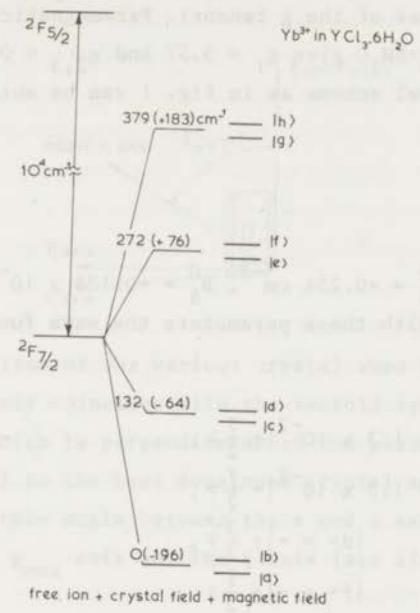

Fig. 1. Energy-level scheme of Yb^{3+} in $YCl_3 \cdot 6H_2O$, according to Harrop. The levels at 0 cm^{-1} (-196 cm^{-1}) and 132 cm^{-1} (-64 cm^{-1}) are observed by infrared spectroscopy. (Eisenstein's hexagonal spin hamiltonian requires the undetected levels to lie at 74 cm^{-1} and 100 cm^{-1} with respect to the ground state).

$$|a\rangle = (+0.67 - i0.14)\left|-\tfrac{5}{2}\right\rangle + (-0.18 - i0.23)\left|-\tfrac{1}{2}\right\rangle + (0.53 - i0.30)\left|+\tfrac{3}{2}\right\rangle + (-0.26 - i0.08)\left|+\tfrac{7}{2}\right\rangle,$$

$$|b\rangle = (-0.28)\left|-\tfrac{7}{2}\right\rangle + (0.42 + i0.45)\left|-\tfrac{3}{2}\right\rangle + (-0.24 + i0.17)\left|+\tfrac{1}{2}\right\rangle + (0.59 + i0.33)\left|+\tfrac{5}{2}\right\rangle,$$

$$|c\rangle = (-0.31)\left|-\tfrac{7}{2}\right\rangle + (0.11 + i0.64)\left|-\tfrac{3}{2}\right\rangle + (0.47 - i0.01)\left|+\tfrac{1}{2}\right\rangle + (-0.30 - i0.40)\left|+\tfrac{5}{2}\right\rangle,$$

$$|d\rangle = (+0.48 - i0.12)\left|-\tfrac{5}{2}\right\rangle + (-0.37 - i0.28)\left|-\tfrac{1}{2}\right\rangle + (-0.50 + i0.43)\left|+\tfrac{3}{2}\right\rangle + (+0.24 + i0.20)\left|+\tfrac{7}{2}\right\rangle.$$

The calculated g values are $g_1 = 5.68$, $g_2 = 0.25$ and $g_3 = -0.86$ (referring to the principal axes of the g tensor). Paramagnetic resonance results [4] in 1% $Yb:YCl_3 \cdot 6H_2O$ give $g_1 = 5.57$ and $g_{2,3} < 0.5$.

The same energy-level scheme as in fig. 1 can be obtained from a hexagonal hamiltonian

$$H = \sum_{m,n} B_n^m O_n^m \qquad (2.2)$$

with $B_2^0 = +3.53\ cm^{-1}$, $B_4^0 = +0.254\ cm^{-1}$, $B_6^0 = +0.123 \times 10^{-2} cm^{-1}$ and $B_6^6 = -5.25 \times 10^{-3} cm^{-1}$. With these parameters the wave functions of the four doublets become

$$\begin{aligned}
|a\rangle &= -\left|-\tfrac{5}{2}\right\rangle - 1.3 \times 10^{-2}\left|+\tfrac{7}{2}\right\rangle, \\
|b\rangle &= -\left|+\tfrac{5}{2}\right\rangle - 1.3 \times 10^{-2}\left|-\tfrac{7}{2}\right\rangle, \\
|c\rangle &= -\left|-\tfrac{3}{2}\right\rangle, \qquad |d\rangle = -\left|+\tfrac{3}{2}\right\rangle, \\
|e\rangle &= -\left|-\tfrac{1}{2}\right\rangle, \qquad |f\rangle = -\left|+\tfrac{1}{2}\right\rangle, \\
|g\rangle &= +\left|-\tfrac{7}{2}\right\rangle - 1.3 \times 10^{-2}\left|+\tfrac{5}{2}\right\rangle, \\
|h\rangle &= +\left|+\tfrac{7}{2}\right\rangle - 1.3 \times 10^{-2}\left|-\tfrac{5}{2}\right\rangle.
\end{aligned} \qquad (2.3)$$

In view of the measured value of $g_\perp$ (section 5) we have assumed an admixture in the $\left|-\tfrac{5}{2}\right\rangle$ state of 1.3×10^{-2} of $\left|+\tfrac{7}{2}\right\rangle$. The other parameters are fixed by the energy-level scheme and the wave functions of Harrop. The g values derived from this hexagonal spin hamiltonian are $g_{/\!/} = 5.7$ and $g_\perp = 0.08$.

2.3. *Direction of the pseudohexagonal axis.* About the value of χ_0, which determines the direction of the magnetic axis, there are two conventions, Dieke and Crosswhite [2a], Harrop [9] and others define χ_0 by a rotation of the crystal with respect to a magnetic field (denoted in the following by χ_0^H), while e.g. Jeffries et al. [4] give the position of the magnetic axis with respect to the crystal ξ axis, as is illustrated in fig. 2, hereafter denoted by χ_0. The derivation of χ_0^H from Harrop's crystal-field parameters, based on the angular variation of the Zeeman splitting, gives $\chi_0^H = 116^\circ$, while the experimentally determined value [2a] is

$\chi_0^H = 109^\circ$ (we found $\chi_0 = 70^\circ \pm 2$).

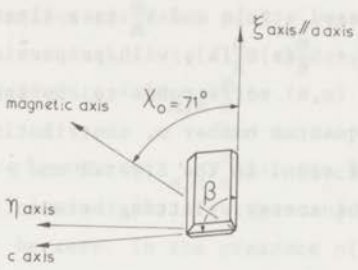

Fig. 2. Orientation of the various crystal axes in the chloride hexahydrates. The ζ axis coincides with the twofold symmetry axis (b axis) of the crystal, which is perpendicular to the plane of the figure. The ξ axis is parallel to the best developed crystal edge (a axis). β is defined as the obtuse angle between the a and c axes and χ_0 as the angle between the g_{max} axis and the ξ axis (see also text).

3. Electron spin-lattice relaxation in Yb:$YCl_3 \cdot 6H_2O$. The theory of the direct electron spin-lattice relaxation process as developed e.g. by Orbach [12] is given especially for hexagonal crystals. This theory is briefly summarized in section 3.1, including the existing methods to estimate the matrix elements of the orbit-lattice interaction potential. Section 3.2 is concerned with the theory for monoclinic crystals. It will be shown that two parameters are necessary to describe the electron spin-lattice relaxation rate. In section 3.3 a formula for T_{1e} is given, based on hexagonal symmetry. Only one parameter remains in the formula. A comparison between the two formulas is made in the same section.

3.1. *Orbach's relaxation theory.* The general expression, obtained by Orbach for the electron spin-lattice relaxation rate (T_{1e}^{-1}) when determined by one-phonon relaxation processes, is

$$T_{1e}^{-1} = \frac{3}{2\pi\rho v^5 \hbar} \left(\frac{\delta_{ab}}{\hbar}\right)^3 \coth\left(\frac{\delta_{ab}}{2kT}\right) \left|\langle a| \sum_{m,n} V_n^m |b\rangle\right|^2. \qquad (3.1)$$

The orbit-lattice interaction potential V_{OL}, responsible for the electron spin-lattice relaxation, is expanded in series of V_n^m: $V_{OL} = \Sigma_{m,n} \varepsilon V_n^m$. ε denotes an averaged strain and V_n^m is a linear combination of O_n^m and $O_n^m(s)$: $V_n^m = b_n^m O_n^m + b_n^m(s) O_n^m(s)$, with proportionality constants b_n^m and $b_n^m(s)$. The notation (m,n) corresponds to the spherical harmonics of degree n and azimuthal quantum number m, contributing to O_n^m and $O_n^m(s)$. v is the velocity of sound in the crystal and ρ the density of the crystal. δ_{ab} denotes the energy splitting between the lowest levels $|a\rangle$ and $|b\rangle$.

For hexagonal crystals Orbach gives the following estimate for the dynamic V_n^m. He sets the orbit-lattice terms V_n^m (which in the case of hexagonal symmetry can be written as $b_n^m O_n^m$) approximately equal in magnitude to the static crystal-field parameters $\overline{V}_n^m = B_n^m O_n^m$:

$$b_n^m = |B_n^0| \quad \text{when } n = 2 \text{ or } 4; \quad b_6^m = (|B_6^0|^{6-|m|} |B_6^6|^{|m|})^{1/6} \tag{3.2}$$

This very rough approximation can be understood, see e.g. Orton [13], in the following way: $V_{OL} \propto (\partial B_n^m/\partial R)\Delta R \propto -(n+1)B_n^m \varepsilon$, in which ΔR is the displacement in the ligand position, R, caused by the lattice vibrations and $\varepsilon = \Delta R/R$. Scott and Jeffries [14] relate the dynamic V_n^m to the static $\overline{V}_n^m$ by the normalizing factors g_n^m:

$$V_n^m = g_n^m |\overline{V}_n^m|. \tag{3.3}$$

Relation (3.3) is obtained from the good empirical rule $|\widehat{B_n^m}| = |\widehat{B_n^0}|$, where $\widehat{B_n^m}$ are the coefficients of the static crystal-field interaction $H_c = \Sigma_{n,m} \widehat{B_n^m} r^n Y_n^m(\theta,\phi)$ with n = 2,4,6 and $|m| \leq n$. This equality gives rise to eq. (3.3), because in the dynamic spin-lattice interaction $H_c' = \Sigma_{n,m} \widehat{b_n^m} r^n Y_n^m(\theta,\phi)$ it can be assumed that $|\widehat{b_n^m}| = |\widehat{B_n^m}|$ in a first approximation (see above).

3.2. *Relaxation theory for monoclinic crystals.* The estimates of Orbach and Scott and Jeffries are not applicable to monoclinic crystals. For example, Harrop's coefficients, expressed as $\widehat{B_n^m}$, are unequal for different m values at the same n, while expression (3.3) is based on the

rule $|\widehat{B_n^m}| = |\widehat{B_n^0}|$. Because of the problems involved in estimating the magnitude of the dynamic crystal-field parameters, we shall try to derive only a qualitative expression of T_{1e}, starting from the general equation (3.1), i.e. our task is to find the angular and field dependence of the matrix elements $\langle a|\Sigma_{m,n} V_n^m|b\rangle$.

3.2.1. *The matrix elements* $\langle a|\Sigma_{m,n} V_n^m|b\rangle$. Since the ionic ground state is a Kramers doublet, $|a\rangle$ and $|b\rangle$ are time-conjugate states and the matrix elements will be zero. In the presence of a magnetic field wave functions of higher states are admixed to those of the ground doublet and these must be substituted for $|a\rangle$ and $|b\rangle$ in the matrix elements. We shall confine ourselves to the experimental situation (fig. 3), in which the monoclinic ζ axis is directed in the horizontal x-y plane, while the direct-current field $\vec{H}_{dc}$ can be rotated in this plane. Let ϕ denote the angle between $\vec{H}_{dc}$ and the ζ axis, θ the angle between $\vec{H}_{dc}$ and the pseudohexagonal axis (the g_{max} axis), ε the angle between the g_{max} axis and the vertical z axis and δ the angle between the ξ axis and the y axis. The x axis is chosen parallel to the monoclinic crystal axis. We label the wave function of the ground doublet with the symbols $|\pm\frac{1}{2}p\rangle$, and of the first higher state with $|\pm\frac{1}{2}q\rangle$. The $\pm$ signs are related to the time-conjugate character of the two eigenstates in the absence of a magnetic field. The energy difference between the $|p\rangle$ and $|q\rangle$ states is denoted by Δ_q. Admixture of the other states gives the same angular and magnetic-field dependence as the $|\pm\frac{1}{2}q\rangle$ state in the matrix elements, and are for simplicity omitted in this derivation. First-order perturbation theory gives for the admixed state $|-\frac{1}{2}p'\rangle$ and $|+\frac{1}{2}p'\rangle$:

$$|-\tfrac{1}{2}p'\rangle = |-\tfrac{1}{2}p\rangle - A\vec{H}_{dc}\cdot(\langle-\tfrac{1}{2}q|\vec{J}|-\tfrac{1}{2}p\rangle|-\tfrac{1}{2}q\rangle + \langle+\tfrac{1}{2}q|\vec{J}|-\tfrac{1}{2}p\rangle|+\tfrac{1}{2}q\rangle)/\Delta_q,$$

$$|+\tfrac{1}{2}p'\rangle = |+\tfrac{1}{2}p\rangle - A\vec{H}_{dc}\cdot(\langle-\tfrac{1}{2}q|\vec{J}|+\tfrac{1}{2}q\rangle|-\tfrac{1}{2}q\rangle + \langle+\tfrac{1}{2}q|\vec{J}|+\tfrac{1}{2}p\rangle|+\tfrac{1}{2}q\rangle)/\Delta_q, \qquad (3.4)$$

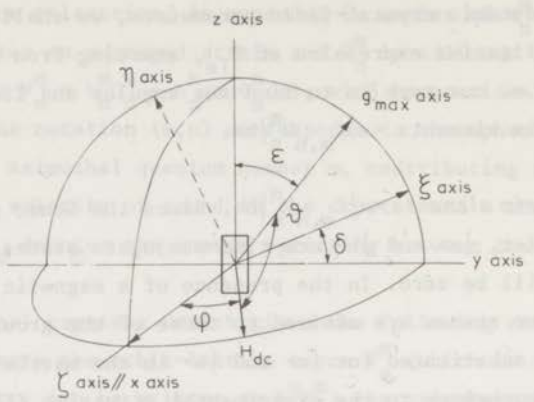

Fig. 3. In the experimental situation the chloride crystals were mounted with the ξ-η plane vertically. The angle between $\vec{H}_{dc}$ and the ζ (laboratory x) axis is denoted by ϕ, while θ denotes the angle between the g_{max} axis and $\vec{H}_{dc}$. δ is defined as the angle between the crystal ξ axis and the horizontal plane, and ε as the angle between the g_{max} axis and the vertical z axis. The positions of the ξ, η, and ζ axes with respect to the laboratory frame are found by cross-relaxation experiments after adiabatic demagnetizations, as described in I.

with $A = \Lambda\mu_B$. Λ denotes the Landé factor and μ_B the Bohr magneton. Choosing the ζ axis as quantization axis and omitting zero terms, eq. (3.4) becomes

$$|-\tfrac{1}{2}p'\rangle = |-\tfrac{1}{2}p\rangle - (AH_{dc}\sin\phi(j_\eta^-\sin\delta + j_\xi^-\cos\delta)|-\tfrac{1}{2}q\rangle$$

$$-AH_{dc}\cos\phi j_\zeta^-|+\tfrac{1}{2}q\rangle)/\Delta_q,$$

$$|+\tfrac{1}{2}p'\rangle = |+\tfrac{1}{2}p\rangle - (AH_{dc}\sin\phi(j_\eta^+\sin\delta + j_\xi^+\cos\delta)|+\tfrac{1}{2}q\rangle$$

$$-AH_{dc}\cos\phi j_\zeta^+|-\tfrac{1}{2}q\rangle)/\Delta_q,$$

with

$$j^{-}_{\xi,\eta} = \langle -\tfrac{1}{2}q|J_{x,y}|-\tfrac{1}{2}p\rangle, \qquad j^{+}_{\xi,\eta} = \langle +\tfrac{1}{2}q|J_{x,y}|+\tfrac{1}{2}p\rangle,$$
$$j^{-}_{\zeta} = \langle +\tfrac{1}{2}q|J_{z}|-\tfrac{1}{2}p\rangle, \qquad j^{+}_{\zeta} = \langle -\tfrac{1}{2}q|J_{z}|+\tfrac{1}{2}p\rangle. \tag{3.5}$$

The matrix elements $\langle -\frac{1}{2}p'|\Sigma_{m,n}V^{m}_{n}|+\frac{1}{2}p'\rangle$ can now be written, in a first approximation in A/Δ_{q}, as

$$\langle -\tfrac{1}{2}p'|\sum_{m,n}V^{m}_{n}|+\tfrac{1}{2}p'\rangle$$
$$= AH_{dc}\sin\phi(\alpha\sin\delta + \beta\cos\delta) + AH_{dc}\gamma\cos\phi\ , \tag{3.6}$$

with

$$\alpha = -(j^{+}_{\eta}\langle -\tfrac{1}{2}p|\sum_{m,n}V^{m}_{n}|+\tfrac{1}{2}q\rangle + j^{-}_{\eta}\langle -\tfrac{1}{2}q|\sum_{m,n}V^{m}_{n}|+\tfrac{1}{2}p\rangle)/\Delta_{q},$$
$$\beta = -(j^{+}_{\xi}\langle -\tfrac{1}{2}p|\sum_{m,n}V^{m}_{n}|+\tfrac{1}{2}q\rangle + j^{-}_{\xi}\langle -\tfrac{1}{2}q|\sum_{m,n}V^{m}_{n}|+\tfrac{1}{2}p\rangle)/\Delta_{q},$$
$$\gamma = -(j^{-}_{\zeta}\langle +\tfrac{1}{2}q|\sum_{m,n}V^{m}_{n}|+\tfrac{1}{2}p\rangle + j^{+}_{\zeta}\langle -\tfrac{1}{2}q|\sum_{m,n}V^{m}_{n}|-\tfrac{1}{2}p\rangle)/\Delta_{q}.$$

In our experimental configuration the matrix elements are dependent on the magnitude of the magnetic field, the angle between the ξ axis and the y axis (δ), and the angle between $\vec{H}_{dc}$ and the monoclinic symmetry axis (ϕ). The coefficients α, β and γ are determined by the orbit-lattice interaction potential and the wave functions of the various doublets in the $^{2}F_{7/2}$ multiplet.

3.2.2. *Equation for the electron spin-lattice relaxation.* With the aid of the expression derived for the matrix elements of the dynamic crystal-field interaction between the states of the lowest Kramers doublet in the presence of a magnetic field, the expression for T^{-1}_{1e} becomes

$$T^{-1}_{1e} = -\frac{3}{2\pi\rho v^{5}\hbar}\left(\frac{g_{max}\mu_{B}H_{dc}\sin\phi\sin\varepsilon}{\hbar}\right)^{3}$$
$$\times \coth\left(\frac{g_{max}\mu_{B}H_{dc}\sin\phi\sin\varepsilon}{2kT}\right) H^{2}_{dc}A^{2}\gamma^{2}|\cos\phi + \kappa\sin\phi|^{2}, \tag{3.7}$$

where $\kappa = (\alpha\sin\delta + \beta\cos\delta)/\gamma$ is in general a complex coefficient. In the derivation of eq. (3.7) we have set $\delta_{ab} = g_{max}\mu_B H_{dc}\sin\varepsilon\sin\phi$, because of the small g_{min} value. For Yb^{3+} in $YCl_3 \cdot 6H_2O$ eq. (3.7) can be written as

$$T_{1e}^{-1} = 0.32 \times 10^{-2} H_{dc}^5 (\sin\phi\sin\varepsilon)^3 \gamma^2 |\cos\phi + \kappa\sin\phi|^2 \coth(\delta_{ab}/2kT), \tag{3.8a}$$

in which H_{dc} denotes the magnetic field in kOe and with T_{1e}^{-1} in s^{-1}. Eq. (3.8a) becomes in the high-temperature approximation $\delta_{ab} \ll kT$:

$$T_{1e}^{-1} = 1.7 \times 10^{-2} H_{dc}^4 T(\sin\phi\sin\varepsilon)^2 \gamma^2 |\cos\phi + \kappa\sin\phi|^2. \tag{3.8b}$$

Besides the known parameters of field strength, lattice temperature and the angles ε and ϕ, two unknown parameters γ and κ determine the electron spin-lattice relaxation rate. The value of γ is independent of the orientation of the pseudohexagonal axis, but the value of the complex quantity κ may change when ε is varied.

3.3. *Hexagonal symmetry*. Starting from the hexagonal crystal-field parameters, listed in eq. (2.2) we derive according to the procedure of Orbach for the electron spin-lattice relaxation rate

$$T_{1e}^{-1} = 0.32 \times 10^{-2} H_{dc}^5 \cos^3\theta (0.64\sin\theta + 0.012\cos\theta)^2 \coth(\delta_{ab}/2kT). \tag{3.9a}$$

Again H_{dc} denotes the magnetic field in kOe and $\delta_{ab} \simeq g_{\parallel}\mu_B H_{dc}\cos\theta$. In the high-temperature approximation eq. (3.9a) can be written, neglecting the small term $0.012\cos\theta$, as

$$T_{1e}^{-1} = 1.7 \times 10^{-2} H_{dc}^4 T\cos^2\theta (0.64\sin\theta)^2. \tag{3.9b}$$

In eq. (3.9b) there is only one parameter, which has to be determined from experiment. This parameter, 0.64, is calculated according to Orbach, but using the estimate of the dynamical crystal-field parameters of Scott and Jeffries the coefficient becomes a factor 10^2 larger. However, once this parameter is fixed by experiment, all data can be

described independently of the value of the angle ε. From a comparison between eq. (3.8) and eq. (3.9) it is obvious, that when nearly hexagonal symmetry is present, eq. (3.9) is to be preferred, because of the occurrence of only one unknown parameter in the relaxation formula.

In both eqs. (3.8) and (3.9) we have neglected the value of $g_\perp$. When taken into account, δ_{ab} remains unequal to zero for $\phi = 0$ (or $\theta = 90^\circ$), with $T_{1e}^{-1} \neq 0$ as a consequence for this angle. It may be remembered that the admixture of $|\frac{5}{2}\rangle$ and $|\frac{7}{2}\rangle$ in the ground state, responsible for the $g_\perp \neq 0$ value, gives rise to a finite relaxation time in the parallel direction ($\theta = 0^\circ$), which is more than a factor 10^3 slower than in the $\theta = 45^\circ$ direction.

4. Relation between proton and electron spin-lattice relaxation times.

It is generally acknowledged that proton spin-lattice relaxation at low temperatures proceeds practically entirely via paramagnetic impurities. Various mechanisms for nuclear spin-lattice relaxation via electron spins have been discussed in ref. 1 with particular emphasis on the proton relaxation in dilute Dy- and Yb-ethyl-sulfate single crystals. The electron spin system must be considered to consist of a Zeeman system, corresponding to the Zeeman energy splitting in a magnetic field, and a dipole-dipole system or reservoir (abbreviated as DDR), which is determined by the spin-spin interaction between the electron spins. It was demonstrated that nuclear relaxation to the lattice proceeds via the electron-spin Zeeman system, called Bloembergen relaxation, and via the DDR, referred to as dipole relaxation. The two processes could be untangled by creating such circumstances of electron-spin concentration, magnetic field and temperature that one is favoured above the other. It was also shown that proton-spin diffusion plays an important role, for example in the ratio between T_{1e} and T_{1n}. Since the single-ion properties of the Yb ions in the Y-chloride lattice qualitatively resemble those of the Yb and Dy ions in yttrium ethyl sulfate and since further also the temperature and magnetic-field regimes are the same, we expect the same mechanisms to be operative. In analogy to the situation in Yb:YES, relaxation via the DDR is expected to dominate the Bloembergen relaxation for Yb concentrations of the order of 1 at.%. When the

concentration, c, becomes very small or the ratio between magnetic-field and lattice temperature, H/T, sufficiently high, electron spin-lattice interaction gives nuclear relaxation, because the wave functions of the electron-spin Zeeman system are admixed with those of the proton-spin Zeeman system by the dipolar interaction. If, like in Yb:YES and Dy:YES, a sufficiently rapid spin diffusion is supposed, even to protons nearest to the Yb ion, the Bloembergen relaxation rate becomes

$$T_{1n}^{-1} = 0.53 \times 10^{-2} H_{dc}^{-2} T_{1e}^{-1} \, c/\cosh^2\chi, \tag{4.1}$$

with $\chi = \delta_{ab}/2kT$ and H in kOe. In the derivation of eq. (4.1) the minimum proton-ytterbium distance, r_1, is assumed to be $r_1 = 3.0$ Å (section 2.1). Combining eq. (3.8a) and eq. (4.1) results in

$$T_{1n}^{-1} = 0.34 \times 10^{-4} c H_{dc}^{3} (\sin\phi \sin\varepsilon)^3 \gamma^2 |\cos\phi + \kappa \sin\phi|^2 / \sinh 2\chi, \tag{4.2}$$

for the monoclinic symmetry, while a combination of eq. (3.9a) and eq. (4.1) gives for the hexagonal crystal-field symmetry

$$T_{1n}^{-1} = 0.34 \times 10^{-4} c H_{dc}^{3} \cos^3\theta (0.64\sin\theta + 0.012\cos\theta)^2 / \sinh 2\chi. \tag{4.3}$$

In the following the term $0.012\cos\theta$ will be omitted, because even for $\theta = 0^\circ$ this term is most likely dominated by other processes.

5. Experimental results on T_{1n} in Yb:$YCl_3 \cdot 6H_2O$. The proton relaxation times were measured by determining the time constant of the decay of the NMR signal as a function of time after the protons had been polarized by rotational cooling. The continuous-wave method was applied as is described in I. We shall first present the experimental data and give some general features, while in sections 5.2 and 5.3 the influence of Bloembergen- and dipole-relaxation mechanisms are discussed. Section 5.4 is concerned with the cross-relaxation region near $\theta = 90^\circ$ and in section 5.5 attention is given to the influence of proton-spin diffusion in the T_{1n}/T_{1e} ratio.

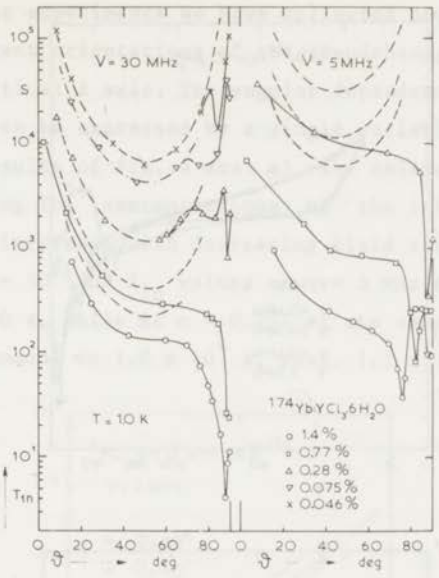

Fig. 4. Proton spin-lattice relaxation time T_{1n} (in s) in ^{174}Yb:$YCl_3 \cdot 6H_2O$ measured at ν = 30 MHz and ν = 5 MHz, and T = 1.0 K, as a function of the angle θ, plotted for various Yb concentrations. θ is the angle between magnetic field and the g_{max} direction. The full-drawn lines connect the experimental data points, while the theoretical predictions are dotted in the figure. The ν = 30 MHz data show, that varying the Yb concentration at this field by a factor 30 (at $\theta = 50^o$) results in a change in T_{1n} by a factor 50. At ν = 5 MHz a change of a factor 50 in T_{1n} (at $\theta = 50^o$) is obtained by varying the concentration by only a factor 5.

5.1. *Experimental data.* In fig. 4 the measured proton spin-lattice relaxation time T_{1n} in Yb:$YCl_3 \cdot 6H_2O$ is plotted versus the angle θ, subtended by the direct-current field H_{dc} and the pseudohexagonal axis. The results on various concentrations ($0.05\% \leq c \leq 1.4\%$) of the rare-earth ion have been simultaneously shown in one figure. All data in the diagram are taken at the same temperature, T = 1.0 K, and at two different

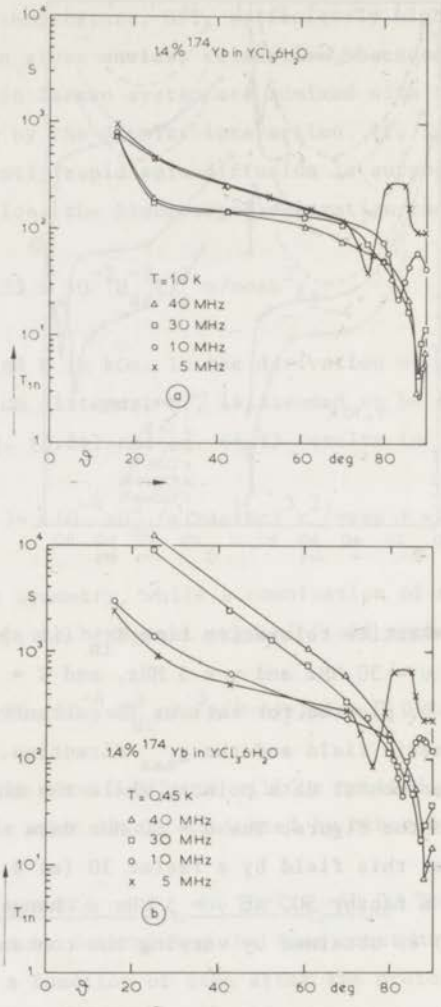

Fig. 5. T_{1n} (in s) in $YCl_3 \cdot 6H_2O$ with 1.4% ^{174}Yb, measured at four frequencies, hence four different magnetic fields, ν = 5, 10, 30 and 40 MHz is plotted versus θ at T = 1.0 K in fig. 5a and at T = 0.45 K in fig. 5b. The high electron-spin polarization values at ν = 30 MHz and ν = 40 MHz, at T = 0.45 K for small θ give a drastic increase in the nuclear-relaxation time with respect to the values at T = 1.0 K.

field strengths, hence two different proton-resonance frequencies (5 and 30 MHz). In our experiments we have collected data on T_{1n} of various crystals at different orientations of the pseudohexagonal axis with respect to the vertical z axis. The angular dependence of the measured relaxation times can be expressed by a single variable, θ. The main features of the results of fig. 4 are: a) the relaxation times become longer at decreasing Yb^{3+} concentrations; b) the influence of the concentration on T_{1n} increases with decreasing field strength. For example at c = 1.4% and $\theta = 50^{o}$ the T_{1n} values at ν = 5 MHz and ν = 30 MHz are resp. 200 s and 130 s, while at c = 0.28% at the same angle the nuclear relaxation times amount to 1.0×10^{4} s, resp. 1.1×10^{3} s.

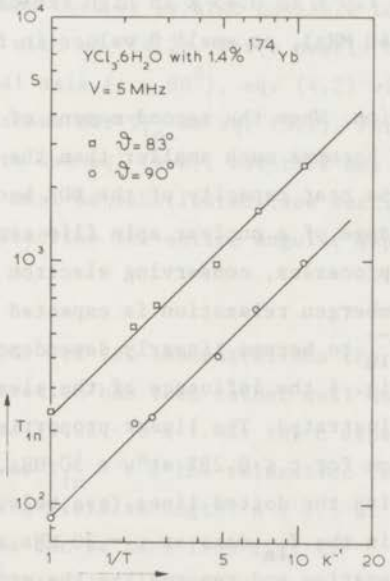

Fig. 6. T_{1n} (in s) in $YCl_3 \cdot 6H_2O$ with 1.4% ^{174}Yb is plotted versus 1/T at ν = 5 MHz. The linear proportionality between T_{1n} and 1/T is expected for a direct relaxation process, when the Zeeman splitting of the electron spins is much smaller than kT.

The temperature dependence of T_{1n} can be judged from the differences between fig. 5a and fig. 5b. The nuclear spin-lattice relaxation

time is measured over the whole angular region for c = 1.4% Yb^{3+} at four frequencies (5, 10, 30 and 40 MHz) and at two different temperatures T = 1.0 K (fig. 5a) and T = 0.45 K (fig. 5b). In fig. 6 two angles $\theta = 90^{o}$, resp. $\theta = 83^{o}$ are selected for a T_{1n} versus 1/T plot down to 0.1 K at ν = 5 MHz using the same crystal as in fig. 5. These data exhibit (for $\delta_{ab} \ll kT$) a linear proportionality between nuclear spin-lattice relaxation rate and temperature, which bears out the occurrence of a direct process in the electron spin-lattice relaxation. When the high-temperature approximation is no longer allowed, T_{1n} becomes proportional to $\exp(\delta_{ab}/2kT)$. This circumstance is responsible for the drastic increase in the nuclear-relaxation time when the temperature is lowered from 1.0 K to 0.45 K in high fields, resp. high frequencies (30 MHz and 40 MHz), at small θ values in fig. 5.

5.2. *Bloembergen relaxation.* When the second moment of the electron-spin resonance line (M_2) becomes much smaller than the squared nuclear Zeeman splitting (Δ_n^2), the heat capacity of the DDR becomes very small, while also the energy change of a nuclear spin flip cannot be matched by electronic flip-flop processes, conserving electron Zeeman energy. Hence, if $M_2 \ll \Delta_n^2$, Bloembergen relaxation is expected to dominate the dipole relaxation, and T_{1n}^{-1} to become linearly dependent on the electron-spin concentration. In fig. 4 the influence of the electron-spin concentration is clearly illustrated. The linear proportionality holds over a wide angular region for $c \leq 0.28\%$ at ν = 30 MHz, which can be seen from a comparison with the dotted lines (see below) in the figure. So we shall try to explain the T_{1n} data at ν = 30 MHz and c = 0.046% in terms of Bloembergen relaxation and renormalize the proportionality constant 1.40 in eq. (4.3) in order to fit the experimental points. As a result we obtain the following relation (dotted in the figure)

$$T_{1n}^{-1} = 1.4 \times 10^{-4} c H_{dc}^{3} \sin^{2}\theta \cos^{3}\theta / \sinh 2\chi. \qquad (5.1)$$

In analogy with the ethyl sulfates we assume eq. (4.1) to be correct and then we arrive at the following relation for the electron spin-lattice relaxation rate

$$T_{1e}^{-1} = 1.3 \times 10^{-2} H_{dc}^{5} \sin^{2}\theta\cos^{3}\theta/\tanh\chi. \qquad (5.2)$$

The relaxation rate, predicted by eq. (5.2) is higher than T_{1e}^{-1}, as calculated from Orbach's formulas in eq. (3.9a) but smaller than the T_{1e}^{-1} value according to Jeffries. Susceptibility measurements [15] in powdered $YbCl_3 \cdot 6H_2O$ at liquid-helium temperatures give for the direct relaxation process $T_{1e}^{-1} = 0.9 \times 10^{-2} H^4 T$. The electron spin-lattice relaxation for a powder, calculated from our T_{1n} data, is given by $T_{1e}^{-1} = 0.92 \times 10^{-2} H^4 T$. This quantitative agreement justifies the diffusion assumption, made in section 4.

It may be remarked that it is also possible to fit the data, represented in fig. 4, with eq. (4.2). For a nearly horizontal direction of the pseudohexagonal axis ($\varepsilon \approx 90^{o}$), eq. (4.2) with $\kappa \approx 0$ and $\gamma^2 = 4.1$ gives the same values for T_{1n} as eq. (5.1). For smaller ε values it remains possible to use eq. (4.2), but this has the disadvantage that a complex $\kappa \neq 0$ must be substituted (see section 3), while eq. (5.1) is capable to describe the entire angular dependence using only one parameter.

5.3. *Dipole relaxation.* For low concentrations the linear dependence of T_{1n}^{-1} on the concentration has been rather well established (fig. 4). At high concentrations ($0.28 < c \leq 1.4\%$) the c dependence is less simple. When written as $T_{1n}^{-1} \propto c^{n}$, the relaxation rate shows a decreasn value with increasing field strength: $n \approx 2.5$ at $\nu = 5$ MHz, while at $\nu = 30$ MHz $n \approx 1.3$, as can be seen from fig. 4.

Khutsishvili [16] has given a survey concerning the influence of the DDR in the nuclear spin-lattice relaxation. He considered a particular situation, in which the contact between nuclear spins and DDR is supposed to be much better than that between nuclear spins and lattice (via the electronic Zeeman system), while also the heat capacity of the dipole system (C_D) is of the same order or smaller than the heat capacity of the nuclear Zeeman system (C_I). Under these circumstances, which are expected to occur at low temperatures and not too low electron-spin concentrations, the nuclear Zeeman and the electronic

dipole systems approach the lattice temperature at a rate T_{1n}^{-1} given by

$$T_{1n}^{-1} = \left(\frac{C_D}{C_I + C_D}\right)T_{DL}^{-1} + \left(\frac{C_I}{C_I + C_D}\right)T_{IL}^{-1} \qquad (5.3)$$

T_{DL} and T_{IL} denote the time constants of the contact between DDR resp. nuclear Zeeman system and the lattice. If $C_D/C_I \gg T_{DL}/T_{IL}$, T_{1n}^{-1} depends quadratically on the concentration of the electron spins; a concentration dependence of the electron spin-lattice relaxation can give a proportionality $T_{1n} \propto c^n$ with $2 \leq n \leq 3$. In view of the measured influence of the electron-spin concentration at $\nu = 5$ MHz ($n \simeq 2.5$) we shall apply eq. (5.3) to the results, obtained at $H_{dc} = 1.17$ kOe ($\nu = 5$ MHz), $c = 1.4\%$ and $T = 1.0$ K. Assuming a homogeneous line-width for the electron spins, gives [16] $(C_D)/(C_I + C_D) = M_2/(2N_nN_e^{-1}\Delta_n^2 + M_2)$, in which N_n and N_e denote the number of nuclear, resp. electron spins per cm^3. By substituting for M_2 the calculated [16] second moment of the dipolar line broadening and for $T_{1e}(= 2T_{DL})$ the result of eq. (5.2) the calculated nuclear spin-lattice relaxation time at $H_{dc} = 1.17$ kOe, $c = 1.4\%$ and $\theta = 50^\circ$ becomes $T_{1n} \simeq 10$ s. This is a lower limit in view of the assumed intimate contact between nuclear Zeeman system and the DDR. Although the experimental $T_{1n} \simeq 10^2$ s does not agree with this dipole relaxation limit, it is very much shorter than the Bloembergen prediction of 10^4 s. Hence we conclude dipolar relaxation to be important.

5.4. *Cross-relaxation.* When the Zeeman splitting of the electron spins becomes commensurate to the dipolar line-width (see I) a minimum in T_{1n} is expected to occur, because of the maximum in the total dipolar heat capacity as a function of θ. When the direct-current field H_{dc} is rotated to the perpendicular direction ($\theta = 90^\circ$) the dipolar heat capacity first increases because of the combination of the dipole and Zeeman systems. If the $g_\perp$ value is very small the contribution of the Zeeman energy vanishes at $\theta = 90^\circ$. The angle θ_{min}, corresponding with the minimum in T_{1n} as a function θ, satisfies the equation

$$H_{dc}\left[(g_{/\!/}\mu_B\cos\theta_{min})^2 + (g_\perp\mu_B\sin\theta_{min})^2\right]^{\frac{1}{2}} = \text{constant } (\equiv \Delta_{min}). \qquad (5.5)$$

In figs. 7a and 7b the influence of field variation on θ_{min} is shown at two different Yb concentrations, while in fig. 7c the influence of concentration variation is illustrated at constant field H_{dc} = 1.17 kOe. The shift in θ_{min} in fig. 7a and fig. 7b can be represented by eq. (5.5) with $\Delta_{min} = 14.4 \times 10^{-18}$ erg for c = 1.4% and $\Delta_{min} = 7.4 \times 10^{-18}$ erg for c = 0.77%. From the concentration dependence of Δ_{min}, demonstrated in fig. 7c it is concluded that line broadening is indeed responsible for the observed effect. The Δ_{min} value for c = 0.28% according to eq. (5.5) is 2.6×10^{-18} erg. The calculated dipolar (gaussian) linewidths [17] expressed in energy units, are in the same sequence

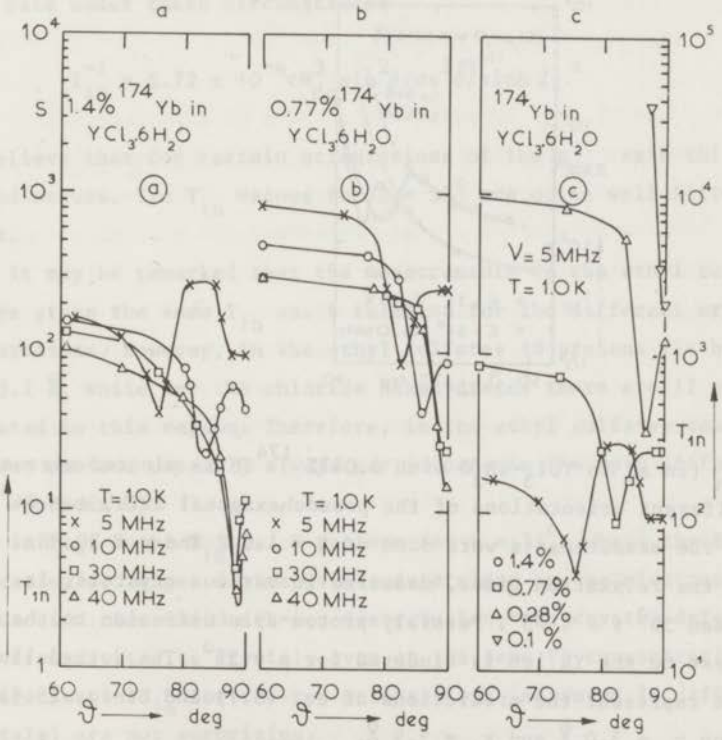

Fig. 7. T_{1n} (in s) in $YCl_3 \cdot 6H_2O$ with 1.4% ^{174}Yb and 0.77% ^{174}Yb is plotted versus θ at four frequencies (ν = 5, 10, 30 and 40 MHz) at T = 1.0 K in figs. 7a and 7b, while in fig. 7c a plot of T_{1n} vs. θ is made at fixed field H = 1.17 kOe (ν = 5 MHz) as a function of the Yb concentration. The figure illustrates the dependence of θ_{min} on H and on Yb concentration.

3.8×10^{-18} erg, 2.8×10^{-18} erg and 1.7×10^{-18} erg. The reasonable agreement between the experimental results and the predictions of eq. (5.5) again confirm, as in the ethyl sulfates, the important role of the electron spin-spin interaction in the cross-relaxation region.

5.5. *Proton-spin diffusion.* In order to observe effects of the monoclinic symmetry, nuclear spin-lattice relaxation measurements were performed with various orientations of the pseudohexagonal axis in the vertical plane ($10^{\circ} \leq \varepsilon \leq 90^{\circ}$). At some orientations of the g_{max} axis T_{1n} appeared

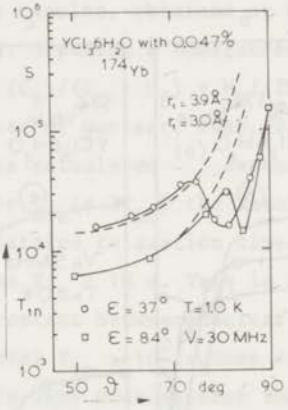

Fig. 8. T_{1n} (in s) in $YCl_3 \cdot 6H_2O$ with 0.047% ^{174}Yb is plotted versus θ for two different orientations of the pseudohexagonal axis, $\varepsilon = 84^{\circ}$ and $\varepsilon = 37^{\circ}$. The measurements were done at T = 1.0 K and ν = 30 MHz. The ratio of the relaxation times, measured in various crystals, is about 2 between $50^{\circ} \leq \theta \leq 75^{\circ}$. Possibly proton-spin diffusion to the protons nearest to the Yb ion is hindered for $\varepsilon = 37^{\circ}$. The dotted lines in the figure represent the predictions of eq. (5.1) and of eq. (5.6), based resp. on r_1 = 3.0 Å and r_1 = 3.9 Å.

to be about two times longer than expected from the $\varepsilon \simeq 90^{\circ}$ results. Fig. 8 gives an illustration of the above-mentioned effect. The nuclear-relaxation time, T_{1n}, is plotted versus θ for two different g_{max}

orientations, $\varepsilon = 84^{\circ}$ and $\varepsilon = 37^{\circ}$. For $50^{\circ} \leq \varepsilon \leq 75^{\circ}$ the ratio of the relaxation times is about 2. A possible explanation of this effect may be the distribution of protons around the rare-earth site. In the chloride hexahydrates twelve protons are situated at a distance of 3.0 Å, while the distance to the next-nearest protons amounts to 3.9 Å. When the proton-spin diffusion to the nearest protons is hindered by the internal field of the Yb ions, but spin diffusion to the next-nearest protons is still possible, the proportionality constant in eq. (4.1) becomes a factor $(3.9/3.0)^3$ smaller. Assuming the T_{1e}^{-1} expression of eq. (5.2) to be valid, we obtain for the nuclear spin-lattice relaxation rate under these circumstances

$$T_{1n}^{-1} = 0.72 \times 10^{-4} c H_{dc}^{3} \sin^{2}\theta \cos^{3}\theta / \sinh 2\chi. \qquad (5.6)$$

We believe that for certain orientations of the g_{max} axis this situation indeed occurs. The T_{1n} values for $\varepsilon = 37^{\circ}$ are quite well fitted by eq. (5.6).

It may be remarked that the measurements in the ethyl sulfates have always given the same T_{1n} vs. θ relation for the different crystal orientations. However, in the ethyl sulfates 18 protons lie between 3.0 and 3.2 Å, while for the chloride hexahydrates there are 12 protons situated in this region. Therefore, in the ethyl sulfates some of the nearest protons possibly always participate in the spin diffusion (see also appendix D).

In fig. 8 the T_{1n} vs. θ pattern for $\theta > 75^{\circ}$, where the Bloembergen relaxation no longer dominates, is determined by the electron spin-spin interaction. Because the Yb-ion distribution, the crystal defects etc. vary from crystal to crystal, even at the same Yb concentration, the differences in T_{1n} for the two orientations (measured in different crystals) are not surprising.

6. The minimum g value. The precise value of g_{min} is of essential importance in the operation of the nuclear-spin refrigerator. In our experiments information on g_{min} is obtained by comparing the maximum nuclear polarization, p_{nm}, as a function of θ at fixed field with the

maximum polarization as a function of magnetic field at fixed angle $\theta = 90^{o}$. The θ dependence of p_{nm} is measured with the pulsed field H_p directed along the z axis in such a way that during the pulse no compensation of the total field component along the g_{max} axis could occur. Cross-relaxation for θ values different from $\theta = 90^{o}$ is possible because of line broadening by the dipolar spin-spin interaction. We define θ_h as the field direction along which the nuclear polarization, p_{nm}, is half the maximum value reached at $\theta = 90^{o}$. The corresponding energy splitting of the electron spins Δ_h is field independent and related to θ_h in the following way:

$$\Delta_h = \{(g_{\parallel}\mu_B H_{dc}\cos\theta_h)^2 + (g_{\perp}\mu_B H_{dc}\sin\theta_h)^2\}^{\frac{1}{2}}. \qquad (6.1)$$

The field dependence of p_{nm}, measured at $\theta = 90^{o}$, is also determined by the dipolar broadening of the resonance line, e.g. for $g_{\perp}\mu_B H_{dc} >> \Delta_h$ no cross relaxation could occur. When the influence of the nuclear and electron spin-lattice relaxation can be neglected, the nuclear polarization will reach half its maximum value at H_h, related to Δ_h by:

$$\Delta_h = g_{\perp}\mu_B H_h. \qquad (6.2)$$

In fig. 9 the result of a p_{nm} vs. θ measurement at fixed field $H_{dc} = 1.17$ kOe is presented. Also shown is a p_{nm} vs. H_{dc} measurement at fixed angle $\theta = 90^{o}$. The polarizations were made in 0.05% $Yb:YCl_3 \cdot 6H_2O$ at T = 0.5 K. The maximum nuclear polarization, at a given H_p, is expressed in arbitrary units. With the data of fig. 9 and the aid of eq. (6.1) and eq. (6.2) it is easy to calculate the value of g_{min}. As a result we obtain $g_{min} = 0.08 \pm 0.01$.

Measurements at higher electron-spin concentrations show increased values of θ_h and H_h, which proves that dipolar line broadening is the relevant mechanism in fig. 9.

A calculation of the third-order electronic Zeeman splitting gives a correction in the electron Zeeman splitting, which is, however, very small, because of the large energy splittings between the various Kramers doublets. In a field of about 0.1 MOe perpendicular to the g_{max}

axis, this correction is only of the order of the nuclear Zeeman splitting. So, third-order Zeeman splitting has no influence on the interpretation of the results of fig. 9.

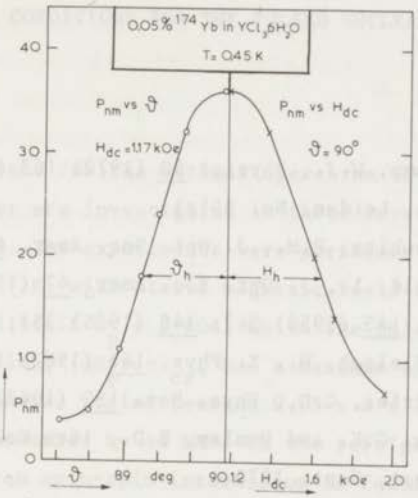

Fig. 9. The maximum obtainable proton polarization (dependent on the magnitude of the pulsed field and therefore given in arbitrary units) is plotted versus θ at fixed field H = 1.17 kOe on the left side and versus H at fixed angle $\theta = 90^{\circ}$ on the right side of the figure. The measurements were made in $YCl_3 \cdot 6H_2O$ containing only 0.05% ^{174}Yb in order to eliminate the influence of nuclear relaxation in the angle and field region concerned. The relation between θ_h and H_h yields a value for g_{min}, namely $g_{min} = 0.08 \pm 0.01$.

7. Conclusion. Proton polarization can be obtained in $^{174}Yb:YCl_3 \cdot 6H_2O$ by the nuclear-spin refrigerator method. As in the ethyl sulfates, the nuclear spin-lattice relaxation can be reasonably well described by the Bloembergen relaxation process at sufficiently low electron-spin concentration. The electron (and nuclear) spin-lattice relaxation appears to be determined by a direct process, which can be understood qualitatively by assuming a spin hamiltonian of hexagonal symmetry. The

experimental data on T_{1n} show an increasing influence of the dipole-dipole reservoir with increasing Yb concentration, completely analogous to the results in Yb:YES and Dy:YES. The measured g_{min} value is too large to make Yb:$YCl_3 \cdot 6H_2O$ a favourable crystal for obtaining large nuclear polarizations.

References.

1) Brom, H.B. and Huiskamp, W.J., Physica 60 (1972) 163 (Commun. Kamerlingh Onnes Lab., Leiden, No. 391a).

2a) Dieke, G.H. and Crosswhite, H.M., J. Opt. Soc. Amer. 46 (1956) 885.

2b) Dieke, G.H. and Leopold, L., J. Opt. Soc. Amer. 47 (1957) 944.

3) Kahle, H.G., Z. Phys. 145 (1956) 347; 145 (1956) 361; 155 (1959) 157. Kahle, H.G. and Kalbfleisch, H., Z. Phys. 166 (1962) 184.

4) Schulz, M.B. and Jeffries, C.D., Phys. Rev. 159 (1967) 277.

5) Kalvius, G.M., Shenoy, G.K. and Dunlap, B.D., 16th Colloque A.M.P.E.R.E., Bucharest, Sept. 1970.

6) Graeber, E.J., Conrad, G.H. and Duliere, S.F., Acta Cryst. 21 (1966) 1012.

7) Marezio, M., Plettinger, H.A. and Zachariasen, W.H., Acta Cryst. 14 (1961) 234.

8) Stohr, J., Olsen, D.N. and Gruber, J.B., J. Chem. Phys. 55 (1971) 4463.

9) Harrop, I.H., J. Chem. Phys. 42 (1965) 4000.

10) Eisenstein, J.C., J. Chem. Phys. 35 (1961) 2097.

11) Hutchings, M.T., Solid State Phys. 16 (1964) 227.

12) Orbach, R., Proc. Roy. Soc. A 264 (1961) 458.

13) Orton, J.W., Electron Paramagnetic Resonance, p. 159, Iliffe Books (London, 1968).

14) Scott, P.L. and Jeffries, C.D., Phys. Rev. 127 (1962) 32.

15) Brom, H.B., Soeteman, J. and Van Duyneveldt, A.J., 17th Colloque A.M.P.E.R.E., Turku, Aug. 1972.

16) Khutsishvili, G.R., Uspekhi Fiz. Nauk 96 (1968) 441, Soviet Physics-Uspekhi 11 (1969) 802.

17) De Boo, N., private communication.

CHAPTER 4

OPTIMAL CONDITIONS FOR THE PULSED NUCLEAR REFRIGERATOR

Synopsis.

The conditions for the optimal operation of the pulsed nuclear spin refrigerator are investigated in three crystals: Dy:YES, Yb:YES and Yb:$YCl_3 \cdot 6H_3O$. The experiments were performed in the temperature range $0.1 \leq T \leq 1$ K, with static magnetic field values $0.5 \leq H_{dc} \leq 10$ kOe and a pulsed field $H_p \leq 2$ kOe, while the pulsed field decay rate at cross-relaxation, $(dH_p/dt)_{cr}$, had a maximum of 50 kOe/s. The magnetic ion concentration was varied between $0.05 \leq c \leq 2\%$. Proton spin temperatures were measured by cw NMR. In the refrigeration process in all crystals, electron spin-spin interaction is found to play an important role, even at the lowest concentrations. In Dy:YES and Yb:$YCl_3 \cdot 6H_2O$, in which $g_\perp$ is determined to be about 0.08, the production of nuclear polarization through proton-electron spin flips is speeded up by spin-spin interaction, in the absence of which cross-relaxation transitions would be very unlikely. Conversely, in Yb:YES, it is concluded in particular from the field dependence of the ratio of the maximum proton polarization and electron-spin polarization, that spin-spin interaction in this crystal forms an obstacle in the polarization method. This appears as a relatively large $g_\perp^2$ value of 7×10^{-5}, compared with the squared proton g_n value of 9×10^{-6}.

Our results in Yb:YES indicate that proton polarizations of more than 70% could be realized. In view of the experiments of Potter and Stapleton it is suggested that an increase of $(dH_p/dt)_{cr}$ by a factor 200, at low Yb concentrations $c \leq 0.05\%$, will circumvent the problems of spin-spin interaction by reducing the apparent Yb spin $g_\perp$ value to $g_\perp \leq g_n$. The low concentrations then required, entail a polarization build-up and decay time of at least a few hours.

1. Introduction. We shall discuss experiments on proton polarization by the nuclear-spin refrigerator method [1-7] in three hexagonal or nearly hexagonal crystals. The samples investigated are $Y(C_2H_5SO_4)_3 \cdot 9H_2O$, doped with Yb^{3+} and Dy^{3+} ions (abbreviated as Yb:YES and Dy:YES resp.) and $YCl_3 \cdot 6H_2O$, doped with Yb^{3+} ions. These crystals have the following features in common. The lowest doublet of the rare-earth ions, which is the only populated energy level at liquid helium temperatures, has a very anisotropic magnetic behaviour. The electron-spin g value has a maximum along the hexagonal axis ($g_{\parallel} = g_{max}$) and a nearly zero value in the perpendicular plane ($g_{\perp} = g_{min} \approx 0$). The maximum g values for Yb^{3+} in YES, Dy^{3+} in YES and Yb^{3+} in $YCl_3 \cdot 6H_2O$ are resp. 3.4, 10.9, and 5.6. Therefore, the Zeeman energy splitting strongly depends on the direction of the magnetic field with respect to the g axes. This is favourable for nuclear-spin refrigeration, which method will now briefly be summarized. The rotation of a magnetic field from a direction where g is large to a direction along which g is small leads to substantial cooling of paramagnetic ions. If simultaneously the electron spins are thermally decoupled from the lattice as a result of anisotropy of the electron spin-lattice relaxation time, the electron spin system can be maintained at low temperatures for some time, typically 1 mK during 1 s. Therefore the electron-spin system can be utilized for cooling, provided that it does not require the lattice for heat transfer. The dipolar coupling between electron spins and nuclear spins, however, provides an effective means of thermal mixing if the nuclear and electron Zeeman energy splittings can be matched for cross-relaxation. The investigation of the matching conditions forms an essential part of this chapter. A more extensive introduction in the polarization method can be found in chapter 2 [6] referred to as I (chapter 3 [7] is referred to as II), where also the experimental equipment is described.

From the above given considerations two requirements can be deduced for the field configuration. One condition is that the magnetic component along the $g_{\parallel}$ axis can be made vanishingly small. Then the Zeeman energy splitting of the electron spins, now determined by the $g_{\perp}$ value, may become of the same order of magnitude as the nuclear Zeeman splitting. Further one requires a large electron-spin polarization just before the

thermal mixing.

The following arrangement of two perpendicular fields can meet both requirements. A pulsed field, H_p, is directed along the vertical z axis, while the hexagonal axis makes a small angle δ with the z axis. It should be emphasized that the pulsed field is large and constant during most of the pulse duration, while the no-pulse period, in which the pulsed field is reduced to practically zero, is comparatively short (see below). The direct-current field, $\vec{H}_{dc}$, is rotatable in the horizontal plane. The angle between $\vec{H}_{dc}$ and the x axis, which is chosen perpendicular to the (z, $g_{//}$) plane, is called ϕ, while θ denotes the angle between $\vec{H}_{dc}$ and the hexagonal axis (see fig. 1). With a pulsed field of

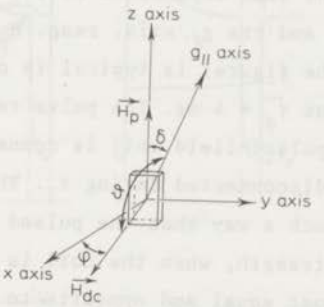

Fig. 1. Experimental configuration. The hexagonal axis makes a small angle δ with the vertical z axis, along which $\vec{H}_p$ is directed. The angle between $\vec{H}_{dc}$ and the x axis, which is perpendicular to the (z, $g_{//}$) plane is called ϕ, while θ denotes the angle between $\vec{H}_{dc}$ and the hexagonal axis.

a few kOe an appreciable electron-spin polarization is attainable, e.g. in Dy:YES H_p = 2.5 kOe at T = 0.4 K gives p_e = 0.98. For cross-relaxation one requires a vanishingly small magnetic field component along the $g_{//}$ axis, which can be fulfilled for small values of ϕ. Let us denote the static field component (rest field) along the hexagonal axis by H_r, which is equal to $H_{dc}\sin\phi\sin\delta$. Then a reduction of the pulsed field to $|H_r|\cos\delta \simeq |H_r|$ gives field cancellation (fig. 2) along the g_{max} axis, provided that the pulsed field is antiparallel to $\vec{H}_r$. If H_p is reduced

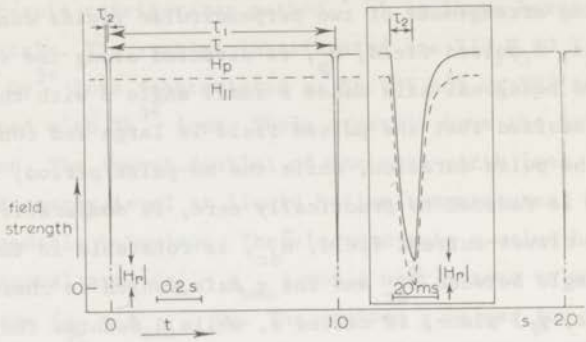

Fig. 2. Illustration of the time dependence of the magnetic-field components along the z axis and the $g_{//}$ axis, resp. H_p and $H_{//}$. The pattern of H_p (drawn line in the figure) is typical in our experiments. The pulse decay time-constant τ_d = 4 ms. The pulse repetition frequency ν_p = 1 Hz, or τ = 1 s. The pulsed-field coil is connected with its power source during τ_1 and disconnected during τ_2. The value of τ_2 = 10 ms in this case is chosen in such a way that the pulsed field has a minimum of 10% of its maximum strength, when the coil is reenergized. This minimum value ($\delta \approx 0^o$) is just equal and opposite to the rest field, $\vec{H}_r$, the component of H_{dc} along the $g_{//}$ axis. So, the time τ_2 is just sufficient for field cancellation along the $g_{//}$ axis, as illustrated by the dotted line ($H_{//}$) in the figure.

sufficiently fast, p_e remains constant until cross-relaxation between electron and proton spins occur. The cross-relaxation process tends to equalize the electron and proton temperature in a time much shorter than the electron spin-lattice relaxation time, T_{1e}.

As an example let us reconsider Dy:YES. If a static field H_{dc} = 1.2 kOe at T = 0.4 K is present, then in a pulsed field of 2.5 kOe, T_{1e} will become 0.05 s. So the equilibrium polarization $p_e \approx 0.98$ will be reached in about 0.2 s. Phonon bottleneck effects give perhaps a somewhat longer T_{1e}, but by choosing a pulse duration, τ_1, of one second the equilibrium polarization value is certainly reached at the end of

the pulse. Thereafter the pulsed field is reduced in a time short compared with T_{1e}, the pulse decay time constant, τ_d, being 3 ms typically. Hence the occupation density of the energy levels will remain constant. The pulsed-field coil is disconnected from its power source during a time τ_2, covering a few times τ_d. This procedure produces field cancellation along the $g_{//}$ axis, after which the pulse cycle is repeated. The complete pulse duration is denoted by $\tau = \tau_1 + \tau_2$. In fig. 3 and fig. 4

Fig. 3.

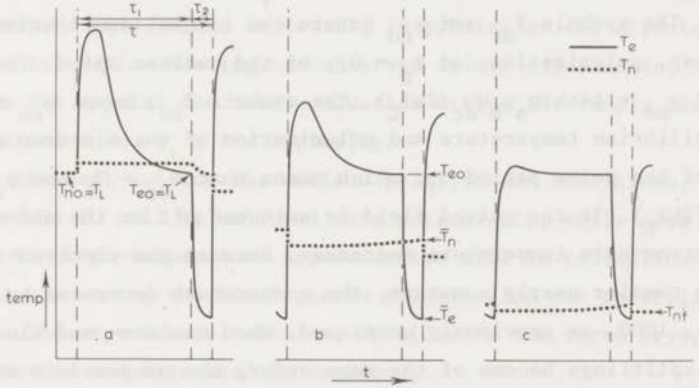

Fig. 4.

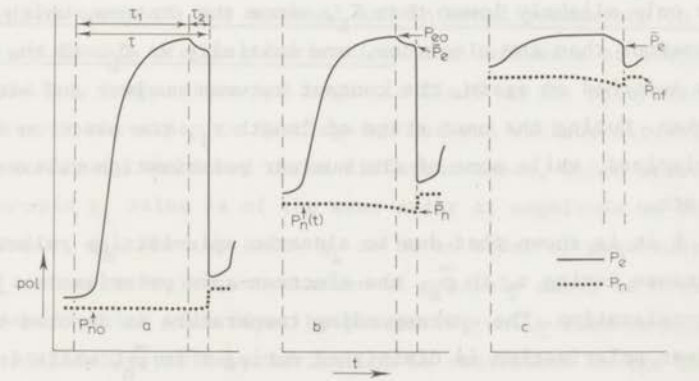

Fig. 3. and Fig. 4. (common caption). Temperature and polarization of electron-and proton-spin system during the refrigeration process. In fig. 3 and fig. 4 the temperature and polarization pattern of electron spins (drawn line) and proton spins (dotted line) are sketched for typical pulse cycles taken at the start, the middle and the end of the

pulse repetition sequence, in the figures a, b and c resp.. Also the various symbols used in section 2 are illustrated. In the initial situation $H_p = 0$ and the temperatures of electron and proton spins are equal to that of the lattice, T_L. If the pulsed field is switched on for the first time the electron-spin temperature rises enormously, for example by a factor thousand, because the occupation number of the electronic Zeeman energy levels remains nearly the same. When $\tau_1 >> T_{1e}$, the electron-spin temperature at the end of τ_1 has reached its equilibrium value. The symbols T_{no} and p_{no} denote the initial equilibrium temperature, resp. polarization (at $H_p = 0$), of the nuclear spins. Thus $T_{no} = T_L$ and $p_{no} = \tanh(g_n \mu_B H_{dc}/2kT_L)$. The symbols T_{eo}, resp. p_{eo} represent the equilibrium temperature and polarization of the electron spins at the end of the pulse period τ_1, which means that $T_{eo} = T_L$ and $p_{eo} = \tanh(g_{//} \mu_B H_p/2kT_L)$. If the pulsed field is switched off at the end of τ_1, the electron-spin temperature decreases. Because the electron-spin polarization remains nearly constant, the temperature decreases by the same factor $\simeq 1000$, as previously mentioned. When nuclear- and electron-spin Zeeman splittings become of the same order, the temperature in both systems become equal. This means that the electron-spin temperature rises till a value only slightly lower than T_L, since the protons, which are much more numerous than the electrons, are initially at T_L. If the pulsed field is switched on again, the contact between nuclear and electron spins is broken. During the next stage of length τ_1, the electron spins will be repolarized, while some of the nuclear polarization relaxes to the lattice etc..

In fig. b it is shown that due to electron spin-lattice relaxation p_{eo} will decrease during τ_2 to $\overline{p}_e$, the electron-spin polarization just before cross-relaxation. The corresponding temperature is denoted by $\overline{T}_e$. The nuclear polarization is diminished during τ to $\overline{p}_n$, while in this case $\overline{T}_n$ gives the corresponding temperature.

In the final situation, see fig. c, in which a steady state is reached, the loss of nuclear polarization through relaxation is just compensated by the increase due to thermal mixing. The maximum polarization in this stage is denoted by p_{nf}, the temperature by T_{nf}. Obviously, in the absence of nuclear relaxation one has $\overline{T}_e = T_{nf}$. However, p_{nf} is in general unequal to $\overline{p}_e$, even if $T_{1n}^{-1} = 0$, see section 2.

we have illustrated the temperature, resp. polarization, behaviour of electron and proton-spin system during the refrigeration process.

The comparatively long electron spin-lattice relaxation times in Yb:YES requires a longer τ_1 than for Dy:YES. With our pulse equipment τ_1 can be varied between rather wide limits $0.001 \leq \tau_1 \leq 100$ s, while a τ_2 value as small as 1% of τ_1 can be realized. There is another limitation for τ_1, imposed by the requirement that the crystal should not be substantially heated during the pulse periods. Potter and Stapleton [5] have analyzed this aspect in detail, in particular the effects on non-resonant relaxation heating. As observed in our experiments, heat transfer from the crystal and heat conduction within the sample limit the pulse duration to $\tau_1 \geq 1$ s typically.

In the next section the various polarization conditions, as already mentioned in I, will be analyzed more extensively, while also the restriction to the high-temperature approximation will be reliquished in the formulas concerning the final proton polarization and polarization build-up rate. The experimental results, obtained in the three crystals, are presented and discussed in section 3.

2. The influence of the external and internal parameters on the maximum obtainable proton polarization. The influence of electron-spin concentration, temperature and magnetic field on the polarization process makes it necessary to distinguish between various situations. In I we have already mentioned three different cases, which arise when the electron-spin $g_\perp$ value is of the same order of magnitude as the proton-spin g value, g_n. When we allow $g_\perp$ to be an order of magnitude higher than g_n a more extensive enumeration of possible cases is desirable. This classification will first be presented, while simultaneously the maximum attainable proton polarization is considered in the limit of negligible nuclear relaxation. The second part of this section is, besides with the maximum polarization, also concerned with the polarization build-up rate taking the influence of nuclear relaxation into account. The various symbols, used in this section for polarization and temperature, are illustrated in fig. 3 and fig. 4.

2.1. *Classification of the polarization process.* Let us first consider the situation in which the electron-spin g_{min} value is less than or equal to the proton-spin g value (= 0.00304, when related to the Bohr magneton): $g \leq g_n$. Then we have to distinguish between the following three cases:

2.1.1. $M_2 << \Delta_{ef}^2 \leq \Delta_n^2$. The nuclear Zeeman splitting Δ_n is larger than or equal to the electron-spin Zeeman splitting at zero field component along the $g_{//}$ axis, Δ_{ef}, while the central second moment of the electron-spin line broadening, M_2, is much smaller than Δ_{ef}^2. Under these conditions the electron spin-spin interaction can be neglected and therefore the paramagnetic ions behave as individual electron spins. Hence the transition probabilities, as formulated by McColl and Jeffries [4] and referred to as MCJ, are applicable. In this individual-ion limit, one can define probabilities f_ε for an ε to 1 ratio of proton to electron spin flip during the cross-relaxation period of the refrigerator cycle. These f_ε have the following dependence on the pulsed field decay rate, $(dH_p/dt)_{cr}$, at the moment of cross-relaxation and on the static field H_{dc}:

$$f_1 = 1-\exp\{a(dH_p/dt)_{cr}^{-1}H_{dc}^{-1}\}$$
$$f_2 = 1-\exp\{b(dH_p/dt)_{cr}^{-1}H_{dc}^{-3}\} \qquad (2.1)$$
$$f_3 = 1-\exp\{c(dH_p/dt)_{cr}^{-1}H_{dc}^{-5}\} \text{ , etc.}$$

with $f_1 \geq f_2 \geq f_3$.
MCJ have shown that the negative coefficients a, b and c are rather complicated functions of the ratio of g_{min} and g_n. Qualitatively it can be seen from eq. (2.1) that an increase of the pulsed-field decay rate or of the static-field strength gives a decrease of the f_ε, which is the stronger, the higher the value of ε.

In the high-temperature approximation the final nuclear polarization, p_{nf}, reached in the steady state, can be calculated from (see I)

$$p_{nf} \approx (<<\varepsilon f_\varepsilon>>/<<\varepsilon^2 f_\varepsilon>>)\bar{p}_e \qquad (2.2)$$

in which $\bar{p}_e$ denotes the electron-spin polarization before the occurrence of cross-relaxation and where the double bracketed $\langle\langle \varepsilon f_\varepsilon \rangle\rangle$ represents an average value of $\langle \varepsilon f_\varepsilon \rangle$ over the distribution of $g_\perp$ values (inhomogeneous line broadening). $\langle \varepsilon f_\varepsilon \rangle$ and $\langle \varepsilon^2 f_\varepsilon \rangle$ are abbreviations, denoting the total effect of all orders of cross-relaxation. For example, when 1:1 and 2:1 spin flips are taken into account $\langle \varepsilon f_\varepsilon \rangle = (1 - f_2)\{2f_2(1 - f_1)^2 + f_1^2 - 2f_1\} + 2f_2$ and $\langle \varepsilon^2 f_\varepsilon \rangle = 8f_2 + (f_1^2 - 2f_1)(1 - 4f_2) - 4f_2^2(1 - f_1)^2$. Here we will restrict our considerations to the situation in which ε has only one value. Eq. (2.2) then simplifies into

$$p_{nf} \approx (\varepsilon f_\varepsilon / \varepsilon^2 f_\varepsilon)\bar{p}_e \approx \bar{p}_e/\varepsilon \qquad (2.3)$$

One can easily generalize this result to cases where the high-temperature approximation is not valid, as, for instance, at high electron-spin polarization. In our experiments this electron polarization is produced by the pulsed field, providing thermal contact with the lattice and establishing a Boltzmann distribution over the electronic Zeeman levels according to the lattice temperature T_L. When the pulsed field decays, the electron spins become thermally isolated. In addition, they may become also isolated from neighbouring spins, when the decay time is short compared with the spin-spin interaction time. However, the concept of spin temperature remains valid as an ensemble average over identical crystals. Equalization of nuclear-spin and electron-spin temperature, taking into account the ε:1 ratio of electron to nuclear Zeeman splitting, leads to $T_{nf} \approx \varepsilon\Delta_n/(2k \operatorname{arctanh} \bar{p}_e)$ for the final nuclear-spin temperature. The final nuclear polarization is then given by the following expression:

$$p_{nf} = \tanh(\varepsilon^{-1} \operatorname{arctanh} \bar{p}_e) \qquad (2.4)$$

When τ_1 is sufficiently long ($\tau_1 > T_{1e}$) and $\tau_2 \ll T_{1e}$, $\bar{p}_e = p_{eo} = \tanh(\Delta_{ei}/2kT_L)$, in which the initial electron spin Zeeman splitting, Δ_{ei}, is equal to $\Delta_{ei} = g_{/\!/}\mu_B H_p \cos\delta \approx g_{/\!/}\mu_B H_p$. In table 1 we have listed the calculated values for p_{nf} as a function of H_p at three values for ε, taken for Dy:YES at T = 0.4 K.

TABLE 1

H_p	$\bar{p}_e = p_{nf}(\varepsilon=1)$	$p_{nf}(\varepsilon=2)$	$p_{nf}(\varepsilon=3)$
1 kOe	0.71	0.4	0.3
2 kOe	0.97	0.7	0.5
2.5 kOe	0.99	0.8	0.6

In the high-temperature approximation $\bar{p}_e/p_{nf} = \varepsilon$, independent of the value of T or H_p. However, from eq. (2.4) and table 1 it follows that the ratio $p_{nf}/\bar{p}_e$ can be increased (at constant ε) by increasing the electron-spin polarization, for instance by decreasing the lattice temperature. This conclusion is of considerable practical significance for circumventing the disadvantage of multiple spin flips.

2.1.2. $\Delta_{ef}^2 < \Delta_n^2 \ll M_2$. This inequality holds under conditions of high electron-spin concentration at low magnetic field strengths. This may be inferred from the concentration dependence of M_2 and the field dependence of Δ_{ef} and Δ_n, since M_2 is proportional to the square root of the number of electron spins per cm^3, N_e, while Δ_n and Δ_{ef} are proportional to the magnetic field strength. The nuclear Zeeman system is in good contact (see I) with the dipolar system of the electronic spins. The two systems combined will be cooled by cross-relaxation with the electron-spin Zeeman system. Because of the important role of the electron spin-spin interaction in the polarization process, we refer to this situation as the "collective limit". After a sufficient number of refrigerator cycles the steady state is reached (see fig. 3c) and the final nuclear-spin temperature will be given by (in the high-temperature approximation) the adiabatic demagnetization formula for the electron spins

$$T_{no}^2/T_{nf}^2 = (2\Delta_{ei}^2 + M_2)/(2\Delta_{ef}^2 + M_2) \qquad (2.5a)$$

which, for $\Delta_{ef}^2 \ll M_2$, becomes

$$T_{no}^2/T_{nf}^2 \simeq (2\Delta_{ei}^2 + M_2)/M_2 \qquad (2.5b)$$

Because $\Delta_{ei} \approx (g_{\parallel}\mu_B H_p + g_{\perp}\mu_B H_{dc}) \approx g_{\parallel}\mu_B H_p$ in practice depends on H_p only, the ratio T_{no}/T_{nf} is independent of H_{dc} or $(dH_p/dt)_{cr}$. Further, eq. (2.5b) predicts that T_{nf} is concentration dependent since a lower electron-spin concentration gives a smaller second moment, which leads to a lower final temperature. Removing the restriction of small electron-spin polarization modifies eq. (2.5b) into

$$T_{no}^2/T_{nf}^2 = (2\Delta_{ei}^2 + M_2(1 - \bar{p}_e^2))/(M_2(1 - \bar{p}_e^2)) \qquad (2.6)$$

as a consequence of the reduction of the central second moment. When the reduction of M_2 becomes so drastic that $M_2(1 - \bar{p}_e^2) = 2(\varepsilon\Delta_n)^2$, the final temperature according to eq. (2.6) becomes $T_{nf} = \Delta_{ei}/\varepsilon\Delta_n$, which means that for these electron-spin polarizations the same result as in 2.1.1 (see eq. (2.4)) is obtained.

2.1.3. $M_2 \approx \Delta_{ef}^2 \leq \Delta_n^2$. In this intermediate situation, the spin-spin interaction causes multiple-electron multiple-proton spin flips, which gives a considerable enhancement of the individual transition probabilities at cross-relaxation. These processes also affect the dependence of the final nuclear polarization on $(dH_p/dt)_{cr}$ and H_{dc}.

For those ions and crystals, in which $g_{\perp} > g_n$, we have to consider three further analogous situations.

2.1.4. $M_2 \ll \Delta_n^2 < \Delta_{ef}^2$. This case corresponds to the individual ion limit 2.1.1. Because $g_{\perp} > g_n$ only ε:1 spin flips with $\varepsilon \approx g_{\perp}/g_n$ can occur. An increase of the pulsed-field decay rate or of the static-field strength leads, in the high-temperature approximation, to $\bar{p}_e/p_{nf} = g_{\perp}/g_n > 1$, while in 2.1.1 in principle $\bar{p}_e/p_{nf} = 1$ can be obtained.

2.1.5. $\Delta_n^2 < \Delta_{ef}^2 \ll M_2$. When spin-spin interaction is dominant in the polarization process, formulas 2.5b and 2.6 remain valid. At cross-relaxation the temperature of the electronic dipole system determines the final nuclear-spin temperature.

2.1.6. $M_2 \approx \Delta_n^2 < \Delta_{ef}^2$. In this intermediate situation the final

electron-spin Zeeman splitting, Δ_{ef}, in eq. (2.5a) can not be neglected. It is plausible that eq. (2.5a) remains applicable, since the transition probabilities, induced by the spin-spin interaction, will be sufficiently large to cause good thermal contact between electron- and nuclear-spin system at cross-relaxation. The final temperature in the limit of small EPR line-width is given by $T_{nf} \simeq (g_{\perp} H_{dc}/g_{/\!/} H_p) T_{no}$. The same result is obtained, when eq. (2.3) is applied.

2.2. *The polarization build-up rate.* Because of the different formulas used in the description of the polarization process, dependent upon whether spin-spin interaction has to be taken into account or not, individual-ion and collective limit will be treated separately.

2.2.1. *Individual-ion limit.* MCJ have calculated the increment in nuclear polarization $\delta p_n(\vec{r}_j)$ of a particular class of protons, namely those situated at a distance $\vec{r}_j$ from their respective neighbouring paramagnetic ion, under the following approximations. First they calculate the change in electron-spin polarization during cross-relaxation assuming the proton polarization to be constant and equal to the proton polarization at the end of the lattice relaxation part of the cycle, $\bar{p}_n$. This should be approximately correct because the protons heavily outnumber the electron spins. Further MCJ include the effect of ε:1 spin flips in the high-temperature approximation. When we also suppose that $\bar{p}_e$ is solely determined by the polarization loss due to spin-lattice interaction during the switch-off period (τ_2), the result for the total increase of nuclear polarization during one cycle becomes

$$\Sigma_j \delta p_n(\vec{r}_j) = N_e\{\langle\langle \varepsilon f_{\varepsilon} \rangle\rangle \bar{p}_e - \langle\langle \varepsilon^2 f_{\varepsilon} \rangle\rangle \bar{p}_n\} - N_e E \langle C \rangle \tau (\bar{p}_n - p_{no}) \tag{2.7}$$

with $E = 4\pi N_n/(3r_1^3)$ and N_n equal to the number of nuclear spins per cm^3. The minimum distance between a proton and a paramagnetic ion is denoted by r_1. The nuclear polarization, when the proton-spin temperature is still equal to the lattice temperature, is written as p_{no}. Further $\langle C \rangle$ denotes the average of the Bloembergen-relaxation coefficient C (see I) over a refrigerator cycle of duration τ. On account of eq. (2.7) the

final proton polarization, reached if $\Sigma_j \delta p_n(\vec{r}_j) = 0$, can be written as

$$p_{nf} = (E<C>\tau p_{no} + <<\varepsilon f_\varepsilon>>\bar{p}_e)/(E<C>\tau + <<\varepsilon^2 f_\varepsilon>>) \qquad (2.8)$$

Furthermore from eq. (2.7) it follows that the instantaneous polarization, $p_n(t)$, see fig. 5, can be expressed by $p_n(t) = p_{nf} - (p_{nf} - p_{no})\exp(-t/\tau_b)$

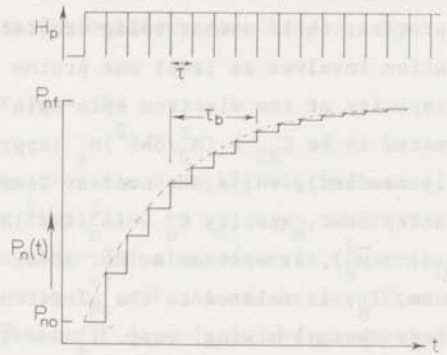

Fig. 5. Proton polarization build-up process. In the upper part of the figure the pulsed-field pattern is sketched. In the lower part, on the same time scale, the stepwise increase of $p_n(t)$ with time is shown as the drawn line. If we connect a $p_n(t)$ value, taken at an arbitrary point in a τ interval, with $p_n(t)$ values at the corresponding points in the other τ intervals, we obtain exponential curves with characteristic time τ_b, of which the dotted curve is one example. For purpose of illustration, in the figure τ_b has the small value $\tau_b = 4\tau$, resulting in $\tau_{bn} = 4$.

in which the build-up rate τ_b^{-1} is given by

$$\tau_b^{-1} = (4\pi N_e <C>)/(3r_1^3) + \tau^{-1}(N_e/N_n)<<\varepsilon^2 f_\varepsilon>> \qquad (2.9)$$

By the influence of nuclear relaxation the final nuclear polarization is of course decreased but on the other hand the build-up rate is increased. When nuclear relaxation rate and electron-spin concentration

are known, $\langle\langle\varepsilon^2 f_\varepsilon\rangle\rangle$ can be calculated from the measured build-up rate. If $T_{1n}^{-1} \approx 0$, the normalized build-up rate $\tau_{bn}^{-1} = (\tau_b/\tau)^{-1} \simeq (N_e/N_n)\langle\langle\varepsilon^2 f_\varepsilon\rangle\rangle$, while the final proton polarization $p_{nf} \simeq \langle\langle\varepsilon f_\varepsilon\rangle\rangle / \langle\langle\varepsilon^2 f_\varepsilon\rangle\rangle$.

2.2.2. *Collective limit.* We shall calculate the average increase in nuclear polarization, δp_n, in order to obtain expressions for p_{nf} and τ_b. We shall assume that only part of the protons are directly involved in the cross-relaxation process, their number being denoted by fN_n. Because each cross-relaxation involves at least one proton spin, $N_e/N_n \leq f \leq 1$. The heat capacity of the electron spin-spin system during cross-relaxation is estimated to be $C_{SS} \simeq (M_2^r/8kT^2)N_e$ (approximately correct when p_{nf} is nearly reached), while the nuclear Zeeman heat capacity is given by the Schottky heat capacity $C_n \simeq (\Delta_n^2/4kT^2)N_n$. The reduced central second moment, $M_2(1 - \bar{p}_e^2)$, is written as M_2^r. After thermal mixing the proton-spin temperature, T_n, is related to the electron- and nuclear-spin temperature just before thermal mixing, resp. $\bar{T}_e$ and $\bar{T}_n$, as follows:

$$T_n^{-1} = F(\bar{T}_e^{-1} - \bar{T}_n^{-1}) + \bar{T}_n^{-1} \tag{2.10}$$

$$F = fN_e M_2^r/(N_e M_2^r + 2fN_n \Delta_n^2) \tag{2.11}$$

Further, if $\tau_1 > T_{1e}$ and $\tau_2 \ll T_{1e}$, compare with eq. (2.5a),

$$\bar{T}_e^2/T_L^2 = (2\Delta_{ef}^2 + M_2^r)/(2\Delta_{ei}^2 + M_2^r) \tag{2.12}$$

For the increase in proton polarization, including the effect of nuclear spin-lattice relaxation, one has

$$\delta p_n = F(p_m - \bar{p}_n) - \langle D\rangle\tau(\bar{p}_n - p_{no}) \tag{2.13}$$

in which $p_m = \Delta_n/2k\bar{T}_e$. If $\Delta_{ei}^2 \gg M_2^r$, it follows from eq. (2.12) that

$$(p_m/\bar{p}_e)^2 \simeq 2\Delta_n^2/(M_2^r + 2\Delta_{ef}^2) \tag{2.14}$$

$\langle D\rangle$ denotes the average nuclear relaxation during a complete cycle.

For Bloembergen relaxation $\langle D \rangle = N_e E \langle C \rangle$, but for dipole relaxation, which process is likely to dominate, $\langle D \rangle$ is quadratic in the electron-spin concentration. From eq. (2.13) one derives for the final proton polarization

$$p_{nf} = (Fp_m + \tau \langle D \rangle p_{no})/(F + \tau \langle D \rangle) \qquad (2.15)$$

while the polarization build-up rate is given by

$$\tau_b^{-1} = (F/\tau) + \langle D \rangle \qquad (2.16)$$

When nuclear relaxation has a negligible influence, eq. (2.15) and eq. (2.16) can be simplified to $p_{nf} = p_m$, which follows directly from the equality of nuclear- and electron-spin temperatures, while the normalized build-up rate $\tau_{bn}^{-1} = F$. As can be seen from eq. (2.11) a calculation of the parameter F depends on the assumptions made about the number of protons, involved in the cross-relaxation process. When we suppose that only one proton spin interacts with one paramagnetic ion at cross-relaxation, or $f = N_e/N_n$, we obtain for the normalized build-up time $\tau_{bn} \simeq (N_n/N_e)$, if $fM_2^r > \Delta_n^2$. It may be remarked that this result is the same as in the individual ion limit for the special case that only 1:1 spin flips are possible with $f_1 = 1$. When during cross-relaxation we wait sufficiently long, we can treat the proton spins as a single system, or $f = 1$. In this situation, with $N_n >> N_e$, we find that $\tau_{bn} \simeq 2N_n\Delta_n^2/N_eM_2^r$. The last equation remains valid if $f > f_c (= N_eM_2^r/2N_n\Delta_n^2)$, which condition always seems to be fulfilled in our experiments.

2.2.3. *Intermediate situation.* This situation can be described as a particular case of section 2.2.1 or section 2.2.2. We shall start from the theory developed in 2.2.2 and consider the situation in which $g_\perp > g_n$. In the estimate of the heat capacity of the spin-spin system during cross-relaxation the contribution of the Zeeman heat capacity can no longer be omitted. So $C_{SS} \simeq (N_e/8kT^2)(M_2^r + 2\Delta_{ef}^2)$, which becomes $C_{SS} \simeq (N_e/4kT^2)\Delta_{ef}^2$ for $\Delta_{ef}^2 > M_2^r$. Neglecting the influence of nuclear relaxation, for $f > f_c$ we get $\tau_{bn} = (N_n/N_e)(\Delta_n^2/\Delta_{ef}^2)$. In other words,

for $\Delta_{ef}^2 > M_2^r$, the normalized build-up time is inversely proportional to the concentration of the electron spins and to the ratio squared of the proton g value and $g_\perp$ value of the electron spins.

It may be remarked that in these very anisotropic crystals the estimate of the electron-spin heat capacity for fields near the perpendicular direction is not very accurate. C_{SS} could exceed our estimate by a factor 2. In that case the values of M_2, deduced from our experiments with the aid of the theory developed in this section, have to be multiplied by a factor 2 to get the correct result.

3. Experimental results and interpretation. This section is first concerned with the experimental arrangement, while we also recall the parameters, which are relevant in the polarization process. Thereafter proton polarization data in Dy:YES, Yb:$YCl_3 \cdot 6H_2O$ and Yb:YES are presented and discussed.

3.1. *Experimental arrangement.* In the experimental set-up, which is already described in I, proton polarizations were measured by cw NMR, using a double T-bridge, adjustable to four fixed frequencies: 5, 10, 30 and 40 MHz. Further, like in earlier experiments, all measurements were carried out on isotopically enriched samples to avoid complications caused by hyperfine interaction. The Dy samples were enriched to 91.0% ^{162}Dy, while for the preparation of the Yb crystals Yb oxide, enriched to 95.8% ^{174}Yb was utilized. The concentrations of the rare-earth ions in the crystals were determined by neutron activation analysis.

For the description of the polarization procedure, as given in section 1, we used the following parameters: the static field $\vec{H}_{dc}$; the lattice temperature T_L; the rare-earth ion concentration c; the strength, decay and duration and off-time of the pulsed field resp. H_p, τ_d, τ_1 and τ_2; and the rest field $\vec{H}_r$. The last parameter enters in the description, mainly because $(dH_p/dt)_{cr} = |H_r|/\tau_d$.

3.2. *Dy:YES.* In order to determine the final degree of polarization obtained in Dy:YES, first the concentration of the paramagnetic ions was optimized. In table 2 the ratio between p_{nf} and p_e is given for

various values of c. The experiments were done in a static field of 1.2 kOe and with a pulse frequency $\nu_p = \tau^{-1} \simeq 1$ Hz. The maximum strength of the pulsed field was varied between $0.5 \leq H_p \leq 4$ kOe, while the crystal temperature was kept constant to $T_L = 0.5$ K. Also experiments were performed at fixed maximum magnetic field strength $H_p = 1.5$ kOe, while the lattice temperature was stepwise decreased to about 0.1 K. Both procedures gave the same result for the p_{nf}/p_e ratio. From the table it can be seen that p_{nf}/p_e becomes constant for electron-spin concentrations below 0.06%. $H_{dc} = 1.2$ kOe was chosen to avoid problems with the third-order Zeeman splitting, e.g. in a field of 7 kOe no nuclear polarization was obtained because in such a relatively high field $g_\perp > g_n$.

TABLE 2

c	1.8%	0.23%	0.13%	0.059%	0.016%
p_{nf}/p_e	0.004	0.03	0.03	0.040	0.043

At c = 0.016% Dy the decay rate of the pulsed field was varied by changing H_r, τ_d and τ_2, thereby varying the time available for cross-relaxation. No influence in the p_{nf}/p_e ratio was detected, except for $\tau_d \geq 20$ ms where we believe the electron-spin polarization to be influenced by too slow a demagnetization compared to the electron spin-lattice relaxation time.

Fig. 6 gives a typical illustration of the exponential character of the polarization build-up process. The difference between the instantaneous and the final polarization, $p_{nf} - p_n(t)$, is plotted versus time on a semi-logarithmic scale. The measurements presented in the figure were done at $T_L = 0.5$ K and $H_{dc} = 1.2$ kOe in two Dy:YES crystals having different concentrations. The data, obtained in 0.059% Dy:YES at a pulse frequency of 1 Hz are shown in fig. 6a, while those of 0.016% Dy:YES at $\nu_p = 0.5$ Hz are given in fig. 6b. Similar experiments at lower ν_p, not shown in the figure, gave essentially the same results.

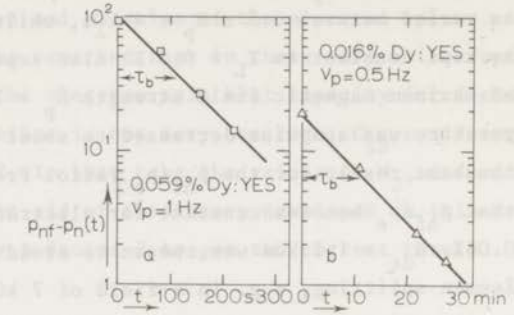

Fig. 6. Polarization build-up rate in Dy:YES. In the figure $p_{nf}-p_n(t)$, in arbitrary units, is plotted versus time on a semi-logarithmic scale, which results in a straight line yielding τ_b. The measurements, done in 0.059% Dy:YES at H_{dc} = 1.2 kOe, T_L = 0.5 K and with a pulse frequency ν_p = 1 Hz give p_e/p_{nf} = 25 and τ_{bn} = 130. From the results on 0.016% Dy:YES, with ν_p = 0.5 Hz, we obtain p_e/p_{nf} = 23 and τ_{bn} = 330.

Analyzing the results presented above with the theory developed in section 2, there appear to be two situations in which the ratio between p_{nf} and p_e becomes constant for decreasing c: the individual-ion limit with $g_\perp < g_n$ or the intermediate situation with $g_\perp > g_n$. However $p_{nf}/p_e = 0.043 \simeq 1/23$ would require at least [4] 22:1 spin flips, which process has a negligible probability in the individual-ion limit. Furthermore, the observed independence of p_{nf}/p_e from $(dH_p/dt)_{cr}$ also excludes the individual limit. On the other hand this independence is consistent with the intermediate situation, in which spin-spin interaction dominates. However, so far only homogeneously broadened EPR lines are considered. When inhomogeneous line broadening is present, M_2 can be written as $M_2 = M_{2i} + M_{2h}$, in which the subscripts i and h refer to inhomogeneous and homogeneous resp.. M_{2i} is in principle independent of the electron-spin concentration and consequently for $M_{2i} > M_{2h}$ and $g_\perp < g_n$, p_e/p_{nf} is also concentration independent. This is easily seen

by solving p_{nf} from eq. (2.15)

$$(p_{nf}/p_e)^2 \approx 2\Delta_n^2/(M_2 + 2\Delta_{ef}^2) \qquad (3.1)$$

The factor f is estimated to be larger than f_c in view of the observed independence of the build-up rate from the cross-relaxation time. Because of the very long nuclear relaxation times, T_{1n}, at the lower concentrations (see I and II) the influence of T_{1n} has been neglected in the derivation of eq. (3.1). In the expression for τ_b (eq. (2.16)) M_2 and Δ_{ef}^2 enter in the same combination as that of eq. (3.1). For $T_{1n}^{-1} \approx 0$ eq. (2.16) leads to

$$\tau_{bn} = (N_n/N_e)(2\Delta_n^2)(M_2 + 2\Delta_{ef}^2)^{-1} \qquad (3.2)$$

The values of p_{nf} and τ_{bn} give therefore only information about the magnitude of the sum of M_2 and $2\Delta_{ef}^2$. The data presented in fig. 6, analyzed with the equations mentioned above, leads to $(M_2 + 2\Delta_{ef}^2) \approx 3.5 \times 10^{-37}\,\mathrm{erg}^2$. By studying the field dependence of p_{nf}/p_e and of τ_{bn} it is possible to disentangle the contributions of M_2 and Δ_{ef}^2. A decrease of the static field by a factor 2 at c = 0.059% gave only a small decrease in the p_{nf}/p_e ratio. This would indicate that $M_2 \ll 2\Delta_{ef}^2$. Hence we shall neglect M_2 and then from $(M_2 + 2\Delta_{ef}^2) \approx 2(g_\perp \mu_B H_{dc})^2 = 3.5 \times 10^{-37}\,\mathrm{erg}^2$, we obtain for the $g_\perp$ value $g_\perp = 0.07$.

It may be noticed that the magnitude of $g_\perp$ is too small to have consequences for the interpretation of the line-width measurements in I. In I the minima, found in the nuclear relaxation time (T_{1n}) near the $\theta = 90^\circ$ direction, were related to the line-width, $\Delta_{\frac{1}{2}}$. From the T_{1n} minimum at H_{dc} = 1.2 kOe in 0.13% Dy:YES, $\Delta_{\frac{1}{2}}$ was determined to be equal to 2.1×10^{-18}erg. From the estimate given above for $g_\perp$ we derive $g_\perp \mu_B H_{dc} \approx 0.7 \times 10^{-18}$erg, which means that the supposed homogeneous line broadening indeed gives the main contribution to $\Delta_{\frac{1}{2}}$. This result is also in agreement with the observed proportionality of $\Delta_{\frac{1}{2}}$ to $\sqrt{c}$.

3.3. *Yb:YCl$_3$·6H$_2$O.* Because of the relatively large $g_\perp$ value, determined in II, high nuclear polarizations are not to be expected in these

crystals. Build-up rate and p_e/p_{nf} were measured in 0.05% Yb:$YCl_3 \cdot 6H_2O$ in a static field H_{dc} = 1.2 kOe at a lattice temperature T_L = 0.5 K with ν_p = 0.1 Hz. As shown in II, already at c = 0.05% and H_{dc} = 2 kOe the polarization method fails, because of too large a $g_\perp$ value. The polarization build-up curve, again exponential in time, gave τ_b = 10 min.. From eq. (3.2), applicable for the same reasons as in Dy:YES, $(M_2 + 2\Delta_{ef}^2)$ is calculated to be 5.6×10^{-37} erg^2. The ratio between p_e and p_{nf} was observed to be $p_e/p_{nf} \simeq 30$. The $g_\perp$ value calculated from these results lies in the region $0.075 \leq g_\perp \leq 0.090$. The agreement with the determination in II, $g_\perp = 0.08 \pm 0.01$, supports the validity of the equations used. In 1.4% Yb:$YCl_3 \cdot 6H_2O$ nearly the same p_e/p_{nf} ratio was obtained in H_{dc} = 7 kOe, which demonstrates that third-order Zeeman splitting in ytterbium chloride hexahydrate is much less than in dysprosium ethylsulfate.

3.4. *Yb:YES.* Till now, Yb:YES is considered as the most suitable substance for the nuclear-spin refrigerator, because of its small $g_\perp$ value. This was the main reason for the detailed analysis of the proton spin-lattice relaxation (see I) and for the polarization study now presented. All available parameters were varied in order to obtain optimal polarization conditions.

In fig. 7 the normalized polarization build-up time is plotted as a function of the pulsed-field decay rate, $(dH_p/dt)_{cr}$, in the cross-relaxation region for various pulse frequencies. The measurements were done in 0.07% Yb:YES at H_{dc} = 7 kOe, H_p = 1 kOe, T_L = 0.5 K and $\delta = 2^o$. Further $(dH_p/dt)_{cr}$ was varied by changing H_r. The pulse decay time-constant τ_d was fixed in this experiment. Two values were chosen for τ_2. One choice was made in such a way, that the pulsed field became almost zero: $H_p \exp(-\tau_2/\tau_d) \ll |H_r|$. In the alternate choice the pulsed field was switched on at the moment of field cancellation along the g_{max} axis (see fig. 2): $H_p \exp(-\tau_2/\tau_d) \simeq |H_r|$. Irrespective of the H_r-variable, no differences in the build-up rate between these τ_2 values were observed. From the figure it can be seen that the dependence of the build-up time on $(dH_p/dt)_{cr}$ is negligible at sufficiently low pulse frequencies. However, at higher pulse frequencies τ_{bn} is seen to increase

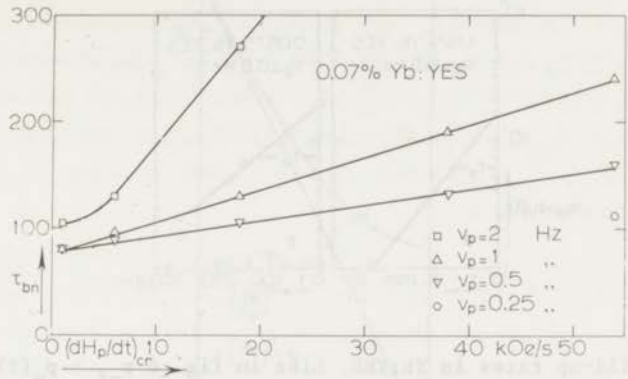

Fig. 7. Plot of the normalized build-up time, τ_{bn}, versus the decay rate of the pulsed field in the cross-relaxation region, $(dH_p/dt)_{cr}$, measured at different pulse repetition frequencies in 0.07% Yb:YES. As can be seen from the figure at sufficiently low pulse frequencies the dependence of τ_{bn} on $(dH_p/dt)_{cr}$ becomes negligible over the measured interval.

with increasing pulsed-field decay rate. This could be caused by the reduction of the effective pulsed field along the g_{max} axis during the pulse. As a consequence, T_{1e} would be longer than with $H_r = 0$, and hence initially $\overline{p}_e < p_{eo}$, which causes a lower build-up rate, as observed.

The dependence of the maximum nuclear polarization on the ratio of pulsed-field strength and lattice temperature, H_p/T_L, has been measured in many crystals at various concentrations. Up to $p_e = 0.6$ (the maximum Yb electron-spin polarization realized in our pulse experiments), the ratio p_e/p_{nf} was found to be constant for given concentration and static field.

In fig. 8 one finds $p_{nf} - p_n(t)$ plotted versus time on a semi-logarithmic scale for two crystals having Yb concentrations of 1.16% and 0.067% at $H_{dc} = 7$ kOe. For these two crystals and also all others in the same concentration region, the observed p_e/p_{nf} ratio lies between 5 and 4.

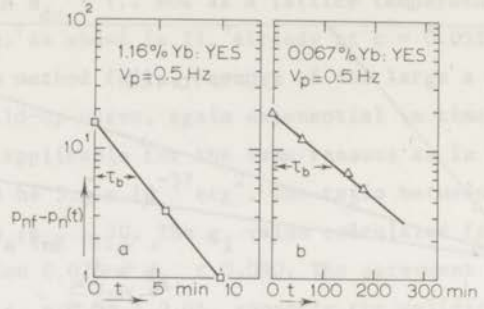

Fig. 8. Build-up rates in Yb:YES. Like in fig. 6 $p_{nf} - p_n(t)$ is plotted versus time on a semi-logarithmic scale in arbitrary units, for 1.16% Yb:YES and for 0.067% Yb:YES. The measurements on 1.16% Yb:YES at H_{dc} = 7 kOe, T_L = 0.5 K and a pulse repetition rate of 0.5 Hz results in $p_e/p_{nf} \approx 5$ and $\tau_{bn} = 1.8$. Those on 0.067% Yb:YES under the same circumstances give $p_e/p_{nf} \approx 4$ and $\tau_{bn} = 60$. As can be seen the influence of the electron-spin concentration, c, is already small for $c \lesssim 1\%$.

In fig. 9 the measured $(p_e/p_{nf})^2$ values are plotted versus H_{dc} on a logarithmic scale. The squared ratio of final nuclear polarization values at two fields $H_{dc} = H_1$ resp. H_2 was found to be equal to the ratio of the normalized build-up times at the same fields: $p_{nf}^2(H_1)/p_{nf}^2(H_2) = \tau_{bn}(H_1)/\tau_{bn}(H_2)$. For example, at H_{dc} = 7 kOe and ν_p = 0.5 Hz the polarization build-up time, τ_b, was found to be about 140 min ($\tau_{bn} = \tau_b \nu_p = 70$), while the squared ratio of p_e/p_{nf} was measured to be 11. At H_{dc} = 1.2 kOe and ν_p = 0.05 Hz we found τ_b = 110 min, hence τ_{bn} = 5.5, and $p_e^2/p_{nf}^2 = 135$. The measurements were, like in fig. 7, performed on 0.07% Yb:YES at T = 0.5 K and with a pulsed field of 1.5 kOe. The pulse frequencies were chosen in such a way that no improvement in the p_e/p_{nf} ratio was obtained at lower values of ν_p. Curve b in the figure is a plot of $p_e^2/p_{nf}^2 - A$, where A is chosen such as to produce a quadratic dependence on H_{dc} (straight line with negative slope 2 in the figure), which requires $A = 8 \pm 1$.

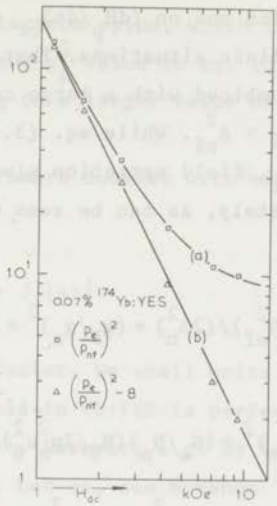

Fig. 9. Magnetic-field dependence of the ratio of electron- to nuclear-spin polarization squared, $(p_e/p_{nf})^2$. Curve (a) connects the experimental $(p_e/p_{nf})^2$ points, plotted versus the static field H_{dc} on a logarithmic scale. The straight line (b) with negative slope 2 is obtained by subtracting $(g_\perp/g_n)^2 = 8$ from the $(p_e/p_{nf})^2$ data. The measurements were performed on 0.07% Yb:YES at $T_L = 0.5$ K with a pulsed field of 1.5 kOe.

Like in Dy:YES and Yb:$YCl_3 \cdot 6H_2O$ nuclear relaxation has no detrimental effect on the polarization process at lower concentrations. The nuclear relaxation times at e.g. c = 0.05% are (see I and II) of the order of 10^4 s.

With the data presented above we can calculate the $g_\perp$ value for Yb:YES and evaluate the inhomogeneous line broadening. Once these parameters are known, the final nuclear polarization can be predicted for a great variety of experimental situations. From the Yb:YES data it is not possible to exclude immediately the individual limit, because only 3:1 to 5:1 spin flips suffice to explain the observed τ_b and p_e/p_{nf}, while in section 3.2 at least 22:1 spin flips were required. However,

like in the other crystals, also in Yb:YES the independence of p_e/p_{nf} on electron-spin concentration and on $(dH_p/dt)_{cr}$ restricts the possible explanations to the intermediate situations. That is, either $g_\perp > g_n$ with $M_2 < \Delta_{ef}^2$ or $g_\perp < g_n$, combined with a large contribution of the inhomogeneous line-width $M_{2i} > \Delta_{ef}^2$. While eq. (3.1) and eq. (3.2) only yield the sum of M_2 and $2\Delta_{ef}^2$, field variation gives the value of $(g_\perp/g_n)^2$ and $(M_2/2\Delta_n^2)$ separately, as can be seen when eq. (3.1) and eq. (3.2) are rewritten as

$$(p_e/p_{nf})^2 = (M_2 + 2\Delta_{ef}^2)/(2\Delta_n^2) = (g_\perp/g_n)^2 + (M_2/2g_n^2\mu_B^2)H_{dc}^{-2} \qquad (3.3)$$

and

$$\tau_{bn}^{-1} = (N_e/N_n)(g_\perp/g_n)^2 + (N_e/N_n)(M_2/2g_n^2\mu_B^2)H_{dc}^{-2} \qquad (3.4)$$

The observed equality of the ratio $p_{nf}^2(H_1)/p_{nf}^2(H_2)$ and the ratio $\tau_{bn}(H_1)/\tau_{bn}(H_2)$ follows directly from these equations. Further, it may be inferred from eq. (3.3) that the difference between $(p_e/p_{nf})^2$ and $(g_\perp/g_n)^2$ depends quadratically on the static field strength. On a logarithmic scale a straight line with negative slope 2 must be obtained in a $\{(p_e/p_{nf})^2 - (g_\perp/g_n)^2\}$ versus H_{dc} plot. Therefore, from curve b in fig. 9 we obtain $(g_\perp/g_n)^2 = 8$, while the intersection with the $H_{dc} = 1$ kOe axis results in $M_2 = 0.9 \times 10^{-37}\,\mathrm{erg}^2$, which agrees with $(M_2 + 2\Delta_{ef}^2) \approx M_2 \approx 6 \times 10^{-37}\,\mathrm{erg}^2$ found at c = 1.4% (see I).

The $g_\perp^2$ value, derived from our results, is nearly the same as estimated by Wolfe and Jeffries [8] from the intensity of the ytterbium ESR line. MCJ explain their polarization data with a $g_\perp$ distribution having width equal to g_n, while Potter and Stapleton [5] assume $g_\perp \leq g_n$. These differences can possibly be explained by the different $(dH/dt)_{cr}$ used in the various experiments. In the rotated crystal refrigerator of Potter and Stapleton $(dH/dt)_{cr} \approx 7$ MOe/s, which is about a factor 200 larger than in our experiments, while MCJ used typically $(dH_p/dt)_{cr} \approx 0.7$ MOe/s. In the experiments of Potter and Stapleton the time allowed for cross-relaxation is very short and may be of the same order as the electron spin flip-flop time, which is comparatively long at the low electron-spin concentrations (c ≈ 0.04%) utilized. Under these circum-

stances the final nuclear polarization is determined by the $g_\perp$ value of the majority of the electron spins, which is apparently smaller than or equal to g_n. However the $g_\perp^2$ value in eq. (3.3) and eq. (3.4) is a weighted average, leading to a larger value of $g_\perp^2$, as will be illustrated by an example.

The $g_\perp$ value of a Kramers doublet with eigenfunctions $|a\rangle$ and $|b\rangle$ is defined as

$$g_\perp = g_L |\langle b|J_+ + J_-|a\rangle| \qquad (3.5)$$

where g_L is the Landé g factor. We shall write for the $g_\perp$ value $g_\perp = g_L|A|$. If the crystal field in Yb:YES is perfectly hexagonal, A = 0 for the lowest Kramers doublet. However, e.g. by lattice strain the symmetry is reduced, giving $A \neq 0$. Let us, see McMahon [9], assume for A a Lorentzian distribution centered around A_o having half-width at half intensity δ (further, for simplicity, we will take A real). If we suppose first $A_o = 0$ and $\delta = g_n/g_L$, the majority of the electron spins has a $g_\perp$ value of about g_n or lower. However, if spin-spin interaction between electron spins differing in $g_\perp$ value up to $6g_n^2$ is sufficiently fast, the $g_\perp^2$ value, which follows from the heat capacity (see section 2.2.2) is about $3g_n^2$. If $A_o \neq 0$, for example $A_o = \delta = g_n$, again the majority of the spins has a $g_\perp$ value of about g_n or lower, but the $g_\perp^2$ value used in the heat capacity expression will become even a factor 8 larger than g_n^2.

The $g_\perp$ values found in Dy:YES and Yb:$YCl_3 \cdot 6H_2O$ probably also comprise, in addition to a bulk $g_\perp$ value, a contribution from spins with larger $g_\perp$ values. We believe, however, that because of the much larger $g_\perp$ in these crystals, the extra contribution is relatively unimportant.

Finally, it may be mentioned that the highest proton polarization reached in our experiments, was achieved in 0.07% Yb:YES with $H_p \simeq 2$ kOe at a lattice temperature $T_L \simeq 0.3$ K in $H_{dc} = 7$ kOe. The p_{nf} value of 0.16 measured corresponds to proton-spin temperatures at $\nu = 30$ MHz and $\nu = 5$ MHz of 4 mK and 0.7 mK resp..

4. Conclusion. In Dy:YES and $YCl_3 \cdot 6H_2O$ the minimum ratio between electron- and final proton-spin polarization, which can be obtained by

the nuclear-spin refrigerator method, is determined to be $p_e/p_{nf} \approx 25$. In Yb:YES p_e/p_{nf}, which is highly field dependent, has a minimum of 3 at low values of the pulsed field decay rate at cross-relaxation, $(dH_p/dt)_{cr}$. The ratio $p_e/p_{nf} = 3$ can be reached at sufficiently low Yb concentrations $c \leq 0.07\%$, combined with static fields $H_{dc} \geq 10$ kOe. This implies that a pulsed field of about 10 kOe at a lattice temperature $T_L = 0.4$ K would be required to obtain a final polarization $p_{nf} = 0.7$. Our experiments show that restrictions resulting from the contact of the electron spins with the lattice, from heat transfer and heat conduction, set an upper limit to the pulse frequency in single crystals of about 1 Hz. As a consequence, at magnetic ion concentrations $c \leq 0.1\%$ the build-up process in single crystals is a matter of hours. Proton polarizations, once reached, can be preserved for a similar length of time, because of the very long nuclear relaxation times involved. The experimental data in all crystals are explained by a model in which electronic spin-spin interaction plays an essential role.

On basis of the above results we have suggested an explanation for the data, obtained by Potter and Stapleton. They found that $p_e/p_{nf} \approx 1$ in 0.04% Yb:YES at high $(dH/dt)_{cr}$, which implies that $p_{nf} = 0.7$ can be reached at these low electron-spin concentrations using a pulsed field of only 3 or 4 kOe at $T = 0.4$ K. Possibly the spin-spin interaction time (compared to the time allowed for cross-relaxation) is long in our experiments but short in those of Potter and Stapleton. This difference can explain the influence of $(dH/dt)_{cr}$ in the nuclear-spin refrigerator.

References.

1) Jeffries, C.D., Cryogenics 3 (1963) 41.
2) Abragam, A., Cryogenics 3 (1963) 42.
3) Langley, K.H. and Jeffries, C.D., Phys. Rev. 152 (1966) 358.
4) McColl, J.R. and Jeffries, C.D., Phys. Rev. B 1 (1970) 2917.
5) Potter, W.H. and Stapleton, H.J., Phys. Rev. B 5 (1972) 1729.
6) Brom, H.B. and Huiskamp, W.J., Physica 60 (1972) 163 (Commun. Kamerlingh Onnes Lab., Leiden, No. 391a).

7) Brom, H.B. and Huiskamp, W.J., Physica, to be published (Commun. Kamerlingh Onnes Lab., Leiden, No. 398a).

8) Wolfe, J.P. and Jeffries, C.D., Phys. Rev. B 4 (1971) 731.

9) McMahon, D.H., Phys. Rev. 134 A (1964) 128.

APPENDICES

Appendix A. The nuclear relaxation coefficient C. In the literature the coefficient C in eq. (3.1) of chapter 1 is derived in various ways, of which two methods will be mentioned here.

A.1. Forbidden relaxation model. Schmugge and Jeffries [1] consider an electronic spin $S = \frac{1}{2}$ and a nuclear spin $I = \frac{1}{2}$, coupled by dipolar interaction, see fig. 2 of chapter 1. The S and I spin are embedded in the crystal lattice, whose thermal vibrations induce relaxation transitions, shown schematically as w_1 etc. The relaxation transitions establish relative populations given by the Boltzmann factors in column a. So the transition rates w_1, w_2, w_3 and w_4 must be weighted by the Boltzmann factor in the final state. For example $w_2^{\uparrow}/w_2^{\downarrow} = \exp\{-(\Delta_e + \Delta_n)/kT\}$, or $w_2^{\uparrow} = w_2\exp\{-(\Delta_e + \Delta_n)/2kT\}$. The transitions w_2 and w_3 are forbidden if the dipolar interaction between the two spins is neglected. However, in the situation considered, the $S_z I_{\pm}$ terms of the dipolar interaction give an admixture of the $|S_z, I_z>$ states, which allow w_1 to induce the w_2 and w_3 transitions at the rate

$$w_2 = w_3 = \sigma w_1 \tag{A.1}$$

For an isotropic electronic g tensor σ is given by

$$\sigma = \frac{9}{4} g_S^2 g_I^2 \mu_B^4 \sin^2\theta\cos^2\theta\, r^{-6}/(g_I\mu_B H)^2 \tag{A.2}$$

θ is defined as the angle between $\vec{r}$ (the radius vector connecting paramagnetic ion and nucleus) and the magnetic field direction. In the derivation of eq. (A.1) it is assumed that the dipolar interaction is small compared to the nuclear Zeeman splitting. Now the total rate of change of the probability density of the nuclear spin state $I_z = +\frac{1}{2}$ can be written as

$$dn_2/dt = n_1N_1w_2\exp\{(\Delta_e + \Delta_n)/2kT\} + n_1N_2w_3\exp\{(-\Delta_e + \Delta_n)/2kT\}$$
$$-n_2N_1w_3\exp\{(\Delta_e - \Delta_n)/2kT\} - n_2N_2w_2\exp\{(-\Delta_e - \Delta_n)/2kT\} \quad (A.3)$$

The contribution of w_4 in eq. (A.3) can be neglected, since it represents the very small direct nuclear spin-lattice relaxation rate. The rate equation for N_2 is approximately given by

$$dN_2/dt = w_1N_1\exp(\Delta_e/2kT) - w_1N_2\exp(-\Delta_e/2kT) \quad (A.4)$$

From eq. (A.3) and eq. (A.4) we obtain for the nuclear and electron spin-lattice relaxation rate resp. T_{1n}^{-1} and T_{1e}^{-1}:

$$T_{1n}^{-1} \simeq 2\sigma w_1\cosh^{-1}(\Delta_e/2kT) \quad (A.5)$$

$$T_{1e}^{-1} \simeq 2w_1\cosh(\Delta_e/2kT) \quad (A.6)$$

Because $\cosh^{-2}(\Delta_e/2kT) = (1 - p_e^2)$ eq. (A.5) and eq. (A.6) relate T_{1n}^{-1} and T_{1e}^{-1} in the following way

$$T_{1n}^{-1} \simeq T_{1e}^{-1}\sigma(1 - p_e^2) \quad (A.7)$$

Comparison of eq. (3.1) of chapter 1 with eq. (A.7) gives

$$C = \frac{9}{4}\, g_S^2 g_I^2 \mu_B^4 \sin^2\theta\cos^2\theta(1 - p_e^2)T_{1e}^{-1}/(g_I\mu_B H)^2 \quad (A.8)$$

A.2. Density matrix formalism. A more general approach can be given by the density matrix formalism, see e.g. Abragam [2] or Slichter [3]. Let us denote the probability per unit time of a transition from state $I_z = -\frac{1}{2}$ to state $I_z = +\frac{1}{2}$ by W_{-+}. Since the Boltzmann factors of the two nuclear states are nearly equal, we take $W_{+-} = W_{-+} = \frac{1}{2}T_{1n}^{-1}$. In the case that the perturbation $H_1(t)$, responsible for the nuclear relaxation can be written as a simple product $H_1(t) = AF(t)$, where A is an operator acting on the variables of the I-system and F(t) a random

function [2], W_{+-} is given by

$$W_{+-} = |\langle +|A|-\rangle|^2 J_z(\omega_I) \qquad (A.9)$$

where $\omega_I = \Delta_n/\hbar$. Further $J_z(\omega_I) = \int_{-\infty}^{+\infty} G(\tau)\exp(-i\omega_I\tau)d\tau$ is the spectral density function of $G(\tau)$ and $G(\tau) = \overline{F(t)F(t+\tau)}$ is the correlation function of $F(t)$. It may be remarked that eq. (A.9) can also be derived directly with the aid of time dependent perturbation theory (Abragam, p. 273) without introducing a density matrix. From the spin operators of the dipolar interaction between the nuclear and electronic spins the $S_z I_\pm$ terms may induce a nuclear spin flip unaccompanied by an electron spin flip. This process requires only the energy $\hbar\omega_I$, whereas relaxation processes, associated with the remaining bilinear operators, require a much larger energy $\hbar(\omega_S + \omega_I)$. Now it is assumed that the spin S is so tightly coupled to the lattice that the nuclear spin system has no effect on its behaviour. The above arguments allow us to write the perturbation $H_1(t)$ as $H_1(t) = BS_z(t)I_\pm$ with $B = -(3/2)g_S g_I \mu_B^2 \sin\Theta\cos\Theta\exp(-i\Phi)/r^3$. The angles Θ and Φ define the orientation of the vector connecting proton and electron with respect to the magnetic field applied along the z axis. The correlation function $G(\tau)$ becomes

$$G(\tau) = \overline{\langle S_z(t)\rangle\langle S_z(t+\tau)\rangle} = \overline{\langle S_z(0)\rangle\langle S_z(\tau)\rangle} \qquad (A.10)$$

The bar represents an ensemble average and the brackets represent expectation values. Horvitz [4] has shown how $G(\tau)$ can be calculated under conditions of a large electron spin polarization. His calculation is based on the assumption that the evolution of the z component of the S spin is a Markov process, which allows the following expansion of $G(\tau)$

$$G(\tau) = p_1(0)\langle S_z(0)\rangle_1\langle S_z(\tau)\rangle_1 + p_2(0)\langle S_z(0)\rangle_2\langle S_z(\tau)\rangle_2 \qquad (A.11)$$

$\langle S_z(\tau)\rangle_1$ and $\langle S_z(\tau)\rangle_2$ denote the expectation values of $S_z(\tau)$ with the initial condition $\langle S_z(0)\rangle_1 = +\frac{1}{2}$ resp. $\langle S_z(0)\rangle_2 = -\frac{1}{2}$, while the probabilities that at $t = 0$ the spin is in state $+\frac{1}{2}$ or state $-\frac{1}{2}$ are designated by the symbols $p_1(0)$ resp. $p_2(0)$. His final result becomes

$$G(\tau) = \langle S_z \rangle^2 + (\langle S_z^2 \rangle - \langle S_z \rangle^2)\exp(-\tau/T_{1e}) \qquad (A.12)$$

For the derivation of eq. (A.12) the electron spin transitions were weighted, like in A.1, according to $w\uparrow/w\downarrow = \exp(-\Delta_e/kT)$. From eq. (A.12) it is evident that the correlation time, τ_c, equals the electron spin-lattice relaxation time, T_{1e}. For the spectral density function, $J(\omega_I)$, we get

$$J_z(\omega_I) = \langle S_z \rangle^2 2\pi\delta(\omega_I) + \{(\langle S_z^2 \rangle - \langle S_z \rangle^2)2\tau_c/(1 + \omega_I^2\tau_c^2)\} \qquad (A.13)$$

Inserting eq. (a.13) in the expression for W_{+-}, given by eq. (A.9), results in the following relation for C

$$C = \frac{9}{4} g_S^2 g_I^2 \mu_B^4 \sin^2\theta\cos^2\theta(1 - p_e^2)\{T_{1e}/(1 + \omega_I^2 T_{1e}^2)\hbar^2\} \qquad (A.14)$$

This expression is equivalent to that of Schmugge and Jeffries (eq. A.8) when also the influence of the electron spin line-width is accounted for, see e.g. McColl [5].

Appendix B. Induced spin diffusion. Horvitz [4] has shown that paramagnetic impurities can induce nuclear spin diffusion in non-conducting solids. This process may have a decisive influence on the magnitude of the nuclear spin diffusion inside the sphere $r_1 \leq r < d$ (=diffusion barrier), around the paramagnetic impurity. He considers a system of two nuclear spins, interacting with the external field and with the paramagnetic impurity. Further, also the interaction of the two spins is taken into account as a small perturbation. The zeroth order $|+\frac{1}{2},-\frac{1}{2}\rangle$ and $|-\frac{1}{2},+\frac{1}{2}\rangle$ eigenfunctions are not degenerate because of the quasi-static field contribution of the impurity spin being different at the two nuclear spin sites. The dipolar interaction of the two nuclei will admix both states, which can in first order be written as

$$\begin{aligned} |1\rangle &= |+\tfrac{1}{2},-\tfrac{1}{2}\rangle - \varepsilon|-\tfrac{1}{2},+\tfrac{1}{2}\rangle \\ |2\rangle &= |-\tfrac{1}{2},+\tfrac{1}{2}\rangle + \varepsilon|+\tfrac{1}{2},-\tfrac{1}{2}\rangle \end{aligned} \qquad (B.1)$$

Because ε is small, diffusion corresponds to transitions between the

states $|1\rangle$ and $|2\rangle$. The dipolar coupling between S and I spins can induce such transitions, the most important contribution arising from (compare section A)

$$H_1(t) = A_i S_z(t) I_z^i + A_j S_z(t) I_z^j \qquad (B.2)$$

where $A = g_S g_I \mu_B^2 (1 - 3\cos^2\theta)/r^3$, while the subscripts i and j denote the nuclear spins. The spectral density function $J(\omega)$ of the impurity spin can be calculated in the same way as in appendix A, etc. Taking Ce^{3+} in CaF_2 as an example, Horvitz shows that at T = 5 K the spin diffusion coefficient D inside the diffusion barrier is even larger than outside, which clearly illustrates the relevance of this mechanism in nuclear spin diffusion.

Appendix C. Electron spin correlation function in a diamagnet containing paramagnetic impurities, due to dipolar interaction. The fluctuations of the S_z component of an electronic spin due to dipolar interaction with neighbouring electron spins is considered by Melikiya [6]. He has proved that for cubic crystals the time dependence of the correlation function of the j^{th} magnetic ion, $\overline{S_{zj}(t)S_{zj}(t+\tau)}$, is exponential for spin concentration below 2%. The exponential behaviour of the correlation function in appendix A directly ensues from the assumed mechanism (Markov process). For the Fourier component of the correlation function, Melikiya shows that one may use a truncated Lorentzian curve having at half intensity a half width δ. The correlation time τ_c is then given by $\tau_c \approx \delta^{-1}$. It may be noticed that the second moment of the spectral density function (in energy units)

$$M_2 = \mathrm{Tr}\left[H_d, S_{zj}\right]^2 / \mathrm{Tr}(S_{zj}^2) \qquad (C.1)$$

while the second moment of the electron spin resonance line is given by

$$M_2 = \mathrm{Tr}\left[H_d, S_x\right]^2 / \mathrm{Tr}(S_x^2) \qquad (C.2)$$

where H_d equals the truncated dipolar interaction hamiltonian and

$S_x^2 = \Sigma_j S_{xj}^2$. As an example, for isotropic g values in a simple cubic lattice with a magnetic field directed in the [100] direction, the M_2 value of Melikiya is a factor 4.5 larger than according to eq. (C.2).

Appendix D. Discussion of the shell of influence model. In chapter 2 and 3 we employed an average value for the coefficient B of the $S_z I_\pm$ term in the dipolar interaction, which determines the nuclear relaxation. The averaging procedure will be discussed here and its results will be compared with computer calculations.

Let us consider crystals with anisotropic g values, but having axial symmetry $g_x = g_y = g_\perp$, like in Yb:YES, Dy:YES and $Yb:YCl_3.6H_2O$. The coefficient B of the $S_z I_\pm$ term is given by the following expression

$$B = -\frac{3}{2} g_I g_S \mu_B^2 \sin\theta\cos\theta\exp(-i\phi)/r^3 + \qquad (D.2)$$

$$+ g_I g_S^{-1} (g_\perp^2 - g_z^2)\mu_B^2 \sin\theta\cos\theta\{-\frac{1}{4}(1-3\cos^2\theta) - \frac{3}{4}\sin^2\theta\exp(-2i\phi)\}/r^3$$

with $g_S^2 = g_z^2\cos^2\theta + g_\perp^2\sin^2\theta$. The angles Θ and Φ determine the direction of the radius vector between paramagnetic ion and proton with respect to the magnetic field, while θ represents the angle between magnetic field direction and g_z axis. Usually (see chapters 2 and 3) one assumes that the protons are isotropically distributed in the crystal. Then one can take an angular average of B, which gives for $g_z >> g_\perp$

$$|B|^2 = 0.3 g_I^2 g_z^2 \mu_B^4 / r^6 \qquad (D.3)$$

In the nuclear spin-lattice relaxation only those protons adjacent to the paramagnetic ion need to be considered for the calculation of the influence of the $BS_z I_\pm$ term. For the 16 protons in Yb:YES, situated in the shell $3.0 \leq r \leq 3.2$ Å, see fig. 3 of chapter 1, we have computed the average of $|B|^2$ for various field directions. The average so determined was found to be dependent on θ, the influence of ϕ in the final value being very small in these crystals. For example for $\theta = 0^\circ$ it was found that $|B|^2 = 0.92$, while at $\theta = 60^\circ$ and $\theta = 90^\circ$ we calculated $|B|^2 = 0.59$ and $|B|^2 = 0.65$ resp.. The average value from

eq. (D.3) is $|B|^2 = 0.24 \times 10^{-40}$, the factor 10^{-40} being omitted in the presented results for simplicity.

In $Yb:YCl_3.6H_2O$ the same calculations were performed for the 12 protons in the shell $3.0 \leq r \leq 3.2$ Å. The θ dependence was again stronger than the influence of ϕ. However, the latter was more important than in the ethyl sulfates. This may be inferred from the following examples: at $\theta = 0^\circ$ the calculations give $|B|^2 = 1.37$ for $\phi = 0^\circ$ and $|B|^2 = 1.35$ for $\phi = 30^\circ$, while at $\theta = 90^\circ$ $|B|^2 = 0.89$ for $\phi = 0^\circ$ and $|B|^2 = 0.83$ for $\phi = 30^\circ$. The average value from eq. (D.3) is $|B|^2 = 0.69$. It may be remarked that in neither of the two crystals the proton positions are accurately known. Furthermore, we have not taken into account the influence of nuclear spin diffusion, which will give an extra weighting factor for the neighbouring protons involved in the relaxation process.

From these considerations we conclude that the averaging procedure applied in the shell of influence model to derive T_{1n}, is not rigorous, but very convenient when the exact proton positions are not known. A better approach can be given starting from the positions of the protons adjacent to the paramagnetic ion. However, then spin diffusion has to be taken into account also on the interatomic distance scale.

Appendix E. Adiabatic demagnetization. The rotational cooling of paramagnetic crystals is in many respects equivalent to the familiar adiabatic demagnetization method. This refers in particular to the derivations of the relation between initial and final temperature [7]. For both methods one has to take into account the Zeeman and dipolar system and their mutual interaction. Let us denote by H_{ei} and H_d resp. the initial external field and the dipolar, or local, field. The latter is defined by $H_d^2 = \mathrm{Tr}H_d^2/\mathrm{Tr}M_z^2$. If $H_{ei} >> H_d$, the Kronig-Bouwkamp relaxation time, τ_{KB}, is very long [8]. In other words the Kronig-Bouwkamp relaxation process, by which mechanism Zeeman and dipolar system can reach the same temperature, is inefficient.

Let us first consider a reduction of the external field from H_{ei} to $H_{ef} >> H_d$ in a time short compared with τ_{KB}. Then the final temperature, T_f, is related to the initial temperature, T_i, by

$$T_i/T_f = H_{ei}/H_{ef} \qquad (E.1)$$

Under the condition $H_{ef} >> H_d$, the dipolar temperature remains essentially constant. However, it is to be expected that in a time interval of the order τ_{KB} irreversable mixing equalizes the temperatures of both systems. When the Zeeman and dipolar heat capacities are resp. given by

$$C_Z = A(H_e^2/4kT^2) \text{ and } C_D = A(H_d^2/4kT^2) \qquad (E.2)$$

in which A denotes a proportionality constant, one obtains after irreversible mixing a final temperature

$$T_f = T_i(H_{ef}^2 + H_d^2)/(H_{ei}H_{ef} + H_d^2) \qquad (E.3)$$

Eq. (E.3) can also directly be obtained in a rigorous quantum mechanical way, see e.g. Goldman [9]. When the external field is reduced to $H_{ef} << H_d$, it will pass a value ($H_e \simeq 5H_d$) where τ_{KB} becomes very short compared to the switch-off time of the external field. Therefore, in this final stage T_i and T_f are related according to

$$(H_{ef}^2 + H_d^2)^{\frac{1}{2}}/T_f = (\overline{H}_{ei}^2 + H_d^2)^{\frac{1}{2}}/T_i \qquad (E.4)$$

The field value at which the switch-off time of the external field becomes longer than τ_{KB} is denoted by $\overline{H}_{ei}$. Let $\overline{H}_{ei} = aH_d$ with $a \simeq 5$. Then a combination of eq. (E.3) and eq. (E.4) leads - for $H_{ei} >> H_d$ - to

$$T_i/T_f = \{a^2/(a^2 + 1)\}^{\frac{1}{2}}(H_{ei}/H_d) \qquad (E.5)$$

If we start from a high initial field value and if a is not too small, one easily verifies that there is no substantial difference between the result for T_f derived from eq. (E.5) and that obtained from eq. (E.4). Hence we shall use eq. (E.4) in our calculations.

It may be noted that in eq. (E.2) the heat capacity of the dipolar system is given in the high temperature approximation. If this restriction is relinquished, C_D (for effective spin $\frac{1}{2}$) is in a better approximation represented by [10]

$$C_D = AH_d^2(1 - p_e^2)/4kT^2 \qquad (E.6)$$

where p_e denotes the electron spin polarization. As a result of eq. (E.6) the expression on the right hand side of eq. (E.5) has to be multiplied by $(1 - p_e^2)^{-\frac{1}{2}}$: the higher the value of p_e, the higher the T_i/T_f ratio.

Appendix F. NMR method. Working at quite low temperatures ($0.05 \leq T \leq 1$ K) and small paramagnetic ion concentrations requires a low heat input in the proton system, because of the very long relaxation times we have to measure. In view of the stability, combined with a low r.f. level, a separate oscillator was connected in a double T-bridge to the resonance circuit, see also chapter 2. For reasons of phase sensitive detection and low heat input in the cooling salt the derivative of the nuclear absorption signal was measured by 30 Hz modulation of the slowly swept "static" field. In order to minimalize the influence of the level of the helium bath in the adjustment of the bridge, the losses in the coaxial line, leading to the resonance coil, were held constant by liquid nitrogen cooling at the feed-through at the top of the cryostat.

Appendix G. Concentration analysis. In many cases the determination of rare earth ion contents in crystals can be performed by light absorption techniques. However, at the very low amounts of Yb and Dy ions in our crystals, $c \leq 0.1\%$, these methods appeared to be unsuccesful. Therefore we resorted to neutron activation analysis, which will briefly be described in the following.

The crystals measured in our experiments were Dy:YES, Yb:YES and $Yb:YCl_3.6H_2O$. Once the experiments were comleted, a mixture of Y_2O_3 and Yb_2O_3 or Dy_2O_3 was recovered from the samples. The oxides were carefully weighed (typical weight 50 mg), sealed in quartz tubes and subsequently exposed to a reactor flux of about $5 \times 10^{13}/cm^2s$. Comparison of the γ-ray activity, after neutron irradiation, of these mixtures with that of 100% Yb or Dy oxide yields the concentration of the rare-earth ion. To be more precise, the Yb oxides, from which the crystals were prepared, were enriched to 96% ^{174}Yb. This isotope has a neutron cross-section [11)]

of about 50 barn. By activation, ^{175}Yb is formed, which has a half life $t_{\frac{1}{2}} \simeq 100$ hours. This isotope decays by β^- emission to one of the (excited) states of ^{175}Lu. By counting e.g. the intensity of the 396 keV γ-radiation of Lu, a measure of the Yb content in the oxide mixtures is obtained. The Dy oxides, enriched to 91% ^{162}Dy, contained about 1% ^{164}Dy. This isotope has a very large activation cross section of about 2000 barn. The activation product ^{165m}Dy decays in the first minutes after irradiation to ^{165}Dy, the latter isotope's life time being 139 m. ^{165}Dy decays by β^- emission to ^{165}Ho, whose 95 keV gamma radiation was counted. At a reactor flux of $5 \times 10^{13}/cm^2s$, the activation time of the Yb samples was about a minute and for the Dy oxide mixtures a few seconds. Countings were performed with a Ge-Li semiconductor detector.

References.

1) Schmugge, T.J. and Jeffries, C.D., Phys. Rev. 138A (1965) 1785.
2) Abragam, A.; The Principles of Nuclear Magnetism (Oxford University Press, London, 1961), Chapter 8.
3) Slichter, C.P.; Principles of Magnetic Resonance (Harper and Row, New York, 1963), Chapter 5.
4) Horvitz, E.P., Phys. Rev. B3 (1971) 2868.
5) McColl, J.R., Thesis, University of California at Berkeley, 1967 (unpublished).
6) Melikiya, M.G., Sov. Phys. Solid State 10 (1968) 673.
7) Bloembergen, N., Nederlands Tijdschrift voor Natuurkunde 38 (1972) 198.
8) Kronig, R. and Bouwkamp, C.J., Physica 5 (1938) 521.
9) Goldman, M.: Spin Temperature and Nuclear Magnetic Resonance in Solids, Clarendon Press (Oxford, 1970), p. 19.
10) McMillan, M. and Opechowski, W., Canad. J. Phys. 38 (1963) 1168.
11) Lederer, C.M., Hollander, J.M. and Perlman, I.; Table of Isotopes (J.Wiley & Sons, inc., 6th edition, 1967).

Samenvatting.

In dit proefschrift worden resonantiemetingen aan de spins van protonen behandeld. Deze protonen bevonden zich in diamagnetische kristallen, die met bekende hoeveelheden paramagnetische ionen werden verontreinigd. Enerzijds werd getracht de spins van de protonen te polariseren door middel van een speciale rotatiekoelingmethode, anderzijds werd de uitwerking van de verschillende relaxatiemechanismen op het protonspinsysteem bestudeerd. De polarisatiemethode berust op het overdragen van electronspinpolarisatie, die met betrekkelijk weinig moeite kan worden verkregen, naar het protonspinsysteem door middel van het draaien van een magneetveld. Om een analyse van deze methode mogelijk te maken en de optimale omstandigheden voor protonpolarisatie te kunnen bereiken, werd het polarisatieproces onderzocht onder verschillende experimentele omstandigheden. Zo werd bijv. de temperatuur gevarieerd tussen $0.05 \leq T \leq 1$ K en de concentratie van onzuiverheden tussen $0.05 \leq c \leq 2\%$.

Het was bij voorbaat al duidelijk dat de polarisatiegraad zou afhangen van de koppeling tussen protonspins, electronspins en roostertrillingen. Een nadere studie van de warmteoverdracht tussen deze systemen, met name van de kernspin-roosterrelaxatietijd, T_{1n}, was daarom gewenst. Een tweede impuls voor het bestuderen van T_{1n} kwam voort uit de wel zeer gunstige omstandigheden voor een dergelijk onderzoek; vandaar ook het relatief grote gedeelte, dat in dit proefschrift aan relaxatiestudie is gewijd. Immers de zeer lage kernspintemperaturen, die door middel van rotatiekoeling kunnen worden bereikt, vergemakkelijken een kernspinrelaxatiemeting aanmerkelijk. Bovendien is het concentratiegebied van de onzuiverheden beneden 1% zeer geschikt om bijv. de rol van de spin-spinwisselwerking in T_{1n} te analyseren.

In hoofdstuk 1 worden enige experimenten vermeld, waarvoor gepolariseerde kernen nodig zijn en lichten we verscheidene polarisatiemethoden toe. Speciale aandacht wordt geschonken aan de dynamische polarisatiemethode en aan „nuclear-spin refrigeration", zoals de rotatiekoelingmethode in de angelsaksische literatuur wordt genoemd. Verder geven we een kort overzicht van de kernspinrelaxatiemechanismen voor zover ze van belang zijn in onze experimenten. Het belangrijkste

onderwerp dat wordt aangesneden is hoe de kernspins relaxeren via het Zeemansysteem en het dipolaire reservoir van de electronspins. Hierbij komt eveneens de discutabele rol van de spindiffusie ter sprake.

De meetopstelling en meetprocedures worden besproken in hoofdstuk 2. Het grootste deel van dit hoofdstuk handelt over protonpolarisatie en-relaxatie in YES (yttrium-ethylsulfaat), waaraan Yb- en Dy-ionen zijn toegevoegd. Met behulp van gepubliceerde T_{1e}-gegevens ontleden we de T_{1n}-resultaten in drie processen: Bloembergenrelaxatie, dipolaire relaxatie en crossrelaxatie.

Hoofdstuk 3 handelt over rotatiekoeling en relaxatiemetingen in $YCl_3.6H_2O$, met Yb verontreinigd. De T_{1n}-gegevens lenen zich tot een zelfde soort interpretatie als in hoofdstuk 2. Verder wordt aangetoond dat de T_{1n}-metingen leiden tot de veronderstelling van een nagenoeg hexagonale kristalveldsymmetrie ter plaatse van het Yb-ion. Voorts wordt de uit de T_{1n} berekende T_{1e} vergeleken met de direct gemeten electronenspin-roosterrelaxatietijd, zoals die is gemeten in $YbCl_3.6H_2O$-poeder. De overeenstemming blijkt zeer goed te zijn. Tenslotte leiden we de minimum g-waarde van de Yb-spins af door de veld- en hoekafhankelijkheid van de polarisatiegraad te vergelijken.

In hoofdstuk 4 worden de optimale omstandigheden voor de rotatiekoelingmethode onderzocht in dezelfde kristallen als in de voorafgaande hoofdstukken. Een theoretische analyse van de gegevens leidt tot de conclusie dat de dipolaire wisselwerking tussen de electronspins een zeer belangrijke rol speelt in de uiteindelijke polarisatiegraad, die met de rotatiekoelingmethode kan worden bereikt.

Enkele onderwerpen uit de inleiding worden uitvoeriger behandeld in de appendices, aan het eind van dit proefschrift. Zo worden enkele facetten besproken van de afleiding van de grootte van de evenredigheidsconstante tussen T_{1e} en T_{1n}. Verder geven we een beschrijving van een adiabatisch-demagnetisatieexperiment met inbegrip van het Kronig-Bouwkamprelaxatiemechanisme. Tenslotte wordt een aantal opmerkingen gemaakt over de NMR-methode en de concentratieanalyse.

Hoofdstuk 2 van dit proefschrift is verschenen in Physica 60 (1972) 163; hoofdstukken 3 en 4 zullen in hetzelfde tijdschrift verschijnen.

Op verzoek van de faculteit der Wiskunde en Natuurwetenschappen volgt hier een overzicht van mijn studie.

Na een gymnasium-B opleiding aan het Sint Jansenius Lyceum te Hulst begon ik in 1961 mijn studie aan de Rijksuniversiteit te Leiden. Het kandidaatsexamen met de hoofdvakken natuurkunde en wiskunde en bijvak sterrekunde werd in 1964 afgelegd. Sinds oktober van dat jaar ben ik verbonden aan de werkgroep adiabatische demagnetisatie en kernfysica van het Kamerlingh Onnes Laboratorium, waarvan Prof. Dr. W.J. Huiskamp de leiding heeft. In de tijd tussen kandidaats- en doctoraalexamen, het laatste afgelegd in 1967, assisteer ik voornamelijk Dr. J. Lubbers.

Sinds 1965 heb ik diverse functies vervuld bij het natuurkunde praktikum. In juli 1967 werd ik aangesteld als wetenschappelijk medewerker in de werkgroep K IV bij de Stichting voor Fundamenteel Onderzoek der Materie, F.O.M.. In 1968 bezocht ik gedurende een maand de afdeling van Prof. Dr. J. Jeener aan de Vrije Universiteit te Brussel.

Het tot stand komen van dit proefschrift is mogelijk geworden dankzij de bijdrage van vele medewerkers uit het K.O. Lab. en met name uit de werkgroep. De heren J. van Weesel en J. van der Waals hebben talrijke technische problemen opgelost en verzorgden het cryogene gedeelte van de opstelling. De glazen apparatuur werd vervaardigd in de glasblazerij van de heer B. Kret. De heer R. Hulstman ontwierp een groot gedeelte van de electronica. De heer R. Hunik en in het bijzonder drs A. Zweers, die ook vele computerprogrammas schreef, verleenden hulp tijdens de experimenten. De kristallen werden bereid door mevr. M.A. Otten-Scholten.

De methode van rotatiekoeling leerde ik kennen van Dr. J. Lubbers. De contacten met de F.O.M. groep VS-LI betreffende de relaxatiemetingen, en de F.O.M. K IX groep in Petten, vanwege de activeringsanalyse, waren zeer nuttig. Prof. C.J. Gorter toonde zich altijd geinteresseerd in de hier beschreven experimenten.

De heer W.F. Tegelaar vervaardigde het merendeel van de tekeningen. Het manuscript werd getypt door mevr. E. de Haas-Walraven.

Aan hen allen zij hier mijn oprechte dank uitgesproken.